UNIVERSITY RESEARCH PROGRAM IN ROBOTICS

Robotics Technology Development Program

Grant No.: DE-FG04-86NE37967

FINAL TECHNICAL CLOSE OUT REPORT

Completion of Project: May 31, 2004

Principal Investigators

Carl D. Crane, III

James S. Tulenko

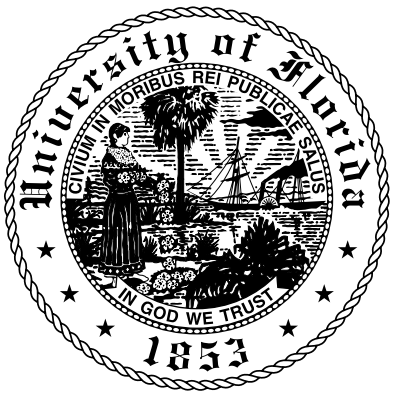

University of Florida

College of Engineering

Gainesville, FL 32611

Table of Contents

Scope & Focus of URPR

An integrated team of five university researchers developing next-generation robotic solutions to DOE technical challenges.

- **Team based**
- **Distinctive competencies**
- **Mid to long-term**
- **Revolutionary solutions**
- **Bringing Together Multiple University Resources**

University Consortium Started in 1986

- **1993 to 2003: Focused on EM to develop robotics capabilities for EM facilities cleanup.**
- **Student-driven research, integrated with training.**
- **Long-term commitment to students : 1-2 years for M.S. and 3-4 years for Ph.D. students.**
- **Balance between basic and applied research, driven by DOE needs.**
- **Archival publications and technology transfer are important elements.**

University of Florida Focus

- **Radiation Hardening Technologies and Force Control**
- **James S. Tulenko, PI; Carl Crane, Co-PI**
- **Sharing and Collabortion of two UF engineering Departments: Nuclear & Radiological Engineering and Mechanical & Aerospace Engineering Departments**
- **Focus now shifted to NNSA**

Research Team Personnel

A. Principal Faculty	B. Associated Faculty	C. Post-Doctoral & Sub Faculty
	Dr. Carl Crane, Co-PI	Dr. G. Ron Dalton
David Armstrong, M.S.		
Prof. J. S. Tulenko, PI	Dr. Chris Niezrecki	Dr. G. Gueorguiev
	Dr. James Kurtz	Dr. Dean Schoenfeld

D. Students Supported and/or Graduated since 1993:

W. Abbassi	Ph.D. Student	Arfath Pasha	Masters Student
M. Alibright	Masters Student	K. Phillips	Project
Baldeep Anand	Masters Student	Integ./Admin	
Jahan Bayat	Ph.D. Student	Ralph Pinherio	Masters Student
Rene Bohren	Masters Student	Shannon Ridgeway	Ph.D. Student
V. Chesney		Jose Santiago	Ph.D Student
Electrical/computer		T. Shawver	Masters Student
Carol Chessney	Ph.D. Student	R. Slovin	Masters Student
S. Clifford	Training/Maint.	Blair Smith	Post Doc
Julio Correa	Ph.D. Student	Sanjay Solanki	M.S Student
D. Haddox	Masters Student	D. Ioannou	Masters Student
Mandeep Jawanda	Masters Student	Zong Su	Ph.D. Student
Ralf Jurcyzk	Ph.D. Student	C. Sun	Masters Student
Jean-F. Kamath	M.S. Student	Vidya Swathamurthy	Masters Student
T. Knight	Masters Student	Memet Unsal	Masters Student
S. Kowkabany	Masters Student	Jiwei Wang	M.S. Student
Hyun Kwon Jung	Ph.D. Student	S. Wang	Post Doc
David Lewis	Masters Student	X. Wang	Ph. D. Student
Jeremy Mayer	Masters Student	C. Will	Ph.D. Student
R. McGhee	Masters Student	Carol Will	Masters Student
Sowmiya Narasimhan	Masters Student	M. Yang	Masters Student
Aditya Nawab	Masters Student	Bo Zhang	Ph.D Student
Sebastien Pamart	Masters Student	Z. Zong	Post Doc

Publications and Presentations

1993-94

- *"The Development of Intelligent Robotic Systems with Practical Applications,"* Crane, C., M. Griffis, and J. Duffy, Second Conference on Mechatronics and Robotics, Univ. of Duisburg/Moers, Germany (1993).

- *"An Implementation of Fuzzy Logic Control for KZA Cybermotion Mobile Robot,"* Dai, H. and R. Dalton, Presented at the 2nd Annual DOE/NE Robotics for Advanced Reactors Student Conference, Gainesville, FL (1993).
- *"ALMR Robotic Inspection: Mobility,"* Gluckman, S., R. Ross, C. Crane, and P. Adsit, Presented at the 2nd Annual DOE/NE Robotics for Advanced Reactors Student Conference, Gainesville, FL (1993).
- *"Using Computerized 3-D Graphical Visualization and Simulation to Determine the most Efficient Maintenance Strategy for the General Electric Advanced Liquid Metal Reactor (ALMR),"* Haddox, D. and R. Dalton, Presented at The 2nd Annual DOE/NE Robotics for Advanced Reactors Student Conference, Gainesville, FL (1993).
- *"Remote Positioning of a Mobile Robot: Development and Testing,"* Ioannou, D., Presented at the 2nd Annual DOE/NE Robotics for Advanced Reactors Student Conference, Gainesville, FL (1993).
- *"Environmental Hardening of a Mobile Manipulator System for Nuclear Environments,"* Jones, S.L., T. Cable, J.S. Tulenko, S, Toshkov, F.R. Sias, Jr., Trans. Am Nuc. Soc., 69: 487-488 (1993).
- *"Three Dimensional Projection Display Using Concave Mirrors,"* Jurczyk, R., Presented at the 2nd Annual DOE/NE Robotics for Advanced Reactors Student Conference, Gainesville, FL (1993).
- *"On-Line Annealing of MOS Devices in Nuclear Environments,"* Mandal, S., R.K. Singh, and J.S. Tulenko, Presented at the 2nd Annual DOE/NE Robotics for Advanced Reactors Student Conference, Gainesville, FL (1993).
- *"Concurrent High-Frequency Annealing of MOS Devices in Nuclear Environments,"* Mandal, S., R.K. Singh, J.S. Tulenko, R.M. Fox, Trans. Am. Nuc. Soc., 69:489-491 (1993).
- *"The Design and Fabrication of a Four Link Articulated Robot,"* Ridgeway, S., C. Crane, and P. Adsit, Presented at the 2nd Annual DOE/NE Robotics for Advanced Reactors Student Conference. Gainesville, FL (1993).
- *"Radiation-Hardened Microcomputers for Robotics and Teleoperated Systems,"* Sias, F.R. Jr. and J.S. Tulenko, Trans Am. Nuc. Soc., 69:488-489 (1993).
- *"Designs for Remote Inspection of the ALMR Reactor Vessel Auxiliary Cooling System (RVACS),"* Sweeney, F., D. Carroll, C. Chen, C. Crane, R. Dalton, J. Taylor, S. Tosunoglu, T. Weymouth, and K. Williams, ANS Fifth Topical Meeting on Robotics and Remote Systems, Knoxville, TN (1993).
- *"An Overview of Robotics Research at the University of Florida,"* Tulenko, J. and C. Crane, Presented at the 2nd Annual DOE/NE Robotics for Advanced Reactors Student Conference," Gainesville, FL (1993).
- *"Utilizing Visual Reality for Design, Construction, Operations Maintenance and Decommission of Nuclear Power Facilities,"* Wang, S., G.R. Dalton, J.S. Tulenko, Presented at the 2nd Annual DOE/NE Robotics for Advanced Reactors Student Conference, Gainesville, FL (1993).

1994-95

- *"Using the Hough Transform for Determining the Length of a Digital Straight Line Segment,"* Ioannou, D. IEEE Electronic Letters, Vol.31, No. I 0. May 11. 1995.
- "*Radiation hardening of Electronics for Robot Applications,*" Tulenko, J.S., G. Youk, D. Ekdahl, H. Liu, H. Zhou, K. Phillips, F. Sias, S. Jones, T. Cable, and H Harvey.. Florida Conference on Recent Advances in Robotics, Orlando, FL (1995).

- "*Model Based Feature Extrusion and Terrain Visualization,*" Wang, S., Y. Huang, D. Haddox, M Rao, C. Crane, B Dewitt. Florida Conference on Recent Advances in Robotics, Orlando, FL (1995).
- *"A Smart Kinestatic Interactive Platform,"* Griffis, M., Crane, C., and Dully, J., Fourth International Workshop on Advances in Robot Kinematics, Ljubjana, Slovenia, 4-6 July 1994.
- *"Design of the Reactor Vessel Inspection Robot for the Advanced Liquid Metal Reactor,"* Spelt, P., Crane, C., Feng, L., Abidi, M., and Tosunogiu, S., " Intelligent Automation and Soft Computing, Trends in Research, Development, and Applications, Volume 1, TSI Press, Proceedings of the First World Automation Congress, Maui, Hawaii, pp. 359-366, 8/1994.
- *"Development of an Articulated Transporter/Manipulator System,"* Ridgeway, S., Adsit, P., and Crane, C., accepted for publication in the Special Issue on Highly Redundant Manipulators of Advanced Robotics, The Transactions of the Robotics Society of Japan.
- *"Real Time Control of the ANDROS Mobile Robot,"* Haddox D., S. Clifford, D. Ekdahl, et. al., DENEB Robotics User Group Meeting Proceedings, pp. 91 - 98, St. Claire, MI, Oct., 1994.
- *"Object Recognition in a Four-Dimensional Hyper-Image Space,"* Wang, S., M. Rao, C. Crane, D. Ekdahl, J. Tulenko, and R. Dalton, Submitted to IEEE Transactions on Pattern Analysis and Machine Intelligence, November, 1994.
- *"CAD-Based Object Recognition from 2D Imagery,"* Wang S., D. Haddox, M. Rao, C. Crane, and J. Tulenko, Submitted to IEEE International Symposium on Computer Vision, Coral Gables, FL, 1995.
- *"Development of a Radiation Hardened ANDROS Robot for Operation in Severe Environments,"* Tulenko, J.S., D. Ekdahl, S. Toshkov, H. Liu, K. Phillips, G. Youk, F. Sias, T. Cable,, S. Jones, and H. Harvey. Sixth Topical Meeting on Robotics and Remote Systems, Monterey, CA, Feb., 1995.
- *"Automatic Updating of Virtual Workcell N-ia Fused Sensor Data,"* Haddox, D., S Wang, J. Tulenko, and R. Dalton, Proceedings of the ANS Sixth Topical Meeting on Robotics and Remote Systems, Monterey, CA, Feb., 1995.
- *"A Fourier Transformation Approach to Image Registration and its Application in Hazardous Waste Cleanup,"* Wang, S., M. Rao, D. Ekdahl, R. Dalton, and J. Tulenko, " Proceedings of the ANS Sixth Topical Meeting on Robotics and Remote Systems, Monterey, CA, Feb., 1995.
- *"Development of a Radiation hardened Robotic System," Intelligent Automation-and Soft Cowutin-2: Trends in Research, Development, and Applications,"* Tulenko, J.S., S. Toshkov, D. Ekdahl, R.M. Fox, and F.R. Sias, Jr., Vol 1, M. Jashidid, et.al., Eds. Albuquerque, NM: ISI Press, pp 373-376.
- *"Real Time Control of the ANDROS Mobile Robot,"* D Haddox, S. Clifford, D Ekdahl, J.S. Tulenko, Trans. American Nuclear Society, 70, pp 111-112, June, 1994.
- *"Autonomous Robotic Navigation and Pipe Inspection: A Simulation Approach,"* Ioannou, D., S. Wang, J.S. Tulenko, Trans. Am. - Nuc. Soc., 70 pp I I I- 1 12, June 1994.
- *"A Fast Model Based 3D Object Recognition System,"* Wang, S., D. loamou, G.R. Dalton, J.s. Tulenko, Trans. Am. Nuc. Soc., 70 pp I 10- III, June, 1994.
- *"A Model Based Segmentation Algorithm,"* S. Wang, M. Rao, R. Dalton, and J. S. Tulenko, The 1994 Florida Conference on Recent Advances in Robotics, Gainesville, FL, April, 1994.
- *"Target Recognition Using Cestrum and Inverse Filtering,"* S. Wang, C. Crane, M. Rao, D. Ekdahl, and J. Tulenko, Proceedings of SPIE, Signal Processing. Remote Sensing and Reconstruction for Three-Dimensional Object and Scenes, Accepted for pub. July 1995.

1995-1996

- *"Virtual Radiation Fields for ALARA Determination,"* Knight, T., R. Dalton and J.S. Tulenko. Trans. AM. Nuc. Soc., 72:105-106, June 1995.
- *"Distance Education,"* Clifford, S., G.R. Dalton, D. Hintenlang, and J.S. Tulenko. Trans. AM. Nuc. Soc., 73:68-69, Oct. 1995.
- *"Virtual Radiation Fields--A Virtual Environment Tool for Radiological Analysis and Simulation,"* Knight, T.W., G.R. Dalton, and J.S. Tulenko. Accepted for publication in Nuclear Technology, February 1997.
- *"Waste Minimization: What a University is Doing to Reduce Waste,"* Coughlin, W., W. Properzio, C. Pitcher, and J.S. Tulenko. Trans. AM. Nuc. Soc., 73:99-100, Oct. 1995.
- *"Development of a Radiation Hardened ANDROS Robot for Environmental Restoration and Waste Management,"* Tulenko, J.S., G. Youk, D. Ekdahl, H. Liu, H. Zhou, K. Phillips, F. Sias, S. Jones, T. Cable, and H. Harvey. Proceedings of the Fifth International Conference on Radioactive Waste Management and Environmental Remediation (ICEM '95), Vol. 11, pages. 1972-1728, Berlin, Sept. 1995.
- *"Development of an Articulated Transporter/Manipulator System,"* Ridgeway, S., Adsit, P., and Crane, C., Special Issue on Highly Redundant Manipulators of Advanced Robotics, the Transactions of the Robotics Society of Japan, Vol. 9, No. 3, 1995, pp. 301-316.
- *"Implementation of a Six Degree of Freedom Manual Controller with Passive Force Feedback,"* Will, C. and Crane, C., SPEE Conference on Telemanipulator and Telepresence Technology, Philadelphia, 1995.
- *"Design, Fabrication, and Control of a Robotic Wall-Crawler for Remote Inspection Operations,"* Adsit, P., Crane, C., Gamble, D., Ridgeway, S., and Tosunoglu, S., IEEE 21st International Conference on Industrial Electronics, Control, and Instrumentation, Orlando, FL, November 6-10, 1995, pp II 0- 1 15.
- *"Target Recognition Using Cepstrum and Inverse Filtering,"* Wang, S., Crane, C., Rao, M., Ekdhal, D., and Tulenko, -J., Proceedings of the SPIE, Signal Processing, Sensor Fusion, and Target Recognition IV, Vol. 2484, April 1995.
- *"Virtual Reality Using Remote Sensing,"* Huang, Y., Wang, S., Haddox, D., Rao, M., Crane, C., Dewitt, B., and Tulenko, J., Proceedings.of SPIE, Signal Processing, Remote Sensing, and Reconstruction for. Three-Dimensional Objects and Scenes, July 95.
- *"Verification and Reconciliation of Virtual World Model for Radioactive Waste Cleanup,"* Wang, S., Haddox, D., Crane, C., and Tulenko, J., Proceedings of SPIE, Intelligent
- Robots and Computer Vision XIV: "*Algorithms, Techniques, Active Vision, and Materials Handling,"* Vol. 2588, October 1995.
- *"A Forward Analysis of a Two Degree of Freedom Parallel Planar Manipulator,"* Ridgeway, S. Crane, C., and Duffy J., 5th International Symposium on Advances in Robot Kinematics, Portoroz-Bemardin, Slovenia, June 1996.
- *"Autonomous Navigation of Heavy Construction Equipment,"* Crane, C., Armstrong, D., Rankin, A., Robotics in Civil Engineering Special Issue of the Microcomputers in Civil Engineering Journal, Vol. IO, No.5, 1995, pp 357-370.
- *"An Evaluation of INS and GPS for Autonomous Navigation,"* Crane, C., Rankin, A., Armstrong, D., Wit, J., and Novick, D., Proceedings of the 2nd IFAC Conference on Intelligent Autonomous Vehicles, Expo, Finland, 1995, pp. 208-213.
- *"Integrated INU/DGPS for Autonomous Vehicle Navigation,"* Rogers, R., Wit, J., Crane, C., Armstrong, D., 1996 IEEE Planning and Navigation Conference, Atlanta.
- *"A Multi-Purpose Off-line Path Planning Based on an A* Search Algorithm,"* Rankin, A., and Crane, C., Proceedings of the 1996 ASME Mechanisms Conference, Irvine, Ca.

- *"Simulating the Motion of a Nonholonomic Robot and its Trailer,"* Rankin, A., Crane, C., and Duffy, J., Proceedings of the 5th International Symposium on Advances in Robot Kinematics, Portoroz-Bernardin, Slovenia, June 1996.
- *"Development and Tuning of an Autonomous Control System for Application to Heavy Construction Equipment,"* Cunningham, S., Crane, C., Armstrong, D., Rankin*, A., Novick*, D., Wit*, J. Duffy, J., Proceedings of the 1996 International Symposium on Robotics and Manufacturing (ISRAM), Montpellier, France, May 1996.
- *"Evaluation of an Integrated Inertial Navigation System and Global Positioning System Under Less than Optimal Conditions,"* Wit, J., Armstrong, D., Crane, C., Proceedings of the 1996 Int'l. Symposium on Robotics and Manufacturing (ISRAM), Montpellier, France, May 1996.
- *"Autonomous Path Planning Navigation System Used for Site Characterization,"* Rankin, A., Crane, C., Armstrong, A., Nease, A., Brown H.E., Proceedings of the SPIE 10th Annual AeroSense Symposium, Orlando, Florida, April 1996.
- *"A System for Performing Site Characterization for Test Ranges Containing Unexploded Ordnance,"* Brown, E., and Crane C., Proceedings of the SPIE I Oth Annual AeroSense Symposium, Orlando, Florida, April 1996.
- *"Virtual Collaborative Robotics,"* Tulenko, J.S., C. Crane, R. Pinheiro, P. Adsit, C. Will, D. Haddox, and G.R. Dalton. presented at the Sixth International Symposium on Robotics and Manufacturing, Second World Automation Congress, Montpellier, France, May 1996
- *"A Program for the Economical Radiation Hardening of Robots,"* Tulenko, J.S., G.R. Dalton, G. Youk, H. Liu, H. Zhou, and R.M. Fox. Presented at the Sixth International Symposium on Robotics and Man., Second World Automation Congress, Montpellier, France, May 1996.

1996-1997

- *"Virtual Collaborative Robotics,"* Crane, C., Pinheiro, R., Adsit, P., Will, C., Haddox, D., Dalton, R., and Tulenko, J., Sixth International Symposium on Robotics and Manufacturing, Second World Automation Congress, Montpellier, France, May 1996, Vol. 3, pp. 209-214.
- *"A Program for the Economical Radiation Hardening of Robots,"* Tulenko, J., Dalton, R., Youk, G., Liu, H., Zhou, H., Fox, R., Sixth International Symposium on Robotics and Manufacturing, Second World Automation Congress, Montpellier, France, May 28, 1996, Vol. 6, pp. 831-836.
- *"Determination of Camera Locations in 6D Based on Image Size and Shape of a Standard Rectangle,"* Dalton, G.R., Proceedings ANS 7th Topical Meeting on Robotics and Remote Systems, Augusta, GA, April 27-May 1997, pp. II I- 1 16.
- *"A Program for the Economical Radiation Hardening of Robots,"* Tulenko, J., Dalton, R., Youk, G., Liu, H., Zhou, H., Fox, R., presented at the ANS Seventh Topical Meeting on Robotics and Remote Systems, Augusta, GA, May, 1997.
- "*Surface Segmentation of Laser Range Images for Automated Facility Mapping,"* Pinheiro, R., Crane, C., and Tulenko'J., SPIE's Photonics East'96, Boston NIA, Nov 96.
- *"Laser Range Image Interpretation for Automated Mapping of Hazardous Environments,"* Pinheiro, R., Crane, C., and Tulenko, J., ANS 7th Topical Meeting on Robotics and Remote Systems, Augusta, Ga., April 1997.
- *"Efficient Barrel Packing,"* McGee, R., Lee, J., Crane, C., and Adsit, P., , 1997 Florida Conference on Recent Advances in Robotics, Miami, I 0- I I Apr 1997.
- *"Development and Testing of a 6-6 Parallel Platform Actuator,"* Abbasi, W., Ridgeway, S., Adsit, P., Crane, C., and Duffy, J., " 1997 Florida Conference on Recent Advances in Robotics, Miami, I 0- I I Apr 1997.

- *"Determination of the Orientation of Two Bodies Connected by a Ball-and-Socket Joint from Three Measured Displacements,"* Zhang, Y., Crane, C., and Duffy, J.,. submitted to the Journal of Robotic Systems.
- *"Determination of the Unique Orientation of Two Bodies Connected by a Ball-and-Socket Joint from Four Measured Displacements,"* Zhang, Y., Crane, C., and Duffy, J., submitted to the Journal of Robotic Systems. 1997-98 Publications
- "*Kinematic Analysis of Robot Manipulators,"* Crane, C. and Duffy, J., Cambridge University Press, 1998.
- *"Determination of the Unique Orientation of Two Bodies Connected by a Ball-and-Socket Joint from Four Measured Displacement,"* Zhang, Y., Crane, C., and Duffy, J., Journal of Robotic Systems, Vol. 15, No. 5, 1998, pp. 299-308.
- *"Investigation of a Special 6-6 Parallel Platform for Contour Milling,"* Abbasi, W., Ridgeway, S., Adsit, P., Crane, C., and Duffy, J., in press, ASME Journal of Manufacturing Science and Engineering, 8 pages.
- *"Modeling the Steering Behavior of an Autonomous Land Vehicle,"* Rankin, A., Crane, C., and Duffy, J., Proceedings of the IASTED International Conference on Applied Modeling and Simulation, Banff, Canada, Jul 1997, pp. 404-407.
- *"Investigation of a Special 6-6 Parallel Platform for Contour Milling,"* Abbasi, W., Ridgeway, S., Adsit, P., Crane, C., and Duffy, J., Proceedings of the ASME Manufacturing Engineering Division 1997 International M.E. Congress and Exposition (IMECE), Dallas, Nov 1997, pp. 373-380.
- *"Development and Testing of a 6-6 Parallel Platform Actuator,"* Abbasi, W., Ridgeway, S., Adsit, P., Crane, C., and Duffy, J., Proceedings of the World Automation Congress, Anchorage, AK, May 1998, 8 pages.

1998-1999

- *"Investigation of a Special 6-6 Parallel Platform for Contour Milling,"* Abbasi, W., Ridgeway, S., Adsit, P, Crane, C., and Duffy, J., ASME Journal of Manufacturing Science and Engineering, Vol. 122, Feb 2000, pp. 132-139.
- *"The Optimum Quality Index for the Stability of In Parallel Planar Platform Devices,"* Lee, J., Duffy, J., Keller, J., Trans. ASME, Journal of Mechanical Design, Vol. 121, March 1999, pp. 15-20.
- *"Hybrid Active/Passive Force Feedback,"* Chesney, C, and Crane, C., Proceedings of the 8th International Topical Meeting on Robotics and Remote Systems, American Nuclear Society, Pittsburgh, Pa, April 1999.
- *"Fusion of Multi-View Laser Range Data With Object Recognition,"* M. Yang, G. R. Dalton, J. S. Tulenko, Nuclear & Radiological Engineering, University of Florida, ANS 8th International Topical Meeting on Robotics and Remote Systems Pittsburgh, PA, April 1999.
- *"Measurement and Mitigation of Radiation Effects on Robotic Electronic Systems at the University of Florida,"* J.S. Tulenko, D.D. Ekdhahl, D.W. Schoenfeld, S. Toshkov, J. Wolf, L. Houssay, at the 8th International Topical Meeting on Robotics and Remote Systems Pittsburgh, PA, April 1999.

1999-2000

- *"Development Of A Radiation-Hardened Absolute-Position Resolver For Advanced Robotic Arms,"* J.S. Tulenko and D.W. Schoenfeld , University of Florida, Nuclear and Radiological

Engineering Department and M. J. Kais, M. Marceau and F. Joffre, CEA LETI, Saclay, France, Accepted for publication for presentation at the Spectrum 2000 International Conference on Nuclear and Hazardous Waste Management, September 2000.

- *"Hybrid Active/Passive Force Feedback,"* Chesney, C, and Crane, C., Proceedings of the 8th International Topical Meeting on Robotics and Remote Systems, American Nuclear Society, Pittsburgh, Pa, April 1999.
- *"Investigation of a Special 6-6 Parallel Platform for Contour Milling,"* Abbasi, W., Ridgeway, S., Adsit, P, Crane, C., and Duffy, J., ASME Journal of Manufacturing Science and Engineering, Vol. 122, Feb 2000, pp. 132-139.
- *"Measurement and Mitigation of Radiation Effects on Robotic Electronic Systems at the University of Florida,"* J.S. Tulenko, D.D. Ekdhahl, D.W. Schoenfeld, S. Toshkov, J. Wolf, L. Houssay, at the 8th International Topical Meeting on Robotics and Remote Systems, American Nuclear Society, Pittsburgh, Pa, April 1999.
- *"The Optimum Quality Index for the Stability of In Parallel Planar Platform Devices,"* Lee, J., Duffy, J., Keler, J., Trans. ASME, Journal of Mechanical Design, Vol. 121, March 1999, pp. 15-20.

2000-2001

- *"Development of a Radiation-Hardened Absolute-Position Resolver For Advanced Robotic Arms,"* J.S. Tulenko and D.W. Schoenfeld , University of Florida, Nuclear and Radiological Engineering Department and M. J. Kais, M. Marceau and F. Joffre, CEA LETI, Saclay, France, Spectrum 2000 International Conference on Nuclear and Hazardous Waste Management, Chattanooga, TN., September, 2000.
- *"Development Of A Radiation-Hardened Resolver-to-Digital Converter For Advanced Robotic Arms,"* Kais, M.J., J. S. Tulenko and D.W. Schoenfeld , University of Florida, Nuclear and Radiological Engineering Department and M. J. Kais, M. Marceau and F. Joffre, CEA LETI, Saclay, France, 9th International Topical Meeting on Robotics and Remote Systems, Seattle, Washington, March 2001.
- *"Development of a Modular Wireless Data Acquisition System For Use in High Radiation Environments,"* James S. Tulenko, University of Florida, Radiological and Nuclear Engineering, ANS 9th International Topical Meeting on Robotics and Remote Systems, Seattle, WA., March 2000.
- *"Design of a Radiation-Hardened Power Amplifier for Induction Motors,"* M. Marceau, LETI CEA Advanced Technologies, J.S. Tulenko and D. W. Schoenfeld, University of Florida, Nuclear and Radiological Engineering Department, Spectrum 2000 International Conference on Nuclear and Hazardous Waste Management, Chattanooga, TN., September 2000.
- *"Development of a Modular Wireless Data Acquisition System for Use in High Radiation Environments,"* J.L.Kurtz, Electronic Communications Laboratory and J.S. Tulenko, Nuclear and Radiological Engineering Department, University of Florida, Radiation Effects on Robotic Systems, Spectrum 2000 International Conference on Nuclear and Hazardous Waste Management, September 2000.
- *"Fuzzy Control for Autonomous Ground Vehicles,"* Jeffrey S. Wit, University of Florida, ANS 9th International Topical Meeting on Robotics and Remote Systems, Seattle, WA., March 2000.
- *"Implementation of Standardized Vehicle Control Commands,"* Carl D. Crane III, Autonomous Systems Sessions of the ANS 9th International Topical Meeting on Robotics and Remote Systems, Seattle, WA., March 2000.

- *"Study of Radiation Induced Resistance Mechanisms in GaAs MESFET and TLM Structures,"* B. Luo, D. Schoenfeld, S. J. Pearton, and F. Ren, The Electrochemical Society, Washington, DC, March 2000.
- *"Use of Radiation Induced Resistance Mechanisms in Standard MESFET to Create a Simple Dosimeter,"* Tulenko, J.S., Schoenfeld, D., Pearton, S., Ren, F., International Conference on Nuclear and Hazardous Waste Management, Spectrum 2000, Chattanooga, TN., September 2000.

2001-2002

- "*Development of a Modular Wireless Data Acquisition System for use in High Radiation Environments*," University of Florida Nuclear & Radiological Engineering, J.S. Tulenko, D. Schoenfeld , UF Electronic Communications Laboratory, J.L .Kurtz, J.M. Cowdery, and Argonne National Laboratory - West, S. Henderson, American Nuclear Society Annual Meeting, Reno, NV, October 2001.
- *"Development of A Radiation-Hardened Resolver-To-Digital Converter For Advanced Robotic Arms,"* Kais, M.J., D. Schoenfeld, J.S. Tulenko, M. Marceau, F. Joffre, , 9th International Topical Meeting on Robotics and Remote Systems, Seattle, Washington, March 2001.
- *"Influence of ^{60}Co X-rays on DC Performance of AlGaN/GaN High Electron Mobility Transistors,"* D. Schoenfeld, University of Florida, et al, American Institute of Physics, Vol 80 No 4, 28 Jan. 2002, pp. 604-606
- *"Development of a Wireless Communication System for use in Radiation Environments,"* James S. Tulenko, D. Schoenfeld, et. al, University of Florida, Spectrum 2002 Conference, August 2002, Reno, NV.
- *"Characterization of High-Dose Gamma Radiation Degradation in Multi-Quantum Well InGaN and II-VI LED Technologies,"* D. Schoenfeld and J. S. Tulenko, University of Florida, and W. V. Schoenfeld, Uniroyal Optoelectronics, 2002 IEEE Nuclear and Space Radiation Effects Conference, Phoenix, Arizona, July 2002.
- "*Rad-Hardened Wireless Communications,*" Applied Physics Letters on results from the evaluation of new electronic materials needed to achieve higher radiation tolerance.
- *"Andros Automation Development of the Intelligent Vehicle Controller,"* Carl Crane, et al, Florida Conference for Recent Advances in Robotics (FCRAR), May, 2002.
- Tech Paper by Samim Anghaie and T. Knight, Association for Unmanned Vehicle Systems International (AUVSI), July 2002.
- *"The Reverse Displacement Analysis of a Tensegrity Based Parallel Mechanism,"* Tran, T., Crane, C., and Duffy, J., 2002 World Automation Congress, Orlando, June 2002.
- *"Development of Object Detection and Obstacle Avoidance Components for JAUGS,"* Crane, C., Armstrong, D., Novick, D., Wit, J., English, R., and Adsit, P., Association for Unmanned Vehicle Systems International (AUVSI) Conference, 2002.
- *"Development of a JAUGS Compliant Intelligent Primitive Driver Component,"* Crane, C., Armstrong, D., and Vinch, P., Association for Unmanned Vehicle Systems International (AUVSI) Conference, 2002.
- *"Development of a Planar Force-Feedback Input Device Using Hybrid Active/Passive Actuation,"* Chesney, C. and Crane, C., Proceedings of the 2002 Florida Conference on Recent Advances in Robotics, Miami, Fla., May 2002.
- *"Development of an Ultrasonic Positioning System for Multiple Vehicle Control,"* MacArthur, D. and Crane, C., Proceedings of the 2002 Florida Conference on Recent Advances in Robotics, Miami, Fla., May 2002.

- *"Implementation of a Sensor Fusion-Based Obstacle-Detection Component for an Autonomous Outdoor Vehicle,"* Novick, D., Crane, C., and Armstrong, D., Proceedings of the 2002 Florida Conference on Recent Advances in Robotics, Miami, Fla., May 2002.
- *"Intelligent Vehicle Controller Development,"* Vinch, P., Crane, C., and Armstrong, D., Proceedings of the 2002 Florida Conference on Recent Advances in Robotics, Miami, Fla., May 2002.

2002-2003

- *"Development of a Wireless Communication System for use in Radiation Environments,"* James S. Tulenko, D. Schoenfeld, et. al, University of Florida, Spectrum 2002 Conference, August 2002 Reno, NV.
- *"Characterization of High-Dose Gamma Radiation Degradation in Multi-Quantum Well InGaN and II-VI LED Technologies,"* D. Schoenfeld and J. S. Tulenko, University of Florida, and W. V. Schoenfeld, Uniroyal Optoelectronics, 2002 IEEE Nuclear and Space Radiation Effects Conference, Phoenix, Arizona, July 2002.
- "*Rad-Hardened Wireless Communications,*" Applied Physics Letters on results from the evaluation of new electronic materials needed to achieve higher radiation tolerance.
- *"Andros Automation Development of the Intelligent Vehicle Controller,"* Carl Crane, et al, Florida Conference for Recent Advances in Robotics (FCRAR), May 2002.
- Tech Paper by Samim Anghaie and T. Knight, Association for Unmanned Vehicle Systems International (AUVSI), July 2002.
- *"The Reverse Displacement Analysis of a Tensegrity Based Parallel Mechanism,"* Tran, T., Crane, C., and Duffy, J., 2002 World Automation Congress, Orlando, June 2002.
- *"Development of Object Detection and Obstacle Avoidance Components for JAUGS,"* Crane, C., Armstrong, D., Novick, D., Wit, J., English, R., and Adsit, P., Association for Unmanned Vehicle Systems International (AUVSI) Conference, 2002.
- *"Development of a JAUGS Compliant Intelligent Primitive Driver Component,"* Crane, C., Armstrong, D., and Vinch, P., Association for Unmanned Vehicle Systems International (AUVSI) Conference, 2002.

2003-2004

- "*Wireless Communications for Robotics in Radiation Environments,*" D. Schoenfeld, J. Tulenko, J. Kurtz and M. Keefe (UF), FCRAR 2003, The 16th Florida Conference on the Recent Advances in Robotics, Florida Atlantic University, Boca Raton, FL, May 2003.
- "*A Radiation-Hardened Encoder for Robotics in Radiation Environments*," FCRAR 2003, The 16th Florida Conference on the Recent Advances in Robotics, Florida Atlantic University, Boca Raton, FL, May 2003.
- "*Development of a Passive Parallel Platform for Force Control Applications,*" B. Zhang and C. Crane (UF), FCRAR 2003, The 16th Florida Conference on the Recent Advances in Robotics, Florida Atlantic University, Boca Raton, FL, May 2003.
- *"Analysis of a Hybrid Tensegrity-Based Parallel Platform,"* M. Marshall and C. Crane (UF), FCRAR 2003, The 16th Florida Conference on the Recent Advances in Robotics, Florida Atlantic University, Boca Raton, FL, May 2003.
- *"Optimized Kinematics of a 6-6 Parallel Mechanism Considering Position and Orientation Errors,"* S. Ridgeway and C. Crane (UF), FCRAR 2003, The 16th Florida Conference on the Recent Advances in Robotics, Florida Atlantic University, Boca Raton, FL, May 2003.

- *"A Robust Boundary Line Extraction Algorithm,"* D. MacArthur, E. Zawodny and C. Crane, FCRAR 2003, The 16th Florida Conference on the Recent Advances in Robotics, Florida Atlantic University, Boca Raton, FL, May 2003.
- *"High Dose Gamma-Ray Irradiation of SiC Schottky Rectifiers,"* The Electrochemical Society, Inc., Electrochemical and Solid-State Letters, Jihyun Kim, S. Nigam, F. Ren, D. Schoenfeld, G. Y. Chung, and S. J. Peartond, Nuclear and Radiological Engineering, University of Florida, Gainesville, FL, 0013-4651 (2003)
- *"Advances in Rad-Hardened Wireless Communications and Robotic Systems,"* J. S. Tulenko, D. W. Schoenfeld, J. L. Kurtz, American Nuclear Society's 10th International Topical Meeting on Robotics and Remote Systems University of Florida Conference Center, Gainesville, FL, March 2004
- *"Reconfigurable Inspection Robots with Climbing Capabilities,"* Jean-Philippe L. Clerc, Gloria J. Wiens, ,American Nuclear Society's 10th International Topical Meeting on Robotics and Remote Systems University of Florida Conference Center, Gainesville, FL, March 2004
- *"Processing of Clinical Images for Guidance of Robotics Assisted Procedures,"* David Hintenlang, American Nuclear Society's 10th International Topical Meeting on Robotics and Remote Systems University of Florida Conference Center, Gainesville, FL, March 2004
- *"Path Planning Algorithm for Non-holonomic Vehicles and Its Application to Radiation Environments,"* Arfath Pasha, Carl D. Crane III, James S. Tulenko, American Nuclear Society's 10th International Topical Meeting on Robotics and Remote Systems University of Florida Conference Center, Gainesville, FL, March 2004
- *"Design Methodology for Parallel Kinematric Mechanisms Considering Metrology Performance,"* Shannon C. Ridgeway, Carl D. Crane III, American Nuclear Society's 10th International Topical Meeting on Robotics and Remote Systems University of Florida Conference Center, Gainesville, FL, March 2004
- *"Special Singularity Analysis for a 6-DOF Parallel Platform,"* Bo Zhang, Carl D. Crane III, Shannon Ridgeway, American Nuclear Society's 10th International Topical Meeting on Robotics and Remote Systems University of Florida Conference Center, Gainesville, FL, March 2004
- *"Static Analysis of Tensegrity Structures,"* Crane, C., Correa, J., and Duffy, J., ASME Journal of Mechanical Design, in press, 2004.
- *"Closed-Form Equilibrium Analysis of a Planar Tensegrity Structure,"* Bayat, J., and Crane, C., On Advances in Robotic Kinematics, Kluwar Academic Press, pp. 313-320, 2004.

Research Laboratories Utilized

Center for Intelligent Machines and Robotics (CIMAR) is an interdisciplinary research group centered in the Department of Mechanical & Aerospace Engineering at the University of Florida. CIMAR's specific research strengths are in the areas hardware/software system development. Several robotic systems and subsystems have been designed, fabricated and tested. These include an autonomous Navigation Test Vehicle (NTV), an Autonomous Survey Vehicle (ASV), and a nuclear reactor vessel inspection robot. CIMAR continues to be a leader in research and development in the areas of mechanisms, autonomous vehicles, and intelligent machines. Significant accomplishments by both the faculty and graduate students have led the way and created new and fruitful areas of research. CIMAR's specific research strengths are in the areas of:

- Hardware/software system development (Several robotic systems have been designed, fabricated, and tested, including an autonomous Navigation Test Vehicle (NTV), an Autonomous Survey Vehicle (ASV), and a nuclear reactor vessel inspection robot).
- Three dimensional geometry and the kinematic analysis of robotic systems.
- Screw theory as applied to position and force control of robot manipulators.
- Real-time computer graphics simulation.
- Integration of computer systems as applied to telepresence system development

The Nuclear & Radiological Engineering Department's Robotics Research Laboratory contains four operating robots, which are used as platforms for research applications, including visual radiation depiction systems and radiation-hardened wireless electronic operating systems. Wireless electronic devices are designed to conduct robotic communications through a hot cell wall from safe distances, without difficulties of a tether or hard-wired control system. Equipment also includes access to university analytical resources for full material & electrical characterizations.

The Robotics Research Laboratory equipment includes:

- Testing equipment (scopes, meters)
- Data acquisition equipment and systems
- Agilent and Tektronix Software operating systems: (Unix, Solaris, Windows 2000 XP &.NT) K2A robots, modernized GE P60 industrial arm robot (new Galil controller and software)
- Glove box system with German Sick laser and video cameras
- Two radiation test chambers (cobalt and cesium)
- PC board LPKF Milling system and Electronics Workbench software
- Access to university analytical resources for full material & electrical characterizations

Electrical & Computer Engineering Department's Electronic Communications Laboratory (ECL) conducts research for the national defense and has received funding continuously since its beginning decades ago. ECL's contract funding from the Army is believed to be the oldest continuing university-funded contract in the Department of Defense. ECL has a tradition of producing relevant research results and its work on the radar proximity fuse is considered one of the three most important scientific developments of World War II.

ECL has eight SUN workstations and many PC's integrated on a high speed network with large storage arrays to support the development of signal processing for radar and communication systems. High speed internet access, electronic systems development software, a wide selection of signal processing software, and a word processing and document production staff support researchers. ECL's primary task for URPR was to develop Rad-hard-electronic robotic communications devices.

Summary of Technology Developed and/or Deployed*

* Code Index V=Developed by UF P=Deployed by DOE or other agency

Autonomous Navigation of an Robot Implementing Modular Architecture = V

Florida researchers developed a modular, autonomous navigation and control system for use on indoor robots. The system was implemented on a Cybermotion K2A standard research vehicle. The system was designed for future use in remediation and decommissioning of Department of Energy (DOE) sites in the DOE Environmental Restoration Program.

The initial system contains four subsystems: A Vehicle Control Unit (VCU), a Mobility Control Unit (MCU), an Operator Control Unit (OCU), and a Positioning System (POS). All subsystems possess hardware modularity through the use of standard power requirements and RS232 serial interfaces. The subsystems achieve their software modularity through the use of structured ASCII messages which are designed to be generic in order to work across different platforms.

The two subsystems of focus during this research were the Vehicle Control Unit and the Positioning System. The primary function of the VCU was to receive control messages from the MCU and drive the vehicle accordingly. The Vehicle Control Unit was developed using a Z-World Systems Little Giant microcontroller. The primary function of the POS was to output the position of the vehicle at a rate of 10Hz. The dead-reckoning Positioning System was developed on a Real Time Devices PC104 system using a KVH Industries Digital Gyro Compass.

The entire system was tested by traversing two different paths which were approximately 12m in length. All systems worked properly and displayed the intended modularity.

CAA - Containment Analysis Automation = V/P

UF played a key role in the total-URPR effort to develop a Processing Unit that could accomplish multiple tasks of developing and commercializing technologies that would allow automating certain DOE and private contract environmental laboratories. This effort was in direct response to the growing need for chemical characterization of soil samples, contents of storage tanks, water samples, and other sample matrices that must take place before environmental remediation could be initiated.

The CAA multiple concept includes: Automated Data Interpretation, Automated System Software for On-Site Standard Analysis Method (SAM), Standard Laboratory Module and Standard Analysis Paradigm, and Chemical Validation of Standard Laboratory Modules.

The CAA systematic analysis program was committed to commercialize standardized technology to ensure broad market availability, low cost and reliability. A technology transfer plan was structured and developed to take the concept to commercial roll out. At the conclusion of the project, a suite of multiple modules were successfully designed, developed and validated and samples were built.

Modeling and Simulation Dense Container Packing = V

The objective of this research was to develop a geometric bin-packing algorithm, which had the capability to control filling a waste container as completely as possible with arbitrary shaped objects. The bin-packing algorithm had to be capable of finding near optimal packing configurations for a set of irregular shaped objects. Some of constraints realized were the effect of gravity on the objects, minimization of center of gravity of the container, and allowable radiation dose and heat levels for the container. Packing configurations that contain interlocking shapes were

also considered an important physical constraint, since configurations are difficult to achieve when the packing is performed with the help of a robotic arm.

The proposed approach used a genetic algorithm to optimize the packing order sequence, and an online packing heuristic that was capable of finding near optimal placements for each object in the sequence. The problem is known to be strongly NP-hard and has many engineering applications in areas such as container loading, stock cutting, layout optimization and rapid prototyping. The 2-dimension algorithm was developed and demonstrated successfully. This technology was presented by UF researchers at a DOE update meeting in Albuquerque in the fall of 2002.

Operations in a Glovebox Environment = V

This research project developed technologies that could assist an operator in performing operations in a glove box. In particular, the project achieved the first stage of developing real-time modeling and graphical displays of the environment inside the glove box.

At the completion of the project, an accurate, high-resolution display of glove box contents was available. However, as research was stopped on this project, full information to an operator engaged in remote manipulation tasks, as well as providing all necessary input for autonomous robotic glove box operations was not achieved.

Initially, a glove box survey was made to identify suitable commercial glove boxes. Sizes and configuratioons were determined from the American Glovebox Society, which provided specifications. Once the specifications were established, sensor selection was made and a placement/movement strategy for the sensor systems was chosen. The primary sensor system chosen was a LMS (Laser Measurement System) 200 from Sick Optic-Electronic. It is a laser range-finder which used a time-of-flight approach to obtain the distance from the sensor to objects. The LMS 200 is fast and has a reasonable level of base resolution. Performance tests proved it gave the proper speed and acceptable accuracies.

The placement/movement strategy selected was to mount the LMS facing downward on a linear track which collected data by sweeping across the width of the glove box. This linear track combined with a pan/tilt mounting will allow for the LMS 200 to gain access to otherwise occluded objects in the glove box.

Upon analysis of the data acquired using the LMS 200 to see if the results fully meet the project objectives, a decision was reached that a supplementary sensor systems with higher levels of measuring accuracy was necessary. Possible choices were considered to complement the LMS 200.

JAUS Interface for Andros Robot = V

In this research effort, an Intelligent Primitive Driver (IPD) was designed to supplement control of a Primitive Driver component defined in the standard published by the Department of Defense Joint Architecture for Unmanned Systems (JAUS). Whereas the Primitive Driver component accepts and blindly executes wrench commands, the IPD uses various subsystems to provide it with the necessary information to make low-level decisions concerning vehicle control. The IPD is accessible by either an onboard autonomous control system; or by a tele-operational control system. For the case of an autonomous control system, the IPD reduces high-level control responsibilities; and therefore reduces processor demands. In the case of teleop control, the IPD serves to ease operator burden by automating intensive operator-controlled processes. A Remotec Andros robot, outfitted with a JAUS-compliant controller, was used to test the viability of the IPD. The challenge was to program the IPD to automate maneuvering up or down a flight of stairs.

The proprietary Andros control stream was reverse-engineered and applied to the Primitive Driver and Intelligent Primitive Driver. The Andros JAUS controller was modified to accept and interpret JAUS commands and make the Andros act upon these commands accordingly. The controller was mounted on the Andros platform, and performed as designed and returned favorable data when the limitations inherent to the Andros platform were taken into account.

However, it was concluded that with the antiquated Andros controller, while the robot could negotiate a set of stairs when controlled by a human operator, with the JAUS controller, a number of factors made the task very difficult and complicated. A host of recommendations were made to increase the controllability of the Andros-IPD system. Specific upgrades were recommended to several of the subsystems, the most important being the embedded controller must be updated to a more modern control scheme. Despite the difficulties encountered, the concept of using an IPD control system to direct a robot in negotiating a set of stairs remains valid.

Joystick Feedback Device = V/P

This research developed improved force-feedback technology with regard to safety and realism. This was accomplished by designing a user-input device that reflected modeled static friction as well as other models of friction. The system evaluated by simulating passive environments incorporating materials with dynamic physical properties. This development task could assist any D.O.E. task that involves teleoperated material handling or object manipulation.

Realistic force-feedback simulation included friction in both the hardware and in the modeled control system. Without damping, it is impossible to reflect a passive environment, and the potential for instability is high. A force-feedback joystick, powered solely with brakes, was previously designed and constructed by UF researchers. The hybrid approach utilizing both brakes and motors accommodated the drawback of the separately applied technologies. Use of passive braking components allowed for the safety benefits as well as increase overall realism for the operator. This improved the safety and increased the maximum amount of force that could be reflected, but sever limitations resulted. Some of these limitations were the inability to reflect generated moments, active environments, or elastic forces. Lost motion and difficulty in calibrating and homing the device were other disadvantages resulting from not using motors. The device was developed, and tested using live volunteers under a monitored test setup to evaluate numerous parameters.

Parallel Compliant Coupler for Force Control: Three Versions = V

The overall objective of this task is to design, fabricate, and apply parallel architecture based mechanisms in the area of force control. Passive mechanisms have been investigated with emphasis placed on improving serial mechanism performance in grasping and assembly tasks. The passive mechanism is named the Parallel Compliant Coupler for Force Control (PCCFC). Specifically, the design and fabrication of compliant end couplers for a serial manipulator has been undertaken. The coupling is based on a parallel architecture for which a reverse analysis has previously been developed. Implementation requires the measurement of displacement in the mechanism connectors and use of this information in calculating applied loads. These loads are used in a force control scheme to improve contact, surface following, and assembly tasks. In parallel with the passive mechanism development, an investigation of methods to control the compliant characteristics of a passive leg connector has been undertaken. The ability to specify and control the compliance of a passive device will increase its adaptability to a particular in-contact force control operation.

V-1: A first prototype was developed utilizing LVDT's for connector length measurement, captive ball type connector joints, and two concepts for the elastic or spring element of the connector. The LVDT's were integrated into the connector structure. The captive ball joints were developed and fabricated in-house. The elastic elements investigated included typical helical springs and elastic cables. The elastic cables were incorporated into the design in a manner that rendered a non-linear spring constant, that "hardened" with as deflections increased. Evaluation of this prototype revealed deficiencies in the joint design and difficulties with repeatability with the elastic cables. The joints exhibited high friction when clearances were reduced for accuracy precision.

V-2: In FY2001 a second prototype of the PCCFC was designed and the fabrication of components was begun. This prototype was sized at ablaut 80% of the size of the first prototype. The joint design was improved from the first prototype by the introduction of a low friction seat material for the ball joints. The connector design was radically changed. A cantilever type beam spring was utilized as the elastic element. Length measurements were made with a rotary potentiometer coupled with a four bar mechanism integrated into the connector that converted linear deflection of the connector into a rotary displacement of the potentiometer. The prototype was completed and evaluated. Calibration of the individual connectors showed good repeatability, and the suitability of the mapping between connector displacement and potentiometer rotation. The device did not perform satisfactorily when assembled. It exhibited a significant zone around the home position in which the pose of the device could not be accurately determined. It would not return consistently to the home position after displacement. Investigation revealed that friction in the ball joints, coupled with the design of the leaf springs, introduced off-axis deflections of the connectors that were un-observable with the potentiometer length measurement scheme.

Also in FY2001 a study of a new platform leg design was initiated whereby the connector would be able to change its compliance characteristics under computer control.

V-3: A third prototype development was initiated to address the deficiencies found in the previous prototypes. The evolution of the design of the PCCFC has allowed the incorporation technological developments that have occurred over the development cycle. Significant advances have been made in position measurement via micro or miniature devices. The third prototype utilizes optical encoders integrated in the connectors for displacement measurement. These encoders were not available when the second prototype design phase was being undertaken. The joint designs for both the previous prototypes lead to failure of the designs. The third design incorporates miniature COT universal or Hooke type joints, along with a rolling element joint, to make up the 5 degrees of freedom the connector needs. The conventional helical springs evaluated in the first prototype proved the most viable, so they have been incorporated in the third design. A linear recirculating ball bearing spline in incorporated into the connector design to minimize off-axis deflections. The prototype was fabricated and assembled.

Rad Hard Andros Robot = V/P

The need to handle radioactive "hot" cleanup jobs, such as nuclear processing facilities, was instrumental in bringing together a robot manufacturer and the radiation hardening researchers at the University of Florida. Their goal was to develop a radiation hardened version of REMOTEC's workhorse ANDROS mobile robot. The work led to the award of a Phase I and Phase 11 Small Business Innovative Research (SBIR) contract with the University of Florida as its Rad Hardening subcontractor. The purpose of the SBIR was to evaluate, redesign, test, and build a hardened version of the ANDROS series of teleoperated mobile vehicles equipped with manipulator and

sensor capabilities. The detailed research and development program developed an ANDROS robot capable of operating in radiation environments with accumulated gamma ray doses exceeding 1 MRad (Si) (10 kgray (Si)).

A radiation hardened and tolerant version of the ANDROS V-A and VI-A system was developed by a team composed of engineers and scientists from the University of Florida and the vendor REMOTEC, Inc. More than 1,200 parts were reviewed and tested. The project completed its Phase I and Phase 11 SBIR redesign with the upgrade of most control components. UF's facilities include a linear accelerator and multiple cobalt irradiators and provided the capability to perform the extensive testing. The commercial production of this radiation hardened ANDROS a mobile platform made available that can serve as a main work and inspection system for hazardous tasks facing the world nuclear industry.

Rad Hard Wireless Communications System = V/P

This program contains two parts, both of which involved extensive research, development and testing at UF.

Part I – The primary objective of the task was to improve a current RF wireless communication system design in terms of functionality, reliability, and radiation tolerance for applications requiring operation to a total dose of approximately 1 Mrad (Si). Relevant DOE applications include use in robotic activities, in material handling systems and any other activities in high radiation areas. The ability to replace umbilical cables with wireless communications offers excellent operational flexibility. Goals for this work include improved reliability, increased data channel capabilities and ease of setup and operation. The radiation tolerance of specific electronic components will be investigated as part of this effort. The long-range goal which was successfully achieved was to extent the radiation hardening to the 100 MRad range and to extend the bandwidth capabilities of the wireless communication equipment.

The research team developed a prototype wireless modem which was developed and successfully tested to communicate commands through a hot cell wall at Argonne National Labaoratory – West. During development, the radiation tolerance of all components was determined, and those failing to meet target rad hardness received additional design changes. Following, a second redesigned circuit of the Wireless Transceiver was successfully developed and tested at the ANL-W labs. Radiation testing on SiGe, AlGaN and GaAs MESFET devices were incorporated and the results published nationally and internationally.

Part II – Rad Hard Resolver Servo

The objective of this task was to implement the radiation hardened Admotec Resolver developed and tested the previous year. This was accomplished by joint efforts with the Mechanical Engineering group to install resolvers into an improved robotic arm that was developed for the K2A robot. Remote operations with the U New Mexico were discussed. Long range plans seek to use the Rad Hard Wireless RF Modem developed at UF for fully autonomous operations.

This task was relevant to any D.O.E. equipment that involves robotic material handling or object manipulation in hazardous radiation environments. Systems with real-time absolute position feedback will provide a new level of path planning and control not currently available. Such advanced systems will have new capabilities to determine inertia and momentum characteristics essential to safe handling of large or fragile objects.

RadPaint Radiation Imaging = V

Officially known as "Radiation Modeling & Simulation for Task Planning," this technology was developed by UF in conjunction with the range imaging camera available at the University of Tennessee. The UF research team took those images and developed a program to change them from range images, already produced for checking purposes, to radiation paint images (RadPaint). These images were first depicted in gray scale and then later researchers developed color-coded images, with an associated guide to indicate gamma ray flux or dose rate.

Examples of the transition are shown in Figures 1 and 2 below.

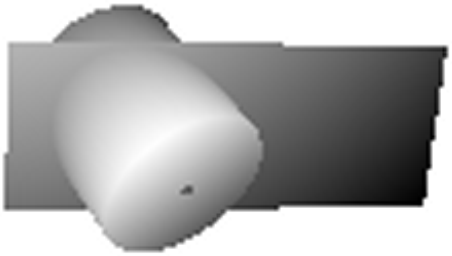

Figure 1: Gray Scale Range Image

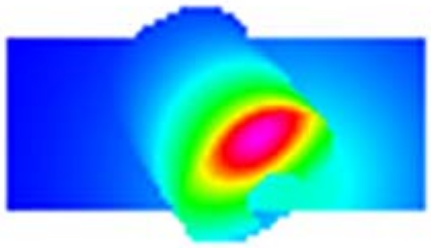

Figure 2: Color Coded Flux Map

The color figure graphically indicates the power of surface colors to indicate the presence, location and strength of a source of radioactive material inside a container. The plane is added to illustrate the ability to select line-of-sight intersections correctly when multiple objects are present. The shadow-like anomaly at the bottom front of the colored drum indicates that there are still some problems with the color presentation of flux values that need to be corrected.

The entire program was developed so that it could be accessed via computer over the internet, with any special programs or interfaces. Having achieved its goals, this program was concluded successfully in 2003.

Open Architecture Controller for the Spar Long-Reach Manipulator = V/P

University of Florida researchers designed and implemented an open architecture controller for the Ontario Hyro Long Reach Manipulator. This manipulator was built by Spar Aerospace for initial use in re-fueling nuclear reactors. The manipulator has five axes configured in the vertical articulation scheme. The five joints are servo-hydraulically controller, with redundant hydraulic power supplies. Alathough never deployed for its intended use, the manipulator was leased from Ontario Hydro by DOE researchers at PNL for use in research concerning tank waste remediation. The manipulator was supplied by Spar Aerospace with a custom closed architecture controller based on early 1980's technology. The controller would not allow joint level control at anything faster than a few Hz. Due to the nature of the intended task, Spar designed several levels of redundancies and fail-safes from both the software and hardware sides. These features limited the usefulness of the manipulator in the research setting.

University of Florida researchers were tasked with designing, developing, and deploying an open architecture controller that would allow joint level control in a real time sense (1-to-2 kHz). The controller designed was based on multiple cpu's located on a VME backplane with the requisite i/o hardware. The operating system utilized was Wind River's VX Works. Programming was completed in the C language. The Spar controller was integrated at the hardware level, and deployment of the UF controller required the same level of integration with the hardware fail-safes and redundancies. The Spar controller was left in place, and could be re-instituted by disconnecting

the UF controller and reconnecting the Spar controller. The UF-developed controller was deployed on site at PNL and joint level control between 1-to-2 kHz was successfully accomplished.

Three-Dimensional Visualization Display Device = V

The computer graphics community has done much work in the area of three-dimensional displays. Existing off-the-shelf technologies utilize techniques such as having the user wear shutter glasses while looking at a two-dimensional computer monitor. The images drawn on the monitor are swapped to show the left eye view and then the right eye view in coordination with the shutter glasses. Head-mounted displays provide separate simultaneous images to the left and right eye. These displays are often combined with head tracking sensors so that the image being presented coincides with the direction that the user is looking towards.

While these techniques have been successful in presenting three-dimensional representations, they are difficult to implement for multiple users who wish to observe a scene at the same time. Also the glasses and head-mounted displays can be burdensome for the operator.

UF researchers attempted to develop a three-dimensional display device that will have the following characteristics:

(1) presents a three-dimensional representation of the object being displayed;
(2) does not require the user to wear any special glasses or head mounted tracking system;
(3) allows multiple users to simultaneously view the same object. Such a device will greatly aid an operator (or a team of operators) in tele-operation and tele-supervision operations.

In the final year, the Three Dimentional Visualization Display Device was completely assembled, tested, and analyzed. The design of the physical display was completed. New features were added to the graphical user interface that made it more efficient and helpful for assembly and testing. The machine was run and the effectiveness of the design could be analyzed. The majority of the work done in the past year involved the physical display. The design was improved several times before and during assembly. Having many components, it was not possible to completely design one without seeing how well another would work. The results were judged successful.

Tensegrity Concept = V

The word *tensegrity* is a combination of the words *tension* and *integrity*. Tensegrity structures are spatial structures formed by a combination of rigid elements in compression (struts) and connecting elements that are in tension (ties). No pair of struts touch and the end of each strut is connected to three non-coplanar ties. The entire configuration stands by itself and maintains its form solely because of the internal arrangement of the struts and ties. A tensegrity structure with three struts is shown in Figure 1.

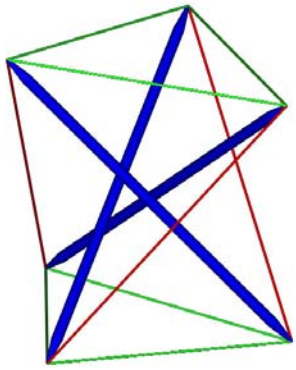

Figure 1: Three-strut tensegrity system.

Research at the University of Florida is focused on the analysis of tensegrity systems with compliant ties. Such devices are referred to as self-deploying tensegrity systems as they deploy automatically to minimal energy configurations. Analyses have been conducted to determine equilibrium positions of such devices for cases with and without external loading. Current research includes the design and analysis of a parallel platform device that incorporates tensegrity. The objective is to develop a parallel platform device whose vibrational characteristics can be controlled and whose top platform can be moved relative to its base in an energy efficient manner. The analysis techniques are currently being applied to problems at the micro scale to impact the process of micro-assembly.

Terms & Acronyms

AND	Computer 2-state Boolean Logic
CMOS	Complementary Metal Oxide Semi-Conductor
COTS	Commercial off-the-shelf
CMOS Resolver	Complementary Metal Oxide Semiconductor EVBU
GaAs	Gallium Arsenide
GaN	Gallium Nitride
GPIP Bus	General Purpose Interface Bus
JFET	Junction Field Effect Transistor
JPG	JPEG, for Joint Photo Experts Group, a photo file format
LMS	Laser Measuring System
LSI	Large Scale Integration
MOS	Metal oxide semiconductor dosimeters (also radfets)
MOSFETs	Metal-Oxide Semiconductor Field-Effect-Transistors
MOT	metal-oxide technology
NAND	Negative 2-state computer Boolean logic
NOR	Negative “also” 2-state computer Boolean logic
OR	“Also” 2-state computer Boolean logic
PCCFC	Parallel Compliant Coupler for Force Control
Quadrature	Compare two wave forms of differing phases
Quantized	Subdivided into small, measurable increments
RADFET	Solid State Radiation Dosimeter Field-Effect-Transistors
RDC	Resolver to Digital Converter
RGB	Red, Green, Blue
SOI	Silicon on insulator
TTL	Transistor logic gate
TLM	Transmission Line Method to determine resistivity
UTMC	Rad hard device manufacturer
Vrms meter	Voltage reading meter
WCPMMI	Weight Compensating Parallel Manipulator/Manual Input
XOR gate	Exclusive “no ambiguous” 2-state computer logic

I.1.1 Rad-Hard Wireless Communications System

I.1.1 Introduction

The present RF wireless system design, developed jointly by the Nuclear and Radiological Engineering (NRE) and Electronic Communications Laboratory (UF/ECL), successfully developed reliable wireless communications for data acquisition in hazardous radiation environments. This radiation-tolerant wireless design consists of a master unit and a slave unit, both of which are implemented solely in hardware. Each board of the design has been tested in the NRE Cobalt Irradiator Facility to at least 1 Mrad (Si) total dose. Each RF wireless modem unit contains five circuit boards, one of which is the RF transceiver board. There is no software or firmware inherent in the system due to the absence of a microprocessor/microcontroller. The data transfer baud rate is currently 9600, and significantly higher baud rates could be obtained with the future system architecture redesign outlined in this report. Incorporating replacement of the dedicated logic circuitry with a microcontroller to handle the transceiver data encoding and decoding circuitry offers greater flexibility and decreased risk of obsolescence.

I.1.2 Future System Architecture Design and Implementation

The original master design consisted of four boards on the master side: RS-232 board, controller board, transmit board and receive board. The controller board was then interfaced to the RF2905 wireless transceiver for over the air transmission. This design was bulky, consumed almost 1 A of current and the circuitry was complicated. A block diagram of the original master design is shown in Figure I.1.1.

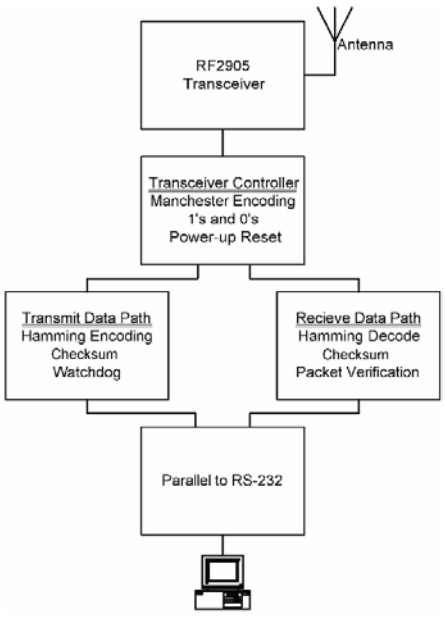

Figure I.1.1: Original Master System Block Diagram

The original design and application utilized a host unit not subject to irradiation because it was outside the hot cell. This master unit was not subject to the limitations of using radiation hardened or radiation tolerant components. This allows for the option of replacing the dedicated logic circuitry with a microcontroller to handle the transceiver data encoding and decoding

circuitry. This report will discuss the original design and justification for redesigning the master, the choices that were available for the redesign, the plans and results of the master redesign and possible future work that can be done.

Although the current implementation was the result of an effort to use off-the-shelf components (COTS) that are inherently radiation tolerant, the absence of any microprocessor or microcontroller leads to inflexibility in system components such as data rate, data structure, error correction, I/O interfaces, and user interface. Further, a microprocessor or microcontroller based design would be very hardware efficient resulting in, at most, two circuit boards—an RF transceiver board, and an interface/controller board. It is conceivable that these functions could later be combined onto one board, if desirable. Progress in the areas of the microprocessor design and RF transceiver were accomplished through a redesign described in section I.1.3

I.1.3 Redesign details

The master redesign was broken down into 3 steps: choosing a suitable technology to implement the redesign, writing the software, and designing the hardware. An overall diagram is shown in Figure 2. The four components of the old design are all contained in the microcontroller code. This saves space, cost and power and allows for faster speeds.

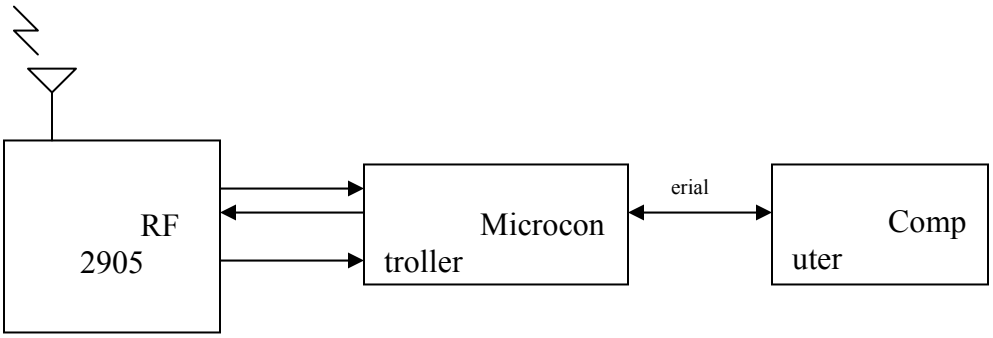

Figure I.1.2. Redesigned Master Block Diagram

I.1.3.1 Researched Options

Three options were considered for the master redesign. These technologies are the three major ones in the digital market today. Only two were recommended for possible consideration to meet budget and time constraints.

I.1.3.2 Application Specific Integrated Circuit (ASIC)

This option would be the most flexible and power efficient and would facilitate a working prototype within a relatively short period of time. Unfortunately, to achieve these benefits, a high cost must be incurred, which would not be justifiable unless units were produced on the order of tens of thousands. Since a single prototype was the goal, this option was excluded.

I.1.3.3 Field Programmable Gate Arrays (FPGA)

This option allows a digital logic design to be input in a schematic editor, a solution generated and input to the FPGA. The logic design on the original master design could be input gate for gate, compiled and programmed into the FPGA and give the same functionality as the four boards of the original master design, without having to change any of the design. This option is less

expensive than the ASIC but consumes a relatively large amount of power. In addition, this design would need external components such as a USART and a analog to digital converter (ADC).

I.1.3.4 Microcontroller

The microcontroller is a relatively cheap design, but is the best compromise on speed, price, and power consumption. Tools such as development boards, programmers, compilers and assemblers are cheap and readily available. This option was selected for its versatility. The major disadvantage and consequently, the major challenge is that the logic circuitry must be converted into a high-level code. Of the available microcontrollers, the Motorola 68HC08GP32 and the Atmel ATMega 128 were considered. The Atmel was chosen because of its low cost development tools.

I.1.3.5 Microcontroller Software Design

The general design is interrupt driven, mainly because of the precise timing needed to decode the data. The code was written in C, a high level programming language allowing for complicated data structures and control algorithms that would take many lines of assembly code. By writing in a high-level language and leaving the computer the task of writing the assembly code reduces the chances of syntactic and logical errors at the lowest levels of code and allows quicker debugging times. The code was developed using HP InfoTech's CodeVision AVR C Compiler, which is an integrated compiler, assembler and programmer.

I.1.3.6 Decoding Algortihm

The decoding algorithm was derived by observing the state of the raw data coming in on the DataOut line from the RF2905. The line would be random ones and zeros until there was actual data, and then there would be synchronization information and finally the data to be decoded. This algorithm is explained below.

I.1.3.7 Monitor Received Signal Strength Indicator

Using one channel of the analog to digital converter (ADC), the Received Signal Strength Indicator (RSSI) output from the RF2905 is monitored. This signal is an analog voltage indicating the relative strength of the signal, where an idle line is about 1.37 V. This signal is sampled 19200 times per second. This coincidentally is twice the data rate, but was empirically determined to be a good rate to reliably sample the RSSI.

If the sampled voltage is above 1.37 V (40_{16} digital), it is said to be above the RSSI threshold. If 192 consecutive samples are above this threshold, it is certain that the incoming signal is not noise but a signal to be decoded. If 192 consecutive samples are not above the threshold, the signal is considered noise and the routine looks for a new consecutive string of 192 samples.

I.1.3.8 Frame Synchronization

When a valid signal is detected, control is transferred to the input capture feature of the microcontroller. Using the input capture system, which can detect the change of levels on a predetermined pin, the data line (DataOut) from the RF2905 is monitored. When a rising edge is detected, the system counter is recorded and stored. When the next rising edge occurs, the system counter is again recorded. The expected data rate is 19200 bits/second, so each bit should be:

$$T_b = \frac{1}{R} = \frac{1}{19200 \frac{bits}{s}} = 52.083 \mu s \qquad (1)$$

The data coming in from the RF2905 (transmitted by the slave) had variable bit widths which forced an increase in the allowable tolerance of bit widths. If the difference in the counters fell within 51.8 μs and 52.1 μs then the incoming data was synchronized on valid edges. This strategy was employed so that if noise were to occur between two edges it would not be mistaken for an actual edge and synchronized to one of the invalid edges. This worked effectively approximately 95% of the time.

I.1.3.9 Frame Field Synchronization

Before the actual packet is transmitted, there is a preamble of ones and then zeros, which come on the line with Manchester encoding. By the time valid data is detected through the previously described steps of the algorithm, the receiver is getting zeros. The microcontroller then Manchester decodes each bit, until a one is decoded. This indicates that the preamble is over and the following data is the packet to be decoded. The following figure describes the packet:

Ones	Zeros	Start Bit	Address	Length	Data	Checksum
3.5ms ≅ 32 bits	3.5ms ≅ 32 bits	1 bit	7 bits	8 bits	1-62x8bits	8 bits

Figure I.1.3: Packet Structure

I.1.3.10 Packet Decoding

The incoming data is written to an array in memory. Each byte of memory (eight data bits) would then be Manchester decoded using a case statement and stored in a new array. This data would then be Hamming decoded using another case statement. The data would be checked for errors using the "exclusive or" equations that define Hamming code error syndromes. If a non-correctable error is detected, the packet is discarded. If a correctable error is present, it is corrected.

I.1.3.11 Transmission to Computer

If the data is correct, it is then sent to the computer using the USART and a prewritten service routine for CodeVision AVR called putchar(), which automatically frames the data for RS-232 serial transmission.

I.1.4 RF Transceiver Design

The current RF transceiver design is based upon a silicon bipolar integrated circuit built by RF Microdevices, the RF2905. The RF2905 operates at 900 MHz and utilizes frequency-shift-keyed (FSK) modulation to convert digital information to an RF modulated waveform containing that information. Testing of the RF transceiver showed that radiation tolerance of 750 kRad to 1 Mrad could be obtained, with an achievable upper limit on the data transfer rate of less than 500 kbit/sec. The actual system data rate was 9600 Baud. While this data rate is more than adequate for many low speed processes (low frequency voltage readings or control of relatively slow processes) it would not be adequate to transfer video signals or images in a sustained fashion. Also, robotic control and other control processes would benefit from higher data transfer rates. In addition, the RF2905 is being phased out by RF Microdevices and may soon be unavailable. These considerations have motivated an investigation of RF transceivers that would be more radiation tolerant and potentially support higher data transfer rates.

Most currently manufactured RF transceivers at 900 MHz utilize CMOS processing which has been shown to have low radiation tolerance. The RF gain and mixing functions needed in the RF transceiver can be implemented efficiently in silicon bipolar and GaAs and several manufacturers provide integrated circuits for these functions. A recently developed technology to achieve these RF functions and one that would support higher data rate communications in radiation environments is based on Silicon Germanium (SiGe) circuits. Radiation tests at the University of Florida have already shown that SiGe amplifier stages provide very high tolerance to radiation with minimal impact to the operating performance parameters (such as gain). Unfortunately, there is not a known single-chip RF transceiver for FSK modulation that uses only GaAs or SiGe fabrication processes.

In view of the availability of radiation-tolerant component, we are investigating integrated circuits to design an RF transceiver using building blocks based on GaAs, SiGe, and/or silicon bipolar components. These building blocks include amplifiers, mixers, phase-locked loop circuits, and combinations of these and other circuit functions. At the same time we will continue to investigate single-chip solutions for the RF transceiver that use a radiation tolerant fabrication process. We have completed the initial design architecture for an FSK RF transceiver using multiple ICs. Specific integrated circuits for some of the circuit functions in the block diagram have been identified. If a single-chip solution can be identified in early 2004, it may be possible to breadboard and test this more desirable approach.

I.1.4.1 Microprocessor Selection and Other Design Options

The data is sent to the computer using the USART and a prewritten service routine for CodeVision AVR called putchar(), which automatically frames the data for RS-232 serial transmission. The microcontroller would be interfaced with the RF2905 using a header and to the computer using a MAX232 chip and a DB-9 port. In addition to this, the microcontroller needs support circuitry, including a crystal oscillator, capacitors and resistors. The completed software design determines the hardware design and provides the specifications.

I.1.4.2 Future work to Redesign Slave Unit

The current design of the packet format of the system is poor, which made redesigning the master difficult. Any future work on the master controller redesign should be preceded by a new packet and slave design. A redesign should follow either the International Organization for Standardization (ISO) Open Systems Interconnect (OSI) model for networking or a similar derivative. The ISO OSI model consists of seven layers:

	Layer	Operation of Layer
7	Application	E-mail, File Transfer
6	Presentation	Syntax & Semantics, Graphics
5	Session	Connections & Disconnections
4	Transport	Packets are Tagged for Resequencing
3	Network	Addressing Packets, Routing
2	Data Link	Frames, ACK
1	Physical	Bits

Figure I.1.4: ISO OSI Seven Layer Model

Even though the master and slave may not interface with other networks, it allows for easy upgrades and changes in technology. A master-slave system would most likely implement layers 1,2,3,4 and 7.

The timing in the slave system has room for improvement as well. When measuring the bit widths of the data received at the master, there was a variance of more than 5% which makes it hard to keep data synchronized using a microcontroller. This is another reason to redesign the slave system in any future projects.

The slave redesign should keep Manchester line encoding at the physical level. In place of Hamming codes, a simple CRC could be considered. Although there would not be forward error correction, if bad packets are received occasionally then CRC might be more effective.

The microprocessor hardware design path is straightforward, and the afforded flexibility requires the addition of software development and a software based error detection/correction scheme. There is also the opportunity to introduce a network communication scheme that supports a multiple-master/multiple-slave environment.

The first phase includes implementing a prototype with off-the-shelf, non-radiation tolerant components (COTS) to prove the architecture and develop the software. Concurrent with this phase a search would be underway for a suitable radiation tolerant microcontroller. Once a prototype is functioning, the software could be ported to the new microcontroller resulting in a radiation tolerant prototype that could be irradiated in a test chamber. While the first prototype using an off-the-shelf microcontroller would probably not require a PCB design (due to the use of a microcontroller evaluation board), the second one using the radiation tolerant microcontroller would require a PCB to be designed so that any required glue circuitry could also be radiation tolerant.

Once a microcontroller is implemented, there would be a host of interfacing possibilities available. Either the master or slave could be easily connected to a computer via RS232, USB, firewire or some other communication method. Likewise, any piece of equipment could be connected to a slave unit by implementing slave interfaces such as A/D, D/A, serial data, parallel data, etc. Some of these interfaces may be inherent features of the microcontroller selected. The entire slave unit could also be incorporated into another device, such as a robotic device, and could, due to the on-board, radiation tolerant microcontroller, be the controller for this device.

I.1.5 Summary and Conclusion

Microprocessors and microcontrollers that are tolerant to a total radiation dose of 1 Mrad are available but are rather expensive. However, there is an offsetting gain in system flexibility, reliability, and ease of use. The selection of more “open architecture” designs and utilizing industrial standard protocols and methods is likely to provide the most immunity from obsolescence. While the addition of programmability does not necessarily simplify the design, it will result in meeting the needs of more applications by its overall flexibility.

I.2 Wireless Components for Rad Environments

I.2.1 Introduction

The primary objectives of this subtask are to develop new rad-hard circuits for mobile robots and remote systems. A new COTS chip color camera under development by industry will be subjected to radiation tolerance testing. The camera is estimated by UF to potentially have a radiation tolerance exceeding 3Mrads(Si). UF plans to interface this camera with a rad-hard COTS 2.4 GHz RF transmitter for live TV applications inside high radiation environments. The small size and low power requirements of this system make it an excellent video candidate for use with robots, mechanical systems, security, surveillance, and basic operations in areas with limited human access. Long range plans seek instrumentation and control interfaces to use the Rad Hard Wireless RF Modem developed at UF for fully autonomous operations.

I.2.2 Background

This development task is relevant to any D.O.E. site that involves robotic material handling, storage, or object manipulation in hazardous radiation environments. Low-cost systems with real-time monitoring of position and environment will provide a new level of path planning and control not currently available. Such advanced systems will have new capabilities essential to safe handling of large or fragile objects and significantly reduce worker exposures.

I.2.3 Approach

Our approach envisions low-cost COTS modular designs coupled with the development advanced robotic arms and mobile robots. Current development plans for the first prototype will feature active video monitoring in color. Future advanced systems require this capability for operations under computer control. The design for these capabilities is scalable for any size robotic arm. Long range plans seek to evaluate the use of this technology with advanced end effectors, and automated waste barrel packing systems.

The selection of components is guided by several important principles. These are: industrial standard interfaces and circuits, likelihood of longevity of supply, interchangeability of multi-sourced components, loosely coupled modular design, and the important radiation tolerance. Thus, system architecture must be a compromise among evolving future technology, a need to limit vendor dependencies, and well-defined interfaces that can support future technology.

I.2.4 Technology Evaluated

- The initial low-cost camera system (the under $80 XCam2 system) was obtained from X10.com and evaluated. Its major components and features are: CCD camera (< 30Krad tolerance), GaAs technology, 2.4GHz wireless operation, and compatibility with battery power.
- The rad-hard camera technology was based on Spectra-Physics Cidtec CID video camera (charge injection device) platform to replace poor radiation tolerance of the CCD (charge-coupled-device) technology.
- Redesigned small modular circuits (with reduced part counts, lower power, reduced size SOIC surface mount package, simple architecture for a bare-bones system) operation and radiation tolerance were studied.

I.2.5 Specifications

I.2.5.1 XCam2 CCD Color Camera Specifications:

Imager CMOS Sensor
Format 1/3"
Array Size NTSC - 510 × 492
Resolution 310 TV Lines
Scanning 2:1 Interlace
Auto Shutter 1/60 to 1/15,000 sec.
Minimum Illumination (f1.8)
Operating Temperature -10°C to 40°C (14°F to 104°F)
Humidity Limits 0 - 95% Humidity
60 Degree Range of View

XCam2 transmits high-quality visual images via 2.4 GHz frequency technology using a circular polarization signal to provide clear, powerful re-transmission of video signals unobstructed by walls, ceilings, furniture, or floors. This results in cleaner pictures, reduced signal interference and multiple channels.

Figure I.2.5.1 – Model XX11A CCD Camera

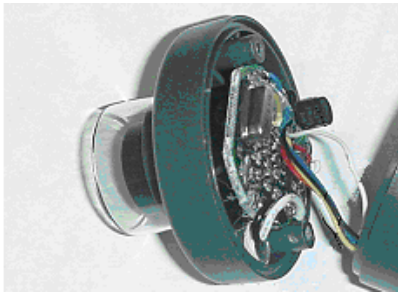

Figure I.2.5.2 – Model XC18A 2.4GHz Video Transmitter

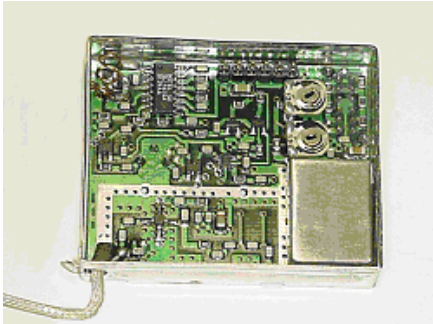

Figure I.2.5.3 Model VR36A 2.4GHz Receiver

The 2.4GHz transmitter broadcasts a wireless video signal to the Video Receiver unit (VR36A) which easily attaches to any video device using the included RCA jacks. Additional information on the XX11A and VR36A can be found at the web address: http://www.x10.com/products/cameras.htm

I.2.5.2 Cidtec CID Video Cameras

The specification for greater than 1Mrad(Si) radiation tolerance is met by the COTS CID technology. The charge injection device structure, principle of operation, and readout techniques are fundamentally different from charge-coupled-devices (CCD's). Each pixel in the CID array is individually addressed during readout. Scanning routines are implemented via electronic switching of row and column electrodes which are fabricated in a thin, clear polysilicon matrix over the surface of the array. While CCD's transfer collected charge out of the pixels during readout (hence erasing the image stored on the sensor), CID's do not transfer charge from site to site in the array. CID readout is accomplished by transferring or "shifting" the collected 'charge packet" within an individually addressed pixel, and sensing displacement values across the electrodes at the site.

Readout is non-destructive because charge remains intact in the pixel after the signal level has been determined. To empty the pixel for a new frame intergration, row and column electrodes are biased to "inject" the charge packet into the substrate collector. This is the basis for the improved radiation tolerance since no charge becomes trapped in an oxide layer. The commercial market availability was found through Symphotic TII Corp or RoperResources Ltd. Their ColorRad CIDTEC solid state color radiation hardened camera (1 and 3Mrads models) is commercially available.

I.2.5.3 Zarlink Semiconductor SL1461 - Wideband PLL FM Demodulator

The SL1461SA is a wideband PLL FM demodulator, intended primarily for application in satellite tuners. The device contains all elements necessary, with the exception of external oscillator sustaining network and loop feedback components, to form a complete PLL system operating at frequencies up to 800MHz. An AFC with window adjust is provided, whose output signal can be used to correct for any frequency drift at the head end local oscillator.

FEATURES

_ Single chip PLL system for wideband FM demodulation
_ Simple low component count application
_ Allows for application of threshold extension
_ Fully balanced low radiation design

_ High operating input sensivity
_ Improved VCO stability with variations in supply or temperature
_ AGC detect and bias adjust
_ 75Ωvideo output drive with low distortion levels
_ Dynamic self biasing analog AFC
_ Full ESD Protection*

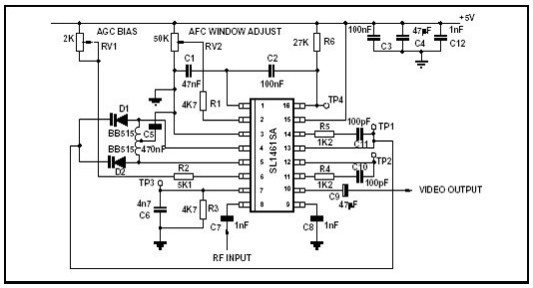

Figure I.2.5.3 Zarlink Semiconductor SL1461 Block Diagram

I.2.5.4 ANADIGICS DBS (Direct Broadcast Satellite) Tuner IC ADC20013

The ADC20013 down-converter is intended for use in the indoor receiver portion of the DBS (Direct Broadcast Satellite) System. .ANADIGICS' 0.5 µm radiation tolerant depletion-mode GaAs process is used to fabricate this device. The chip down-converts inputs in the 950-2050 MHz band to a fixed IF at 480 MHz. The device typically dissipates 300 mW from a standard 16 pin SOIC surface mount package. The ADC20013 ushers in a new era in low cost MMIC applications for consumer electronics.

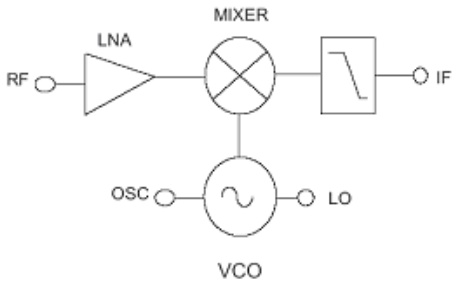

Figure I.2.5.4.1 Anadigics ADC20013 DBS IC Tuner Block Diagram

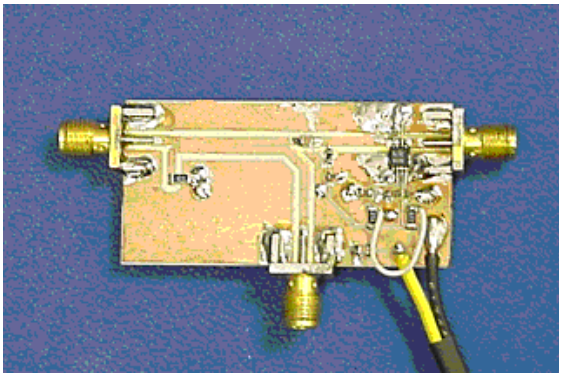

Figure I.2.5.4.2 Anadigics ADC20013 DBS IC Tuner Test Circuit

I.2.5.5 RF MicroDevices GaAs Low-Cost PreAmp and MMIC Amplifier

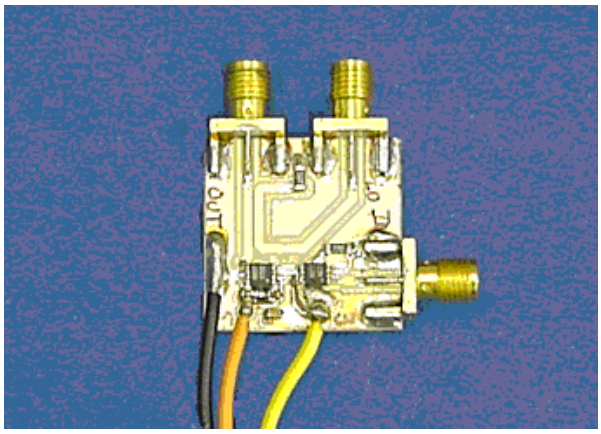

Figure I.2.5.5 RF3805 & RF3819 GaAs Amplifiers

The modular test circuit was construct using a pre-driver amplifier (RF3805) and a monolithic microwave integrated circuit (MMIC) used as a gain block amplifier. The RF3805 preamplifier is specifically designed for wireless applications, and uses a highly reliable GaAs heterojunction-bipolar-transistor (HBT) fabrication process. The RF3819 is a high-performance InGaP/GaAs general purpose RF and microwave gain block amplifier is based on a reliable HBT MMIC design.

I.2.5.6 Phyllips NE564 Phase-Lock-Loop (PLL) Demodulator

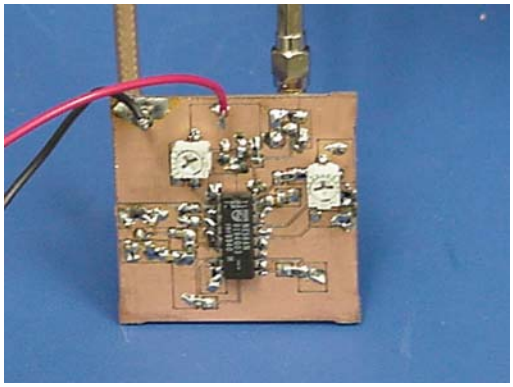

Figure I.2.5.6.1 NE564N Test Circuit

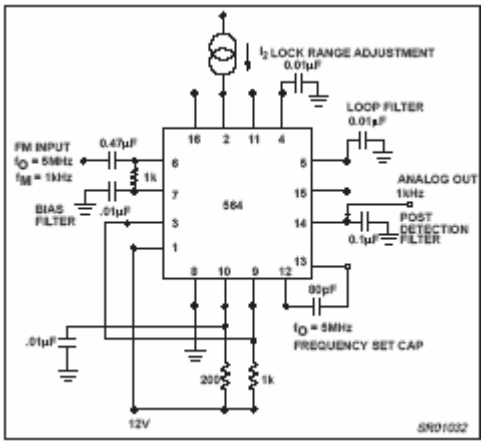

Figure I.2.5.6.2 Block Diagram of PLL

The NE/SE564 is a versatile, high guaranteed frequency phase-locked loop designed for operation up to 50MHz. As shown in the Block Diagram, the NE/SE564 consists of a VCO, limiter, phase comparator, and post detection processor.

I.2.6 Results Summary

The 2.4 GHz wireless Xcam2 video system irradiation demonstrated that the radiation tolerance of the CCD was limited to less than 30Krads(Si). However, independent testing of both the transmitter and receiver portions demonstrated exceptional radiation tolerance. The transmitter was irradiated in excess of 5.4Mrads(Si) without apparent damage, and the receiver was irradiated to 3.8Mrads(Si).

Examination of the commercial circuits in the Xcam2 camera system provided the identified the important components, Zarlink Semiconductor SL1461 and the Anadigics ADC20013 DBS IC Tuner. This was the basis of the design used to develop the modular circuits shown in this report. It was demonstrated in the Electronic Communication Lab (UF ECL) that with a few components, a rudimentary video system can be constructed. Coupling the GaAs HBT devices with the InGaAs MMIC provides the matching circuit radiation tolerance to work with the CidTec CID radiation hard video cameras. Thus, an economical COTS video camera system with a radiation tolerance of 3Mrads(Si) can be constructed. This low-cost system has the potential to fill numerous needs in hazardous environment for DOE.

I.3 RadPaint and Development of a Path Planning Algorithm

I.3.1 Introduction to Path Planning

The RadPaint software was developed by the University of Florida to produce visual images of the radiation hazard present in any work space containing radioactive materials. RadPaint translates information from 3-D source distributions of high energy gamma sources and contaminated objects into color coded images. That research work was reported in previous documents and is completed.

The next phase of the project was the development of a path planning algorithm for a mobile robot to traverse a radiation environment. The objective of the algorithm was to find the safest radiation path from a given start configuration to a goal configuration of a vehicle moving only forward in a radiation environment cluttered with obstacles bounded by simple polygons. The path planning algorithm finds the shortest path in time (n^2logn, and n being the number of vertices in the discritized map) using a radial sweep line method to compute the visibility graph and Dijkstra's algorithm to find the shortest path.

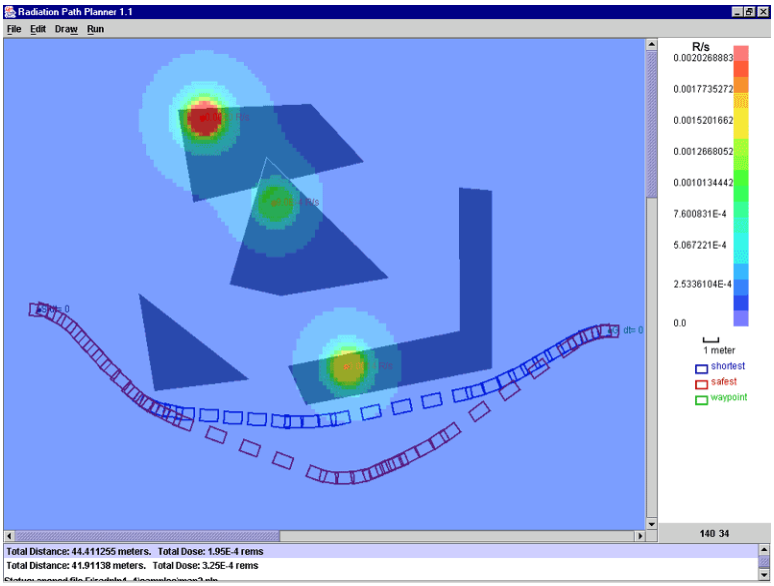

Figure 1.3.1: Radiation Path Planner – Java Applet

Figure 1.3.1 shows a map with point sources of radiation that have exposure rates, 002R/s, 0.00014R/s and 0.0014R/s (top left to bottom right) and a set of obstacles. The shortest path has a distance of 41.9 meters and a cumulative dose of 325e-4 Rem. Also shown is the safest path, calculated from our program. This path has a slightly longer distance of 44.4 meters but has a cumulative dose of 1.95e-4 Rem, which is recommended because it offers less radiation dose by a factor of 166.

In an unbounded environment, any path that steers clear of the radiation sources and travels a minimal distance will result in a safe path. To compute the safest path, the path planner utilizes the fact that the point sources obey the inverse square law and assumes that the gamma ray attenuation from the obstacles is insignificant.

1.3.2 Developing a Path Planning Algorithm

Motion planning is one of the most important components of an autonomous mobile vehicle. It deals with the search and execution of collision free paths by vehicles performing specific tasks. Motion planning is often broken down into two stages--*path planning* and *path tracking*. The path planning stage involves the search for a collision free path, taking into consideration the geometry of the vehicle and it surroundings, the vehicle's kinematic constraints and any other external constraints that may affect the planning of a path. The path tracking stage involves the actual navigation of a planned path, taking into consideration the kinematic and dynamic constraints of the vehicle. This research presents a path planning algorithm for car-like vehicles.

1.3.3 Problem Statement

The objective of this effort is two fold:

1. To develop an efficient offline path planning algorithm that is capable of finding optimal collision free paths from a start point to a goal, for a car-like vehicle moving through an environment containing obstacles bounded by simple polygons.

2. To extend the path planning algorithm in order to find safe paths by imposing a radiation constraint on a mobile robot operating in a radiation environment.

The first objective was intended to be an improvement of the work done by Arturo Rankin. The second objective was intended to facilitate the optimal utilization of robotic vehicles in places such as nuclear power plants where prolonged exposure to radiation can cause substantial damage to robotic equipment.

I.3.4 Kinematic Constraints of Car-Like Robots

The motion characteristics of a robot play an important role in planning its path. Robots that move in a plane generally have three degrees of freedom--translation along the two axes in the plane and rotation about the axis perpendicular to the plane. Certain robots that are car-like cannot move freely in all three degrees of motion due to their steering constraints. The geometry of such robots is presented in Figure 1.3.2 and their equations of motion are given below.

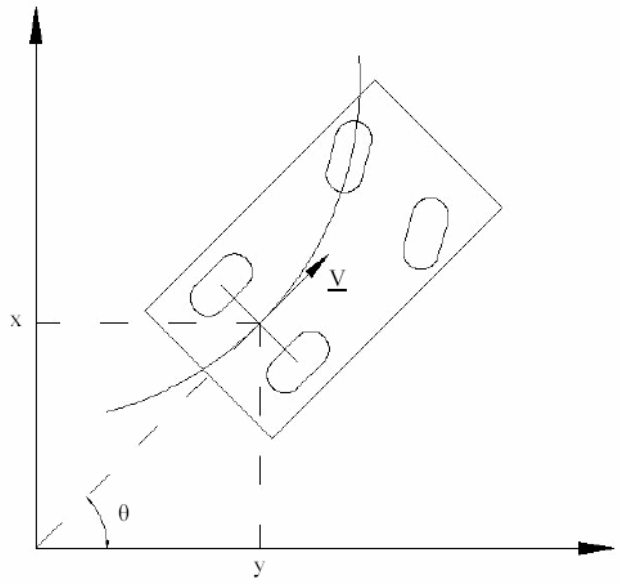

Figure 1.3.2 Geometry of a car-like vehicle

$$\frac{dx}{du} = \cos(\theta).v(u)$$

$$\frac{dy}{du} = \sin(\theta).v(u)$$

$$\frac{d\theta}{du} = \omega(u)$$

In Figure I.3.2, V is a unit vector along the direction of motion of a vehicle moving with linear velocity *v* and angular velocity *ù*. *è* is the angle that V makes with the positive x-axis. The position (*x,y*) of the vehicle is referenced from the midpoint of the vehicle's rear axle. As seen from the equations, a car-like robot has less number of controls (linear and angular velocities) than the number of configuration variables (*x,y,è*), making the equations non-integratable. Vehicles with such kinematic constraints are called *nonholonomic* vehicles. Although nonholonomic vehicles are controllable, their path planning is a difficult task because the motion at any moment is not free. In addition to this, car-like vehicles have a minimum turning radius. The combination of the nonholonomic constraints and the minimum radius of curvature constraint constitute the kinematic constraints of a car-like robot.

I.3.5 Path Planning Algorithms

Over the last decade, path planning for mobile robots has been broken down into two main categories--*offline* and *online* (also called dynamic) path planning. As the names suggest, offline path planning is a global optimization approach while online path planning performs only a local optimization.

Offline algorithms require a priori an obstacle map of the robot's environment. The path is pre-computed and then given to the robot to execute. The robot uses the path information to navigate itself efficiently through the environment with the help of a path tracking algorithm. A number of approaches have been explored using randomized and deterministic algorithms. While randomized algorithms are used to find solutions to the generalized form of the problem that is extremely complex, the problem is often simplified to create deterministic algorithms. The complexity measure of such algorithms is given as a function of the number of vertices present in the discritized input map.

The main objective of online path planning is to avoid obstacles by reacting to data collected from onboard sensors. It may be used when a map of the mobile robot's environment is not known or, if an unexpected obstacle was encountered during the execution of a pre-computed path. Since online path planners run in real time and on onboard computers that usually have very limited computing resources, they have to be efficient in terms of both memory utilization and time. This is accomplished by using a lightweight algorithm or heuristic that works on a highly discritized input. Their efficiency is usually measured by the amount of time they take. The quality of their results depends on the amount of look-ahead distance of the sensors. Path length is usually used as a complexity measure for online path planning algorithms by setting bounds for the worst case path length as a function of environmental parameters such as the sum of perimeter lengths of obstacles.

A natural offshoot from creating a distinction between online and offline algorithms is the development of hybrid algorithms. Hybrid path planning algorithms usually work with sparse or

low resolution maps that do not provide information about obstacles such as rocks, trees etc. These algorithms have both an online and an offline component that work in tandem to provide globally optimal paths.

I.3.6 Offline Path Planning for Car-Like Vehicles

The generalized offline path planning problem for car-like robots is referred to as the *continuous curvature constrained shortest path problem*. The objective of the generalized problem is to find a continuous path that is the shortest among all paths and whose curvature at any point along the path is less than a given upper bound (the inverse of the minimum turning radius). Reif and Wang proved that this problem is NP-hard. This means that there is no existing algorithm that can solve this problem to optimality in polynomial time and it is highly unlikely that one even exists; a justification for the approaches based on discretization used in the past to yield polynomial time algorithms. Fortunately, these approaches have been found to work well for all practical applications.

Discretization techniques simplify the problem by creating a *configuration space* from a map of the vehicle's environment. The concept of configuration space was introduced in the late seventies as a consequence of kinematic constraints on moving objects. The configuration of a mobile robot is a set of parameters that define its position and orientation in a plane. The configuration space defines a subset of the free space in a robot's environment that is reachable by a robot with kinematic constraints. Typically, a configuration space is built by reducing the robot down to a point and increasing the size of the obstacles such that they bound regions of the free space that are inaccessible to the point sized robot. The problem of motion planning then reduces to finding a sequence of feasible robot configurations in free space from an initial to a final configuration. Figure I.3.3 shows the configuration space for a disc robot.

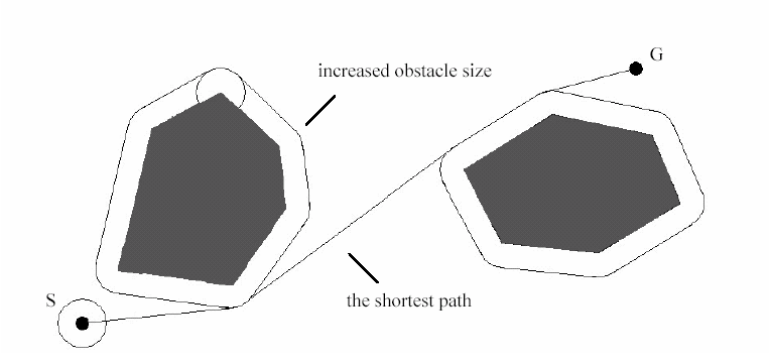

Figure I.3.3 Configuration space for a disc robot.

The planned path is considered to be an image of the final *trajectory* that is executed by the robot. The path may be discontinuous but the trajectory is always continuous. An *admissible trajectory* is a solution of the differential system corresponding to the kinematic model of the robot along with some initial and final conditions. Since the configuration space concept is purely geometric and does not allow for time-dependant constraints (as required by the robot's kinematic model) the goal of a discritized nonholonomic path planner is to find an image of an admissible trajectory--a *collision free admissible path*.

I.3.7 Need for a Path Planner in Radiation Environments

Robots are used in nuclear installations to perform jobs in areas where humans are at risk of being over exposed to radiation. Since radiation is detrimental to human health, the amount of

access that humans have to portions of an installation is limited by regulation 10CFR20 of the Nuclear Regulatory Commission. This limitation may call for the need to employ more labor than needed.

In addition to this, there are as many as 7000 contaminated buildings among Department of Energy nuclear facilities that require decontamination and/or decommissioning. It is estimated that it will take more than 40 years and over 100 billion dollars to clean up these sites [5]. The Department of Energy: Office of Environmental Management, set up a program called the "CP-5 Large Scale Demonstration Project" [6] to find innovative decontamination and decommissioning technologies that can help reduce the cost of this billion dollar effort. Some of the solutions that were developed were radiation imaging systems that could map radiation fields and mobile robots that were capable of finding hotspots in a building. Since robots themselves are affected by radiation and the cost of maintaining or replacing them is high, significant cost savings can be achieved by minimizing their exposure to radiation. One way of doing this is by using a path planner to compute routes that minimize the radiation exposure of mobile robots and thereby extending their life.

I.3.8 Effects of Radiation on Mobile Robots

Gamma rays, beta particles, neutrons and heavy charged particles such as protons and alpha particles are emitted from radioactive materials. Of these, gamma rays, which are photons with very short wave length, pose the greatest threat to electrical and electronic components onboard robots. Gamma radiation is capable of traveling many meters in air and readily penetrates most material, earning itself the name "penetrating radiation." Gamma rays have a very destructive effect on a number of materials used to build robots. Electrical parts such as transformers, motors, thermocouples, relays and circuit boards, which form vital components of a robot may be severely damaged from exposure to gamma radiation. A previous UF researcher, Laurent Houssay, detailed the effects of gamma rays and has referenced tables with threshold values for various materials that are used on robotic systems. The effect of radiation from gamma rays is increased by long exposure (time), close proximity to its source (distance) and the intensity of the source (quantity). Some effects of gamma radiation on commonly used materials are listed in table I.3.1.

Table I.3.1 Effects of gamma radiation to commonly used materials.

Material	Threshold level (Gy) Effect	
Ceramics	5 x 107 (mica) 5 x 1010 (alumina)	Dimensional swelling and decrease in density.
Plastics	100 (Teflon)	Cracking, blistering and embrittlement.
Coatings	2.1 x 106 (vinyl on aluminium) 8.7 x 106 (styrene on steel)	Cracking, blistering and flaking
Adhesives	1 x 106 (neoprene-phenolic) 5 x 106 (epoxy)	Decreases number of adhesive bonds.
Resistors	104 – 107 (carbon film) 105 – 109 (metal film)	Chemical degradation causing a decrease in resistance.
Glass	10 x 106 (quartz)	Darkening.
Magnets	1 x 106 (soft magnets)	Decrease in magnetic strength.

I.3.9 Non-Holonomic Path Planning Algorithm

The algorithm for planning of a collision free admissible path was broken down into four stages as shown in Figure I.3.4 and I.3.5. The algorithm is built on an edge-centric data structure that is listed in Appendix B. All points in the map are referenced to a cartesian coordinate system (x,y). The boundary polygon is treated as the inverse of the obstacle polygon. That is, the final trajectory must be contained by the boundary polygon while lying outside the obstacle polygons. If the operations on the boundary polygon are not explicitly stated, they must be considered as the inverse of the operations performed on the obstacle polygons wherever appropriate.

The pre-process stage of the algorithm validates the input and performs some pre-computation that helps in speeding up the main body of the algorithm. The lists below, detail the validation and pre-computations that are performed on the input. Failure of any of the validity checks may lead to the premature termination of the algorithm.

I.3.10 Input Validation

• Check for non-empty start and goal configurations that lie in free space. That is, the configurations must exist in the input and the position of the start and goal must not lie inside an obstacle polygon or outside the boundary polygon.

• If the set of obstacles and boundary polygons in the map is a non-empty set, ensure that the polygons are non self-intersecting. The reason behind this check is that the orientation of a self-intersecting polygon is undefined. Polygon orientation is required to differentiate between convex and concave vertices of the polygon.

• By convention, the vertices of all polygons are ordered counter-clockwise in the cartesian coordinate system. If the orientation of an input polygon is found to be clockwise, the ordering of its vertices is reversed.

• The length of each edge of an obstacle or boundary polygon must be greater than a minimum length $l_0 = 2R$ ($l_0 = 4R$ for edges between two convex vertices of an obstacle).

• The angle of each concave polygon must lie in the range $[\pi/2, \pi]$.

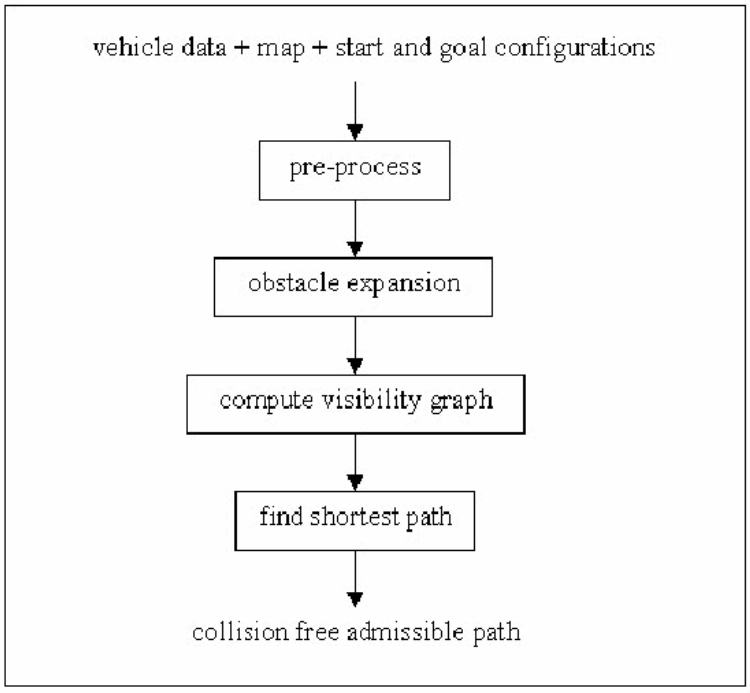

Figure I.3.4. Flowchart of the nonholonomic path planner.

I.3.11 Pre-Computation

• Pseudo obstacles are placed at the start and goal points in order to ensure that the path generated obeys the initial and final orientations of the vehicle. This is as shown in Figure I.3.6. ABCDE forms the pseudo obstacle that forces the path to go through a pseudo start point D.

• Since the shortest path always goes through convex vertices of the obstacle polygons and concave vertices of the boundary, these vertices are tagged as *legal*, while all other vertices are tagged as illegal vertices. This reduces the search time of the algorithm by not considering illegal vertices in the search for the shortest path.

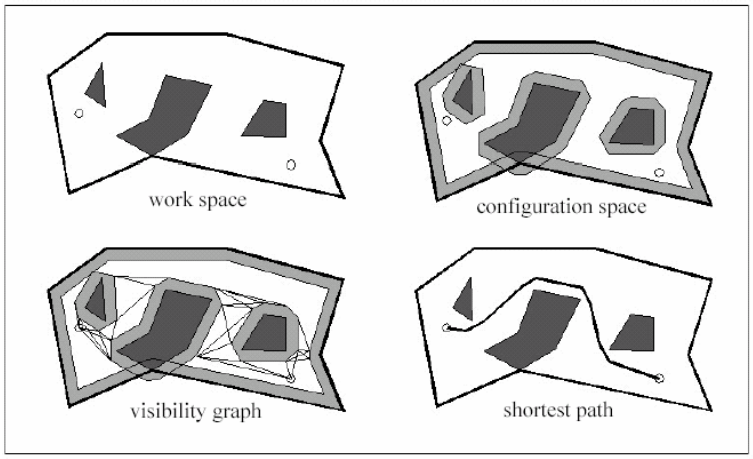

Figure I.3.5: Graphic representation of program flow.

I.3.12 Obstacle Expansion

As stated earlier, a popular simplification of the path planning problem is to grow the obstacles in order to reduce the vehicle down to a point. The obstacle expansion stage of the algorithm is responsible for this transformation of the vehicle to a point in the discretized map. This stage of the algorithm is important from the point of view of the correctness of the output path. The obstacle expansion stage must not only allow for the computation of a collision free path, but must also guarantee that the path is an image of an admissible trajectory. The method used to expand the obstacles and shrink the boundary is described here in detail. It is also proved to guarantee paths that are images of admissible trajectories.

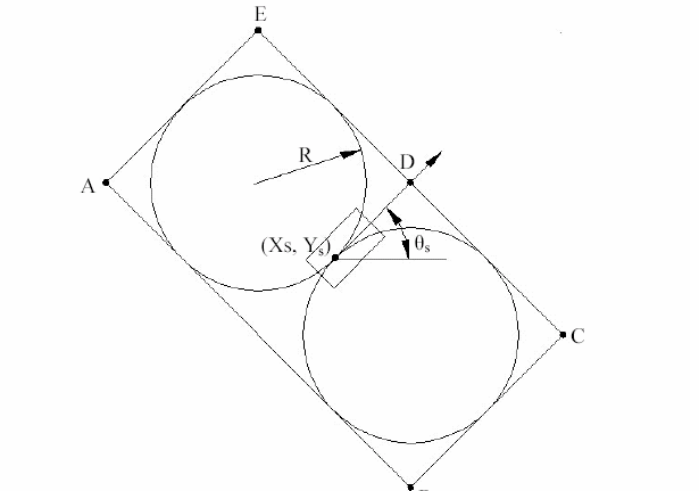

Figure I.3.6 Geometry of a pseudo obstacle placed around the vehicle's start configuration.

Once the obstacles are expanded and the visibility graph computed, the shortest path algorithm finds a piecewise linear path from that start to the goal point. Since the path is highly discontinuous, it must be smoothed in order to make it feasible for a vehicle to follow it. Some researchers like Laumond et al. suggest the use of clothoids to smooth the path into a feasible trajectory. Clothoids are curves whose curvature varies as a function of its length as seen in Figure I.3.7. They have been used successfully in connecting straight line segments and circular arcs with a continuous change of curvature curve for applications such as railway and highway design.

Figure I.3.8 shows how a clothoid can be used to smooth discontinuous paths built out of straight line segments. x_0 is where the clothoid starts and C is the configuration of the robot at the midpoint of the clothoid. σ is the imposed direction of motion and δ is the imposed direction of rotation.

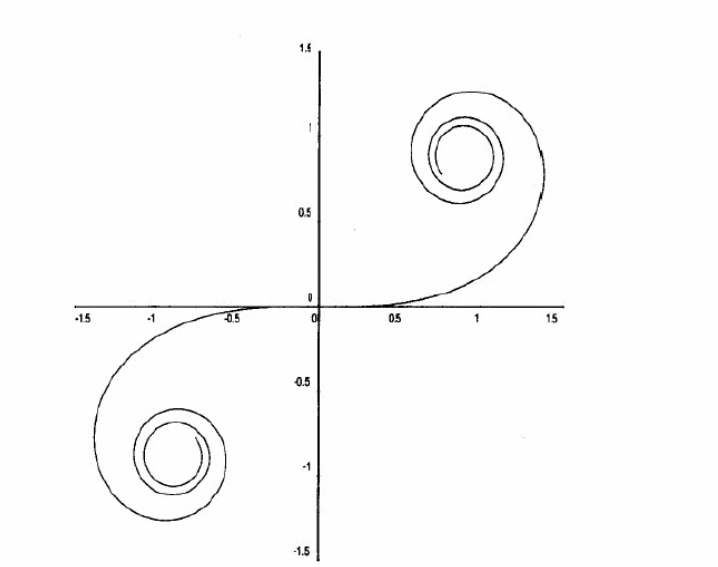

Figure I.3.7 A clothoid (Cornu spiral).

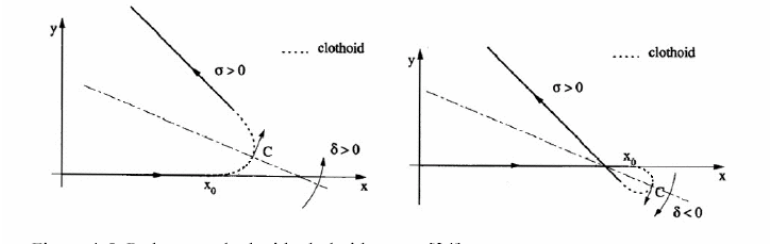

Figure I.3.8 Paths smoothed with clothoid curves.

The expansion algorithm in this paper utilizes another representation of a polynomial curve chosen by the JAUS Committee. Each segment of this curve is defined by three waypoints P_0, P_1 and P_2 and a weighting factor *w*. The parametric form of the curve is as follows:

$$p(u) = \frac{(1-u)^2 P_0 + 2u(1-u) w P_1 + u^2 P_2}{(1-u)^2 + 2u(1-u) w + u^2} \qquad \text{where } u = [0,1],\ w \geq 0$$

In the example curve shown in Figure I.3.9, it may be noticed that p(0) = P_0 and p(1) = P_{22}. The weighting factor *w* has the effect of moving the trajectory closer or further away from the point P_{11}, which is called the control point. This effect can be seen in Figure I.3.10. As the trajectory moves closer to the control point, or further away from it, its maximum curvature κ_{maxmax} tends to increase. κ_{maxmax} can be found by equating the first derivative of equation 4.2 to zero. PPκ κ

$$\kappa = \frac{x' y'' - y' x''}{\left(x'^2 + y'^2\right)^{3/2}} \qquad \text{where (x,y) is a point on the trajectory } p(u)$$

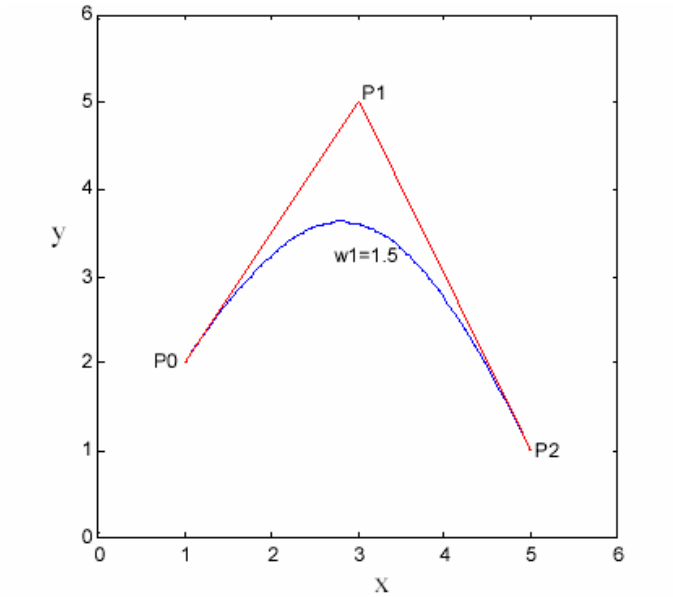

Figure I.3.9 Polynomial curve suggested by the JAUS Reference Architecture for the generation of a trajectory.

An important feature of this trajectory is that the lines P_0P_1 and P_1P_2 are tangent to the trajectory at P_0 and P_2. By choosing P_0 and P_2 to lie between the end points of a path segment, a continuous trajectory may be generated out of consecutive curve segments as seen in Figure I.3.10. P_2 is chosen to lie between the endpoints of the path segment P_1P_3 to yield a trajectory made up of two curve segments that share a common tangent P_1P_3 at P_2.

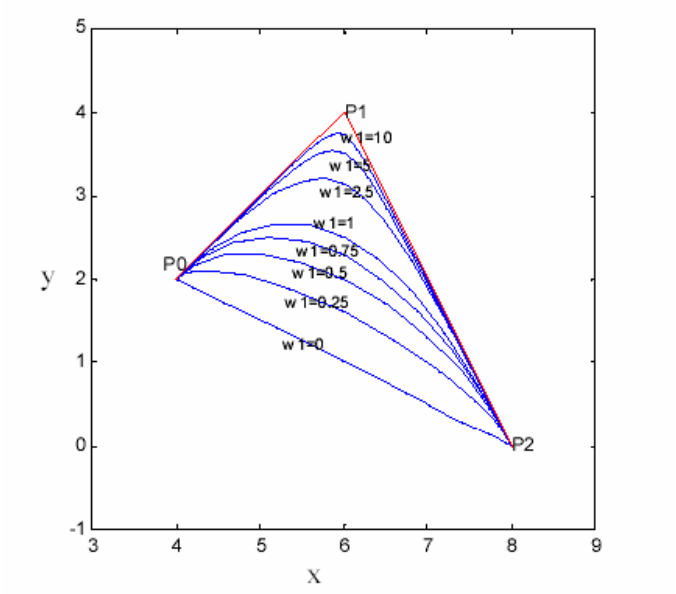

Figure I.3.10 Effect of the weighting *w* factor on the trajectory.

This feature was used to develop an effective expansion method that guarantees an admissible trajectory for any shortest path in the map. Since the waypoints along the shortest path coincide with only convex vertices of the obstacles, the expansion of convex vertices must ensure that any trajectory going through them lies in free space and has a maximum curvature less than 1/R. The concave vertices must be expanded only to maintain a sufficient offset along the walls of the obstacles in order to ensure collision free paths in the concave regions of the obstacles. The following sections describe the geometry behind the expansion method for convex and concave vertices.

I.3.13 Expansion of Convex Obstacle Vertices

The geometry behind the expansion of convex vertices is shown in Figure I.3.11. The convex obstacle vertex P_0 is replaced by two expanded vertices P_1 and P_2. This adds a new edge P_1P_2 to the expanded obstacle for every convex vertex in the original obstacle polygon. The length of the new edge is l_0, and is determined by the minimum edge length constraint. A vehicle that braces the sides of the obstacle will follow a trajectory that comes closest to the obstacle at the midpoint of the new edge P_1P_2. The new expanded points P_1 and P_2 form the control points of this trajectory. By choosing a safe distance *d* that is a function of the vehicle's width *W*, the trajectory shown in Figure I.3.11 will be collision free. The maximum curvature constraint of 1/R may be met by choosing an appropriate weighting factor *w*.

Since the convex angle *è* lies in the range (0,π) the boundary conditions occur when *è 0* and *è* ¡Ö π. The expansions for the boundary conditions are shown in Figure I.3.12. Notice that the minimum offset of the vehicle from the obstacle is min(*d, l*¡Ö*0/2)* in the range *è* =(0,π) when the vehicle moves along any trajectory in the neighborhood of the point P_0.

This feature was used to develop an effective expansion method that guarantees an admissible trajectory for any shortest path in the map. Since the waypoints along the shortest path coincide with only convex vertices of the obstacles, the expansion of convex vertices must ensure that any trajectory going through them lies in free space and has a maximum curvature less than 1/R. The concave vertices must be expanded only to maintain a sufficient offset along the walls of the obstacles in order to ensure collision free paths in the concave regions of the obstacles. The

following sections describe the geometry behind the expansion method for convex and concave vertices.

I.3.14 Expansion of Convex Obstacle Vertices

The geometry behind the expansion of convex vertices is shown in Figure 4-9. The convex obstacle vertex P_0 is replaced by two expanded vertices P_1 and P_2. This adds a new edge P_1P_2 to the expanded obstacle for every convex vertex in the original obstacle polygon. The length of the new edge is l_0, and is determined by the minimum edge length constraint. A vehicle that braces the sides of the obstacle will follow a trajectory that comes closest to the obstacle at the midpoint of the new edge P_1P_2. The new expanded points P_1 and P_2 form the control points of this trajectory. By choosing a safe distance d that is a function of the vehicle's width W, the trajectory shown in Figure 4-9 will be collision free. The maximum curvature constraint of 1/R may be met by choosing an appropriate weighting factor w.

Since the convex angle $è$ lies in the range $(0,\pi)$ the boundary conditions occur when $è \to 0$ and $è \to \pi$. The expansions for the boundary conditions are shown in Figure I.3.12. Notice that the minimum offset of the vehicle from the obstacle is $\min(d, l_0/2)$ in the range $è = (0,\pi)$ when the vehicle moves along any trajectory in the neighborhood of the point P_0.

I.3.15 Main Result: Expansion Method Guarantees Admissible Trajectories

"Any shortest path in a map with expanded obstacles is an image of an admissible trajectory."

Proof: The shortest path between any given start and goal configuration uses the expanded convex vertices of the obstacles as waypoints. The shortest path is piecewise linear and is guaranteed to lie in free space when the obstacles are expanded with sufficient distances d and l_o. The piecewise linear path is converted into a trajectory by using the second degree polynomial curve described by equation I.3.1 to smooth the corners of the path. This is done by choosing the vertices or waypoints of the path as control points of the smoothing curve segments, and endpoints of the smoothing curves along the length of the path segments adjacent to the path vertices. In order to prove that any shortest path among expanded obstacles is an image of an admissible trajectory, it is sufficient to prove that the curve segments used to smooth the path lie in free space and have a maximum curvature of 1/R.

The curve segment shown in Figure I.3.9 can be made symmetric about the control point by choosing segments P_0P_1 and P_1P_2 to be of equal length, say $l_0/2$. Assuming that each path segment has a length of at least l_0, the path will be made up of a sequence of segments of the type,

$$C_a S_b C_a \text{, where } \pi < a \pi/2,\ b\ 0.$$

C represents segments of the polynomial curve used for smoothing and S represents a straight line segment of the path. a represents the acute angle at the control point and b, the length of the straight line segments.

Notice that as the angle of a convex obstacle vertex ranges from $(0, \pi)$, the inner angle at each of the two expanded vertices (P_1 and P_2 in Figure 4-10) has the range $(\pi/2, \pi)$. Therefore the tightest turn that any path can take is a right angled turn. When the curve segment is made symmetric, the maximum curvature occurs at either $u = 0.5$ or $u = 0$ and $u = 1$ depending on the choice of w. A case for which the maximum curvature occurs at $u = 0$ and $u = 1$ is seen in Figure I.3.14 in the plot of κ versus u for the trajectory shown in Figure I.3.15. It may also be noticed that as the angle $P_0P_1P_2$ increases, the maximum curvature κ_{max} decreases when w is kept constant. Also, decreasing the lengths of $P_0P_1 = P_1P_2 = l_0/2$ has a scaling effect on the symmetric curve that increases κ_{max}. Therefore, by fixing the length l_0 and then finding a weighting factor w_1 for which $\kappa_{max} \to 1/R$ for the worst case turn (which happens to be a 90 degree turn), we can ensure that κ_{max} for any

symmetric curve that may be encountered will be less than 1/R as long as each path segment has a length of at least l_0. Figure I.3.15 below, shows the worst case turn.

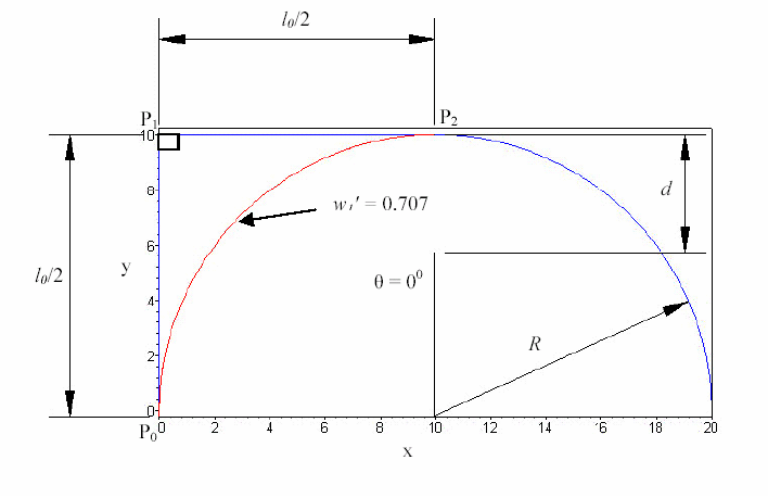

Figure I.3.15 The worst case turn.

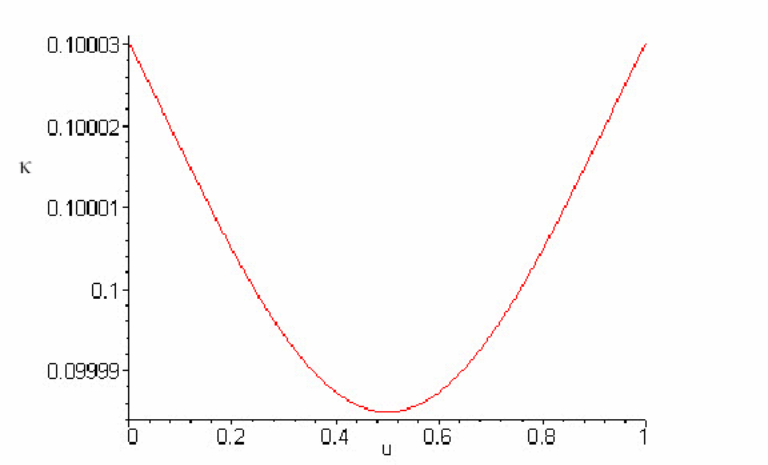

Figure I.3.16 Plot of curvature κ versus parameter u for a symmetric curve with $w = 0.707$

The offset distance d may be set at half the vehicle width $W/2$ plus some corner clearance cc to account for inaccuracies such as drift that occur when the path is being tracked by the vehicle. Therefore, when $l_0 = \max(2R, d)$, w must be 0.707 for κ_{max} ¡Ü 1/R.

d, l_0 and w_1 in the equations above will guarantee that any trajectory will be collision free and have a maximum curvature less than 1/R as long as the length of each path segment is at least l_0.

Unfortunately, the assumption made about the minimum length of each path segment does not hold for the general case. There may be cases when the length of a path segment is much smaller than l_0. This occurs when a path segment spans the free space between two obstacles as against bracing an obstacle edge.

$$d = \frac{W}{2} + cc$$

$$l_0 = \max(2R, d)$$

$$w_1 = 0.707$$

I.3.16 Path Planning With A Radiation Constraint

This section describes one possible way of planning paths in a constrained environment using the path planner. The algorithm described here utilizes the path planner to lower the dose received by a mobile robot moving in a radiation field. We look at the problem in the plane of the robot and for the sake of simplicity, assume that the radiation sources are point sources that are placed in the same plane. The algorithm was initially designed and implemented without considering attenuation from obstacles. An extension that allows the algorithm to consider attenuation was later designed and is available.

I.3.17 Radiation Basics

Of the many different forms of radiation emanated from radioactive materials, gamma rays are by far the most harmful from the point of view of robotic equipment. Exposure to gamma radiation can be minimized by following a basic ALARA principle that states, by reducing the amount of *time* spent near a source of radiation, increasing the *distance* between the source and the robot, and by using *shielding* material placed between the source and the robot reduces the exposure to radiation.

The effect of radiation exposure may be measured using the units *rad* (radiation absorbed dose) and *rem* (Roentgen Equivalent Man). Rad is used to measure the quantity of absorbed dose in terms of the amount of energy actually absorbed by a material, while rem is used to derive an equivalent dose based on the type of radiation being emanated. Since different types of radiation have different effects, the absorbed dose in rad was multiplied by a quality factor Q, unique to the incident radiation, to get the equivalent dose in rem. In recent years, these units have been replaced by two new SI units – *gray* (*Gy*) and *sievert* (*Sv*).

One gray represents the energy absorption of 1 joule per kilogram of absorbing material. That is,

$$1\ Gy = 1\ J\ Kg\text{-}^{1} \quad (5.1)$$

The unit Gray replaced rad as the choice of absorbed dose and sievert replaced rem as the new choice for equivalent dose. The equivalent dose in sievert for a given type of radiation was defined as

$$H = D \times wh \quad (5.2)$$

H is the equivalent dose in sievert, *D* is the absorbed dose in gray and *wh* is the radiation weighting factor that is dependant on the type of incident radiation.

The amount of radiation absorbed by a material per unit time is given by the *equivalent dose rate* or simply dose rate. Dose rate is usually measured in sieverts per unit time, that is Svh^{-1} or more usually $mSvh^{-1}$. The cumulative dose is the integral of dose rate over time and represents the total amount of radiation absorbed.

The intensity of the absorbed radiation depends on the absorption of radiation by the air and the shape and size of the source relative to the distance from which it is viewed. Gamma rays are not scattered by air and therefore, their intensity is determined as a function of the distance from the source. Most numerical computations and simulations that deal with gamma radiation consider the shape of the source to be a point, line or an extended source. Point sources are used when the radioactive material is believed to be emitting equal quantities of radiation in all directions. Line sources represent pipe like structures while extended sources are used to represent large areas like walls and floors.

The algorithm proposed here assumes that all sources are point sources and obey the inverse square law. The inverse square law states that the radiation intensity at a point away from the source is the inverse of the square of the distance from the source. This implies that the radiation spreads over larger areas with decreasing intensity in all directions.

I.3.18 Algorithm Description

The problem of finding the shortest safe path is a multi-objective problem with two objectives – minimum distance and minimum dose. Due to this, the overall objective of the problem may be stated in several different ways. From the practical standpoint, more is gained from minimizing dose than distance. Therefore, one possible way of defining the global optimal path Popt is, a path with the least dose absorption. That is, no other path in the map has a cumulative dose absorption less than the path P_{opt}.

Sources may be limited to regions beyond which the radiation dose rate is so insignificant that it is not considered to be a risk to the robot. The radiation beyond these regions is considered to be zero. When the map contains no boundary, any path that steers clear of the circular regions around the sources that contain significant radiation is an optimal path. Paths P_a and P_b in Figure I.3.17 are optimal paths. But, maps that contain boundaries can make the problem very challenging.

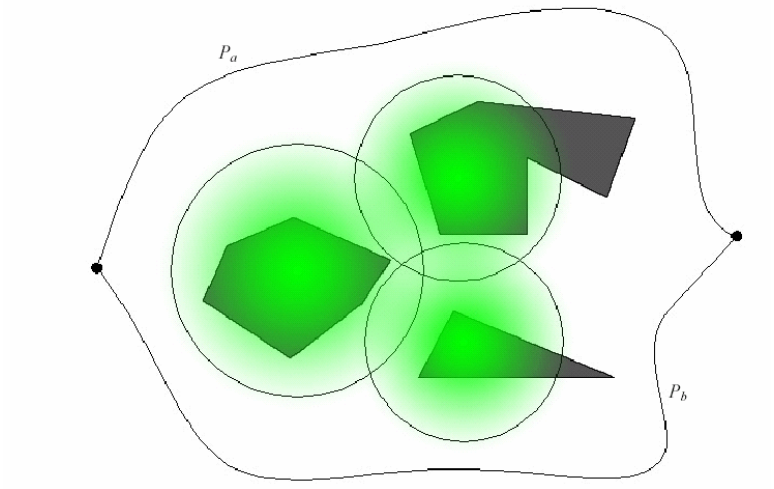

Figure I.3.17 Optimal paths in a map with no boundary.

When a boundary is present, it is not always possible to steer clear of the sources. There may be situations where every possible path in the map receives some significant dose and this calls for a more guided and maybe even exhaustive search for the optimum path. Besides, the optimum path does not necessarily have to pass through the vertices of the discretized map. This implies that a graph type algorithm can only achieve a near optimal result. From this point of view, it may be better to approach this problem using some other approach like the potential field method or a randomized heuristic. But, due to the complex nature of radiation fields, these approaches also cannot guarantee the global optimal path. They may only provide better approximations when compared to a graph search method, but at higher computational costs.

The cumulative dose absorbed by the robot is lessened by using the path planner to enforce the basic ALARA principle of increasing the distance of the robot from the sources to reduce exposure. The exposure is minimized by beginning with the shortest path and moving this path away from the radiation sources. At first, circular pseudo obstacles of unit radius are drawn around each source. The circles are then grown incrementally such that the intensity of the radiation at their circumference reduces by some small amount, say 1 $mSvh^{-1}$ with each iteration. Figure I.3.18 illustrates this concept. The pseudo obstacles create a new type of configuration space where the dose at every point in free space, contributed by any given source, is less than or equal to the intensity at the circumference of the pseudo obstacles. Circles that enclose radiation sources with relatively smaller intensities grow at slower rates than circles that enclose high intensity sources. With each iteration, the pseudo obstacles are grown and the path planner is executed to find if a path still exists. The iterations continue until either all the circular pseudo obstacles have been grown to their maximum limit, (intensity of 0.1 $mSvh^{-1}$ at the circumference to prevent d from going to infinity) or when a path cannot be found. In the former case, the shortest path happens to be the optimum path. In the latter case, the path found in the second last iteration represents a near optimal path. When the optimal path is found, the cumulative dose for the entire path is computed by interpolating dose per source per unit time absorbed along the length of each path segment and summing the total dose received from all the sources. The speed of the robot is found to have a scaling effect on the amount of radiation absorbed along a given path.

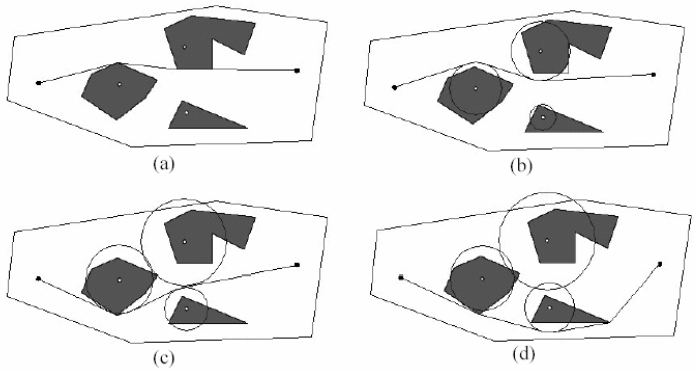

Figure I.3.18 Growing pseudo obstacles around radiation sources to find an optimal path.

There may be two special cases when the radiation sources are placed in series or in parallel with respect to a path between the start and goal points. When they are placed in parallel, there may be cases where the optimal path found passes through the irradiated intersection regions of two or more radiation sources as shown in Figure I.3.19. The combined dose from both sources for the resulting path may be higher than an alternate path like P_{alt} that traverses through a region of possibly lower radiation intensity. But, a path like P_{alt} tends to go closer to the source (where the intensity can spike) and travels a longer distance in the irradiated region. Therefore, there is very

little gained, if any, by the alternate path P_{alt}. Finally, there is the case when the radiation sources are placed in series. When this is done, there may be a possibility where a path is not found due to the intersection of only one pseudo obstacle with the boundary or two or more obstacles as shown in Figure I.3.21. The intersecting pseudo obstacle C_1 that can make the map disjoint is referred to as the *constricting pseudo obstacle*. Pseudo obstacles belonging to other sources (non-constricting pseudo obstacles) may have the potential to be grown further to reduce the cumulative dose by freezing the growth of the constricting pseudo obstacle in successive iterations until all the pseudo obstacles are found to be constricting, or have reached their maximum growth limit (dose at their circumference equals zero).

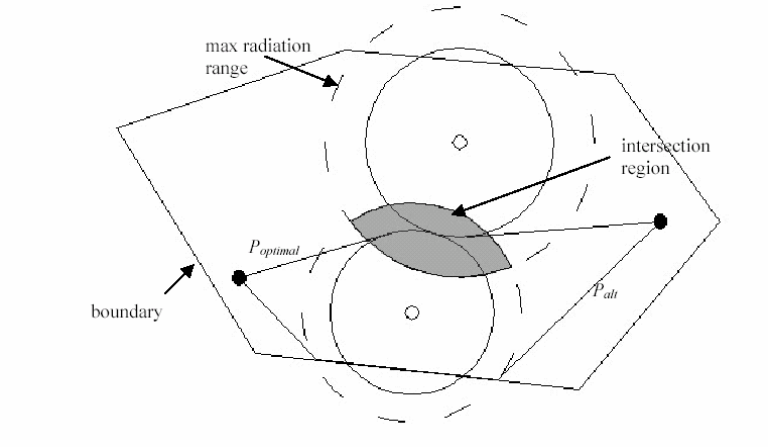

Figure I.3.20 Radiation sources placed parallel in a path between the start and goal points.

In Figure I.3.21, the circle C_2 may be expanded to its maximum limit C_3 after C_1 has been frozen in order to yield a safer path P_2 when compared to the path P_1 found at the point of constriction. Finding constricting pseudo obstacles is not a trivial task though. There may be two or more constricting pseudo obstacles in a single iteration that prevent a path from being found. In order to identify all these obstacles, first an intersection check is done to find a set S_c of all pseudo obstacles that have at least two points of intersection with the boundary, or intersect with two or more obstacles, or the boundary and at least one obstacle (including other pseudo obstacles). The path planner is then executed once for each of the pseudo obstacle in the set S_c. In each of these executions, one obstacle from S_c is retained in the map while all other obstacles belonging to S_c are removed from the map. If a path still does not exist under these conditions, the retained pseudo obstacle is considered as a constricting pseudo obstacle.

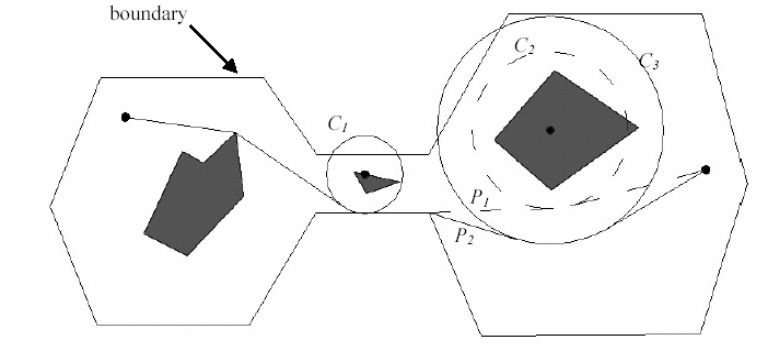

Figure I.3.21 A case with a constricting pseudo obstacle.

The algorithm described thus far is illustrated in the form of a flowchart in Figure I.3.22. A copy of the most recent successful path in the iterations is maintained in the variable *lastPath*. c*urrPath* represents the path found in the current iteration. *maxDose* is the intensity of the largest intensity radiation source, and dose Circumference is the intensity at the circumference of all the pseudo obstacles.

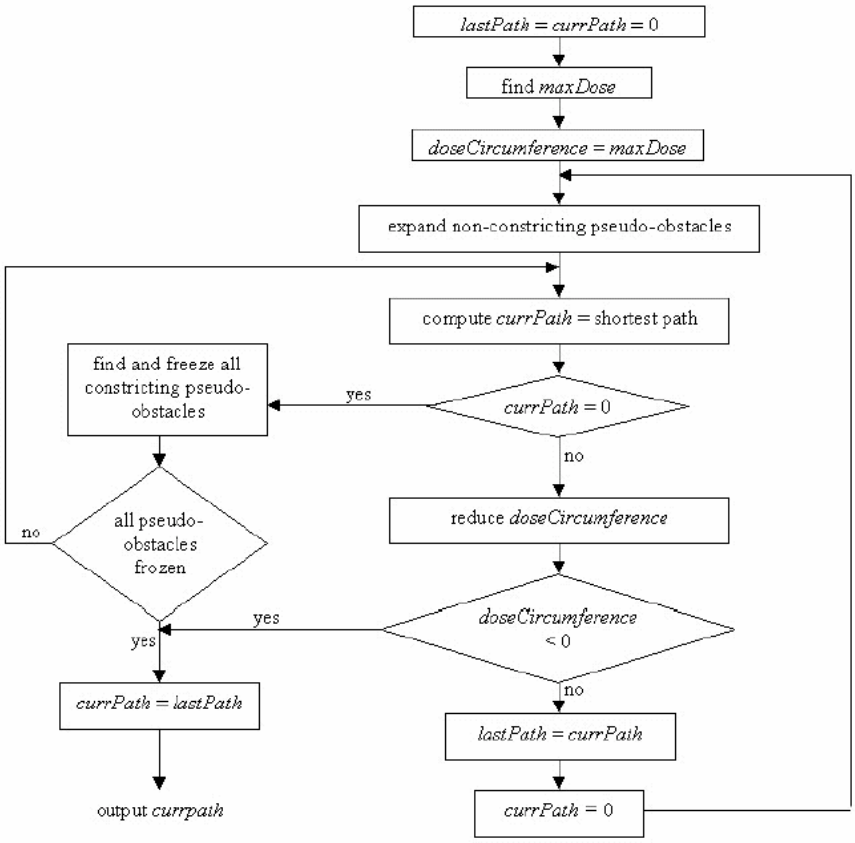

Figure I.3.22 Flow chart of the path planner with a radiation constraint.

I.3.19 Results And Conclusions

The algorithms were implemented in C and were tested with the help of an interactive graphical user interface developed in Java1.2. m. The interface was linked to the C implementation through the Java Native Interface for C. The C implementation was built on a simple and efficient data structure that is general enough to be used for other map based algorithms like the path sweep algorithm or path planning among moving obstacles.

Results from sample runs of both the path planner and the path planner with radiation constraints are shown below. Figure I.3.22 shows a path being generated among a set of expanded non-convex obstacles and a boundary. Pseudo obstacles are used to enforce the initial and final configurations of the robot.

Figure I.3.23 shows a case where a constricting pseudo obstacle's expansion is frozen while all the other pseudo obstacles are expanded to their maximum limit to yield an optimal path.

The path planner was also used successfully for online path planning onboard the UF Eliminator. The data from onboard sensors was discretized using image processing algorithms developed by Donald McArthur. The discretized map was then used to find a path to a local goal.

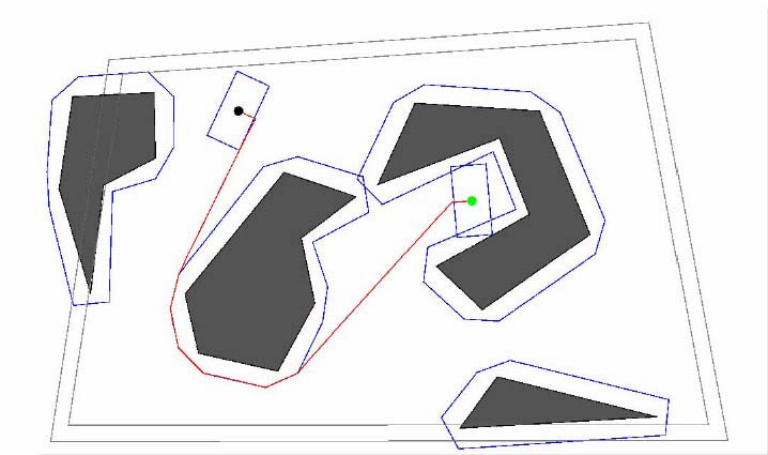

Figure I.3.24 Shortest path in a map with non-convex obstacles and a boundary.

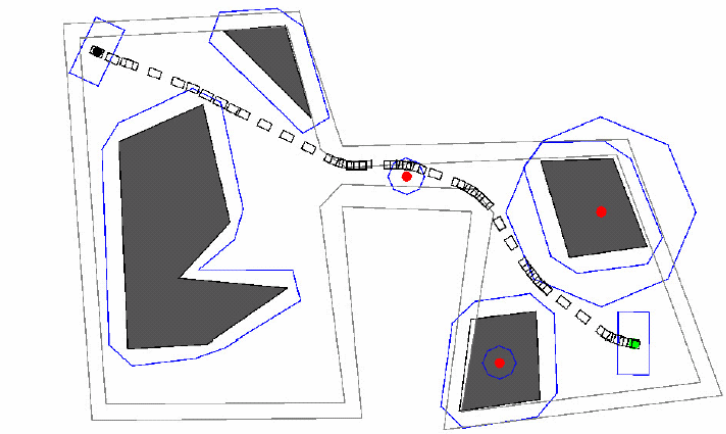

Figure I.3.25 A case with a constricting pseudo obstacle.

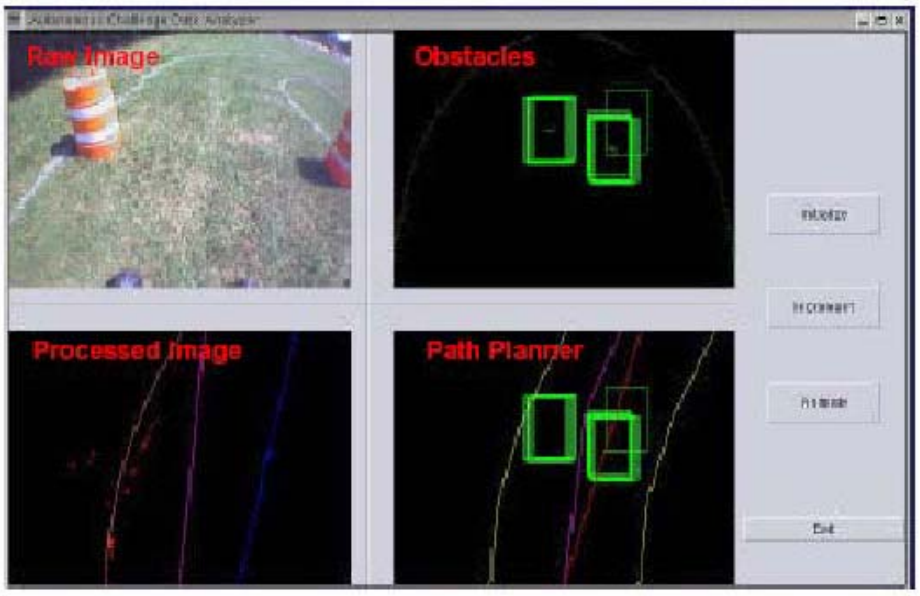

Figure I.3.26 Path planner used for online path planning.

I.3.20 Attenuation

By considering attenuation, a better approximation of the safest path may be achieved. Although the current implementation does not consider attenuation, a method that can be incorporated has been developed and is described here from a purely geometric perspective. The radiation intensity after attenuation for a point source of radiation is computed with the help of equation below

$$I_x = \frac{I_0}{x^2} e^{-\mu t}$$

where, t is the thickness of a homogeneous absorbing material with an attenuation coefficient μ. In Figure I.3.27, the intensity after attenuation at point P_1 along the horizontal can be computed using equation A.1, but at P_2 (which is at an angle *è* with the horizontal) the intensity is given by the equation following.

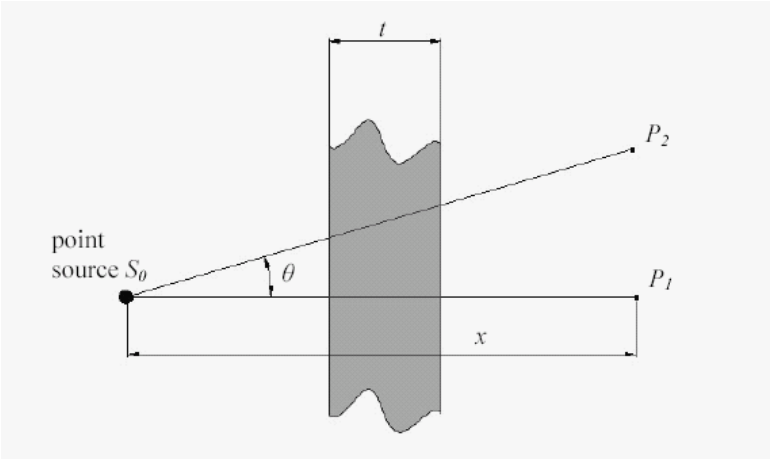

Figure I.3.27 Attenuation from a plane shield in front of a point source of radiation.

From the equation below, it is seen that if the effective distance traveled by a ray inside the shielding material can be found, and if the attenuation factor of the material is known, the intensity of the radiation at a point on the other side of the shield can be computed. In the case of a map with obstacles and radiation sources, the effective distance can be found if we can find the edges of the obstacles that attenuate the rays passing through them for each ray from the sources to points on the path. These edges can be found by applying the radial sweep line algorithm used in the path planner to compute the visibility graph.

$$I_{p2} = \frac{I_{s0}}{(x \sec \theta)^2} e^{-\mu t \sec \theta}$$

Thus the path planning algorithm has proven its ability to affect a simple and efficient data structure that is general enough to be used for other map-based algorithms, like the path sweep algorithm or path planning among moving obstacles. The algorithm has successfully designed the safest radiation path from a given start configuration to a goal configuration of a vehicle moving only forward in a radiation environment cluttered with obstacles bounded by simple polygons.

I.4 Optimized Waste Container-Packing

A new solution to the two dimensional bin packing problem is presented. The purpose of this implementation is to better understand the problem and to assess the previous work. However, instead of simply reprogramming the previous implementation, a new but similar approach was created.

I.4.1 Problem Statement

Two dimensional bin packing problem is defined as follows: given n two dimensional shapes {p1, p2, p3… pn} each one with size S = {s1, s2, s3 … sn} and a container C with a fixed width and infinite height, find a placement of the n shapes such that the void or unused area in the minimized.

The Waste Container-Packing problem belongs to a general class called combinatorial optimization problems. Combinatronics is a mathematical field of study that deals with finding an arrangement and selection of given objects. The main difference between combinatronics and combinatorial optimization is that in the former one wishes to answer a decision question such as if a particular arrangement of the input objects exist. On the other hand, combinatorial optimization tries to find the optimal arrangement of such objects for a specified objective function, which usually takes the form of minimization or maximization.

Most combinatorial optimization problems are *NP-Hard*. *NP* (non polynomial) optimization problems are said to be non-solvable in polynomial time $O(n^k)$ for some constant k. Another class of problems known as *NP-Complete* are those decision problems that cannot be solved in polynomial time but there exist a polynomial time algorithm that can check the correctness of a given input. An optimization problem is said to be *NP-Hard* if its associated decision problem is *NP-Complete*. Furthermore an optimization problem is Strongly NP-Hard if its associated decision problem is still *NP-Hard* even when the input is bounded. The geometric three dimensional bin packing problem belongs to the complexity class *Strongly NP-Hard*, since its associated combinatronic decision problem is still *NP-Hard* even when bounding the volume of the container and the input objects.

There are multiple instances of bin packing such as the knapsack problem which is a one dimensional variant, stock cutting problem which is two dimensional in nature and three dimensional packing which takes objects in Euclidean representation. The general form for the three dimensional bin packing takes the objects of arbitrary shapes and sizes. There are several reductions from the general case which restrict the objects to predetermined shapes such as cubes, boxes, convex hulls, or any other geometric representation.

I.4.2 Bin Packing Applications

The goal of this research is to provide a 3D bin packing algorithm that can be used in nuclear waste sites. The general bin packing problem has many other uses outside this specific task. The most notable one is on any packing related task. Industries that directly relate to such ways of optimization are postal services such as UPS and FedEx, and transportation industries such as airlines, trains, freighters, etc. Bin packing is also related to the manufacturing industry in Rapid Prototyping [IB97] and stock cutting. Another area that is recently being explored is that of 3D product layout. Most of these applications are being derived from the work of Szykman and Cagan [Sy95] which are being geared towards computer chip layout, mechanical assemblies, aerospace applications and automobile engine compartments.

I.4.3 Approximation Algorithms

Even though there is no proof to support the claim that *NP* problems can be solved in polynomial time there is abundance of evidence that suggest the opposite. One only has to consider the many *NP* problems that have been studied and no polynomial algorithm has ever been developed. Many scientists believe that in fact there is no such solution and it is because of this that other strategies have been developed that can find a near optimal and in some cases optimal solutions to these kind of problems in polynomial time. These algorithms are called, appropriately, approximation algorithms and they have proved to be very useful in approaching *NP* problems. There are two kinds of approximations algorithms: deterministic and non-deterministic or randomized algorithms. As the name implies the solution of deterministic approximation algorithms does not change for a specified input. On the other hand the outcome of randomized approximation algorithms can vary for a pre-specified input in the same number of runs. Or to put it in another way a randomized approximation algorithm can obtain the same solution for a given input but with varying running times.

An approximation algorithm can be measured by the amount by which the approximated solution relates to the optimal solution. This amount is called the *performance ratio* or ρ(n). Generally speaking for any input n the performance ratio of an approximation algorithm is defined below.

Maximization Problem:

$$\rho(n) \geq \frac{C^*}{C} \qquad \text{for} \qquad 0 < C \leq C^*$$

Minimization Problem:

$$\rho(n) \geq \frac{C}{C^*} \qquad \text{for} \qquad 0 < C^* \leq C$$

Where C and C^* are the approximate and optimal solutions respectively. Notice that ρ(n) is always greater than 1 since if ρ(n)=1 implies that $C=C^*$ which implies the algorithm obtained an optimal solution and therefore is no longer an approximation.

A *(1+ε)-approximation algorithm* has a performance ratio that is ε apart from the optimal, for some ε>0. This notation usually denotes an approximation scheme for a particular approximation algorithm. If for some specified ε the algorithm runs in polynomial time then we call this a *(1+ε)-polynomial approximation scheme*. Notice that the running time will increase as ε is decreased since we are that much closer to the optimal solution. When ε is decreased by a constant factor and its corresponding running time increases by a constant factor as well the algorithm is said to be a *fully polynomial approximation scheme*.

We limit the topic of approximation algorithms to randomized or non-deterministic ones since they offer the most promise in terms of the problem at hand. In fact there are already implementations for the three dimensional bin packing problem based on simulated annealing and genetic algorithms.

I.4.4 Monte Carlo Simulation

Monte Carlo methods provide a way of simulating a physical process. As long as we can relate the sampling variable with a random number we can simulate the intrinsic process. As a basic example consider the following problem:

Find the probability density function of the sum of two six sided fair dice.

The theoretical solution to this problem is well known and follows from basic statistical knowledge. Each dice has six faces therefore N1 = 6 and N2 = 6. The total number of events are

N=N1*N2 = 36. The discrete probability is equal to $p_i = 1/36$. Table I.4.1 shows these 36 possibilities.

Table I.4.1

1,1	2,1	3,1	4,1	5,1	6,1
1,2	2,2	3,2	4,2	5,2	6,2
1,3	2,3	3,3	4,3	5,3	6,3
1,4	2,4	3,4	4,4	5,4	6,4
1,5	2,5	3,5	4,5	5,5	6,5
1,6	2,6	3,6	4,6	5,6	6,6

If we sum the dice for each outcome we come up with the probability for the sum of the two dice as shown in Table I.4.3.2-2.

Table I.4.2

n1+ n2	p(n1+n2)
2	1/36
3	2/36
4	3/36
5	4/36
6	5/36
7	6/36
8	5/36
9	4/36
10	3/36
11	2/36
12	1/36

To obtain this probability density function via simulation one must first find a way of simulating the discrete probability density function depicted above. For discrete random variables distributed uniformly the sampling uses the following function:

$$n = INT(N * \eta) + 1$$

Where n is the sampling random variable, N is equal to the total number of possible outcomes, η is a random generated number between 0 and 1. The INT function truncates the calculated number to its integer. For our case N = 36, and the above function uniformly outputs a number between 1 and 36. Therefore we have a way of randomly outputting numbers between 1 and 36 and each one represents a possible outcome of the throw of two dice. Using the sample r.v. we can look up the associated outcome by numbering all the cells of the matrix shown in table x.1 from 1 to 36 (we can number it row by row or column by column, for this example we use the latter one). For example let's say we the computer generated the random number $\eta = 0.3745$, then:

$$n = INT(36 * 0.3745) + 1 = 14$$

Therefore our random variable came to be 14 and by looking up Table I.4.1, event 14 corresponds to drawing a 3 on the first dice and a 2 on the second and the sum of the two dice was 5. If we repeat this process thousands of times and count the number of times each of the possible outcomes was drawn we will end up with the same Table I.4.2. A flowchart for this simulation is presented in Figure I.4.1

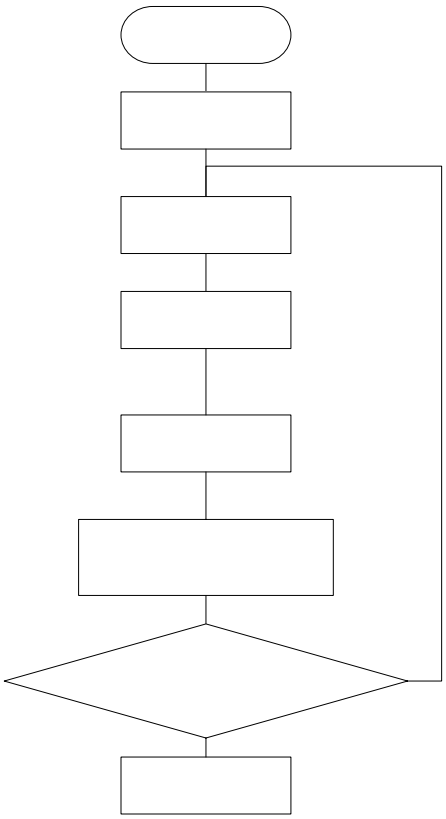

Figure I.4.1

Of course this is a very simple problem and only considers uniformly distributed random variables, but it is enough to give the reader a basic understanding of what a Monte Carlo simulation is and their relevance in sampling the solution space of a given problem.

I.4.5 Metropolis Algorithm

In 1953 a researcher tried to simulate the energy states of a solid which was subjected to heat and slowly allowed to reach equilibrium [Me53]. The simulation would generate a series of states based on Monte Carlo. The main difference was the method incorporated to accept or reject the generated state. Each state had an associated energy and the next state would be accepted depending on the following perturbation function:

$$p = e^{-\frac{(E_2 - E_1)}{K_B T}}$$

Where E_1 and E_2 represent the current and proposed next energy state of the system, K_B is the Boltzmann constant, and T the current temperature. Named after its creator the procedure is called the Metropolis Algorithm.

I.4.6 The Simulated Annealing Algorithm

Thirty years after the inception of the Metropolis Algorithm a connection was made between the physical state of the solid represented by Metropolis and the solution to an optimization problem [Ki83]. The physical state would represent the solution to the optimization problem and the energy associated with this energy state would represent the cost of the objective function. Since the acceptance of a specified state is associated with the perturbation function, the simulated annealing process can sometimes accept inferior solutions. This capacity allows the algorithm

search the solution space more extensively since it has a device that lets it escape local minimums. The annealing process then becomes lowering the temperature of the perturbation function slowly enough to let the solution come to "equilibrium." On a simulated annealing algorithm the temperature will start off high giving the algorithm the opportunity to search large areas of the solution space. As the temperature is lowered the probability of accepting inferior states is reduced which lets the algorithm to find good local minimums and possibly a global optimum. In fact if the temperature is lowered slowly enough the algorithm will find the global optimum but this process may take a large amount of time. The simulated annealing algorithm can be found here [Sa99].

Szykman and Cagan at Carnegie Mellon University developed a simulated annealing algorithm for the three dimensional packing problem [Sy95].

I.4.7 Genetic Algorithms

The Genetic Algorithm is based on survival of the fittest for searching the solution space of a given optimization problem. On a genetic algorithm the population is encoded by a series of strings which represent points from the solution space. The population is then sampled which will provide a set of parents and a new offspring is generated by crossing the selected parents. The offspring is then reintroduced to the population and the process is repeated.

In a genetic algorithm a possible solution is usually represented by a chromosome and its constituent parts are called genes. The values a specified gene can take are called the alleles. Each chromosome has an associated fitness value. Just as in simulated annealing the state represents a possible solution and its associated energy the cost of the objective function, in GA the chromosome represents a particular solution and its fitness value the associated cost. A typical GA algorithm first generates a population by randomly assigning alleles to the genes of the chromosomes. The fitness value for each of the chromosomes is then evaluated. Chromosomes are then selected by a process called reproduction. The chromosomes are selected at random but there is a higher probability to select chromosomes with higher fitness values. Once the chromosomes are selected they undergo crossover and mutation procedures to produce an offspring. In crossover certain genes from each parent chromosome are passed to the offspring. This procedure is usually done by a crossover operator. There are multiple crossover operators but all of them have the property of producing offspring with segments of the parent's chromosomes. The resulting chromosome from the crossover procedure is then subjected to a mutation function which with some probability will swap genes of the offspring. Finally the fitness value is calculated and offspring is introduced to the population and the procedure repeated.

Genetic Algorithms have some desired properties that make them very useful for searching the solution space. The most obvious one is their simplicity to implement. In addition GA's do not have any limitation with respect to the solution space such as continuity, gradients etc. Also since each iteration (Reproduction, Crossover, and Mutation) is independent from the previous one, unlike simulated annealing, the process of searching the solution space is more extensive and theoretically the algorithm can avoid being trapped on a local minimum with ease.

There are two implementations of GA for bin packing problems. The first one was done by Ikonen [Ik98] for three dimensional bin packing. Pasha [Pa03] developed a hybrid GA for the two dimensional bin packing problem.

I.4.8 Tabu Search

First introduced by Glover in 1989 and thoroughly explained here [Gl97], Tabu Search is a generalized form of the local search algorithm. In local search a region of the solution space is searched, if a solution is found to be better than the existing one then the new solution is accepted. This process is repeated until no more better solutions are found. The basic flaw of local search,

and that which Tabu Search builds on, is that on local search there is no way for the algorithm to exit the region which is currently exploring, thus it will always converge to the optimum of that region which in most cases is a local optimum. One key feature of Tabu Search is the fact that it contains a memory of the search space which was visited. Simulated Annealing and Genetic Algorithms do not posses this property since the process is completely probabilistic and thus a solution could be visited more than once, thus affecting their running time.

The algorithm starts with a feasible solution to the problem at hand. A neighborhood that surrounds that solution is generated and a sample of solutions from that region is compared. The best solution from that sample is taken as the current solution if certain criterion is met. Notice that the new solution does not necessarily have to be better than the original one. To prevent cycling, that is revisiting a previous solution; Tabu Search maintains a list properly called *Tabu List* which ensures this from happening. A Tabu List stores the move properties from going from one solution to the next one. Therefore the move properties of the candidate for the current solution can't be on the *Tabu List*. However an unvisited solution may have the same move attributes as a previously visited one. To allow the algorithm to explore these solutions, the candidate solution is subjected to an *aspiration criterion*. There are several *aspiration criterions* but the most common one is that the solution of the candidate is better than the current best solution. The process can now be summarized as follows:

Starting from a feasible solution S_0, generate a neighborhood of that solution $N(S_0)$. Take a sample of solutions from $N(S_0)$ and select the best solution S from that sample as the candidate. Next the move attributes of S are checked in the *Tabu List*. If the attributes are not listed then take S as your new current solution. If the attributes of S are in the *Tabu List* then check the *aspiration criterion* for your algorithm and this will decide whether or not to accept S. Ultimately if S is accepted then its move attributes are added to the *Tabu List* and S is taken as the current solution for the process to be repeated. If S is not selected then the moves are regenerated for a new sample of solutions. The algorithm repeats this process until some stopping criteria is met.

I.4.9 Simulated Evolution

Genetic Algorithms take their inspiration on survival of the fittest to pass good qualities to their offspring; on the other hand Simulated Evolution is based on the adaptation or evolution of organisms for a better chance of survival. Simulated Evolution first appeared on the work of Kling and Banerjee [KB87] and shares much of the properties of SA and GA. In a Simulated Evolution (SimE), a population is randomly generated which satisfies the constraints of the problem. Notice that unlike GA in SimE a population is actually one solution to the problem and contains within it individuals which make up the solution. The population is then subjected to *Evaluation*, *Selection*, and *Allocation* operators. *Evaluation* calculates the goodness of each of the individuals that make up the population. The goodness is defined as the ratio of an estimated cost of the individual and the actual cost of such individual on its current location within the entire population. The goodness as much of the inner workings of this algorithm depends greatly on the problem at hand. After *evaluation* the population is subjected to a *selection* process which basically partitions the population into two sets based on their individual goodness values. The two sets are called selection and remaining sets. The process of *selection* is non-deterministic since there is a probability associated with the selection. Of course just as GA the higher the goodness value the higher the probability of not being selected. Once the two sets are generated it is the *allocation* operator's job to generate a new population by mutating the selected partition of the population. The allocation will move the locations of the selected set by performing a number of trials and selecting the best among the ones sampled. The number of trials usually starts of high and steadily

decreases as new populations are generated. Finally once the *allocation* process produces the new population the process is repeated until some stopping criteria is met.

I.4.10 Stochastic Evolution

Stochastic Evolution is the work of Youssef Saab [Sa89]. As all the algorithms presented here Stochastic Evolution is a search technique for approximating a combinatorial optimization problem. A combinatorial optimization problem is given as follows (from [SY99]):

Given a finite set M of movable elements and a finite set L of locations, a state is defined as a function $S:M \rightarrow L$ satisfying certain constraints.

The algorithm uses a variable ρ which decides when to stop the algorithm. The variable R represents the number of iterations that the algorithm will require to improve the current solution. The variable is dynamic and depends on the algorithm finding better solutions. The variable p is used to determine if a solution that is worse than the current one should be accepted. This variable gives the algorithm the ability to escape local minimums.

At first an initial feasible state S_0 is provided as input along with the parameters R, ρ, and p. The cost of S_0 is calculated and stored and a function called PERTUB is called. PERTURB then makes trial moves of the objects to new locations thus generating new states. Each move has a gain which is calculated as the difference in the cost of the current state and the new state generated by PERTUB. The new state is then accepted if the gain is greater than a random number generated between –p and 0. Since the random number is negative all the moves that lead to a positive gain are automatically accepted, but accepting an inferior move, one that has negative gain, still plausible. If the new state is accepted a function called MAKE_STATE ensures that constraints are met and if not reverses the moves generated by PERTURB until the constraints are satisfied. If the new state is accepted its cost is compared to the cost of S_0, the original state cost, and if the cost is the same the value of p is increased by some factor. What this means is that there is the possibility that the algorithm has reach a minimum and has no way of getting out of it, therefore p is increased to give more opportunity to the algorithm to search elsewhere. After this the cost of the new state is compared to the best cost obtained so far. If the new cost if better than the best so far the value of ρ is decreased by R, otherwise ρ is incremented. This process is then repeated until ρ is greater than R.

By using this scheme the algorithm becomes dynamic since the stopping criteria vary depending on the success of the algorithm. At the initial iterations the algorithm will always find better solutions therefore the number of iterations to run will increase. As the algorithm progresses more and more local optimums will be found and the chances of finding a better local optimum than the current one decrease, thus the remaining iterations are lowered since the algorithm may have reached an optimal or near optimal solution.

I.4.11 Ant Colony Optimization

Ant Colony Optimization ACO is based on the observation on how ants find the traveling path between the nest and a food source. In real ants this path tends to be the shortest one. The reason behind this is based on the pheromone trail each ant leaves behind as it walks. Consider a nest and two paths that lead to a food source. Initially the first ant that arrives at the intersection of the paths will choose either one of them with uniform probability. As more and more ants traverse the same path more pheromones are deposited in the paths, however the shortest path will eventually carry more pheromones since the returning ants are also leaving pheromones, thus the shortest path will have higher concentrations of pheromones.

Dorigo and Caro found an analogy between an optimization problem and the way ants behave and in 1999 published their results [DD99]. A simplified version of ACO will be presented

next for the case of finding the shortest path between two nodes of a graph. We can define the graph as G = (V,E) with n vertices and m edges also denote the source and destination vertices as s and d respectively. Each edge of the graph will carry a variable p(i,j) which represents the artificial pheromone that is present in edge E(i,j). Each ant will start at s and from there individually will select an edge to take. The selection process is based on probability and the amount of pheromone present in the outgoing edges of the current vertex. Once the ant has selected an edge to traverse it will add a small amount of artificial pheromone to the already existing quantity the edge already has.

However using this method alone can lead to local optimums and a limited exploration of the solution space, therefore a mechanism that allows the ants to travel to some other path must be in place. This mechanism was also taken from the ant's analogy since the deposited pheromones will eventually evaporate. This leads to an evaporation function of the amount of artificial pheromones associated with each edge. At each iteration of the main algorithm the amount of pheromone present in each edge p(i,j) is reduced by a percentage ρ. The evaporation function allows the ants to search other less visited routes and search more of the solution space. This method is in actuality referred to as the Simple Ant Colony Optimization and a more general technique for combinatorial optimization is presented here [DD99].

I.4.12 Particle Swarm Optimization

Particle Swarm Optimization takes its inspiration from birds flocking and fish schools and it was first introduced by Eberhart and Kennedy in 1995 [EK95]. The birds or particles represent solutions to the problem. Clearly of all the particles there will be some which have better solutions than the rest. At each iteration the move of a particle is updated such that is closer to the particles that have the best solution so far. This allows the algorithm to search the solution space and as the number of iterations progresses get closer to an optimum. Each particle carries with it two values. The first one is the best solution obtained so far from by the individual particle. The second value is the overall best solution among all the particles.

Using these two values the velocity of each particle is updated using the following equation:

$$v(i) = v(i) + c_1 * \eta_1 * (pbest(i) - p(i)) + c_2 * \eta_2 * (gbest(i) - p(i))$$

Where v(i) is the velocity of the particle, pbest represents the best value obtained by the i^{th} particle, gbest is the overall best solution, η_1 and η_2 are generated random numbers, and p(i) is the present value of the current particle. The position of the particle is then updated as follows:

$$p(i) = p(i) + v(i)$$

Once the position (or solution) for each particle has been updated, pbest and gbest are calculated once more and the process is repeated.

I.4.13 Problem Solution Approach

Throughout this work the term part is referred as a two dimensional non-intersecting polygon which is one of the objects to be packed. A container is referred to as the place where the parts will be placed into. The container also contains a profile which is the collection of previously packed parts and where the next incoming part will be placed onto.

The proposed approach involves the decoupling of the problem into two separate problems: offline ordering and online placement. Online placement deals only with the placement of one single incoming part into the existing profile. The offline placement problem objective is to minimize the void or non-utilized area of the incoming part, without any knowledge of the subsequent parts only the current one. The offline ordering problem deals with the generation of good orderings of parts to be placed. In this work a Simulated Annealing – Genetic Algorithm (SA-

GA) hybrid technique will be used for the offline ordering while a heuristic will be used for online placement.

Figure I.4.2 shows the general layout of the proposed algorithm. Initially a random ordering is randomly generated (2,1,3 in the Figure). This ordering is passed to the online placement heuristic which packs the objects and returns the void area associated with that ordering. The online algorithm takes this void area and evaluates a new ordering (3,2,1 in the Figure) based on the parameters set by the SA-GA technique. This new ordering is passed to the placement heuristic and a new void area is obtained and the process is repeated.

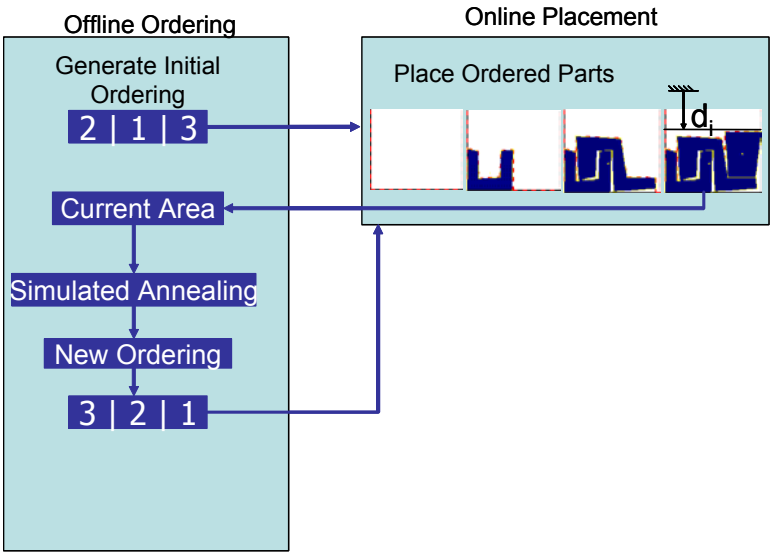

Figure I.4.2: Proposed algorithm general structure.

I.4.14 Online Placement Heuristic

The placement heuristic is based on the proof by Sitharam and Wu for Two Dimensional Non-Oriented Placement. The proof takes into consideration two piecewise linear functions f(x) for the part and g(x) for the profile. The proof shows there are at most m+n breakpoints as the part travels thru the profile and that the minimum area exists in one of these breakpoints, where m and n are the number of vertices of the part and profile respectively. The case is non-oriented which means that rotation of the part is not considered. Figure I.4.3 shows the succession of moves a part needs to take as it travels thru the associated breakpoints.

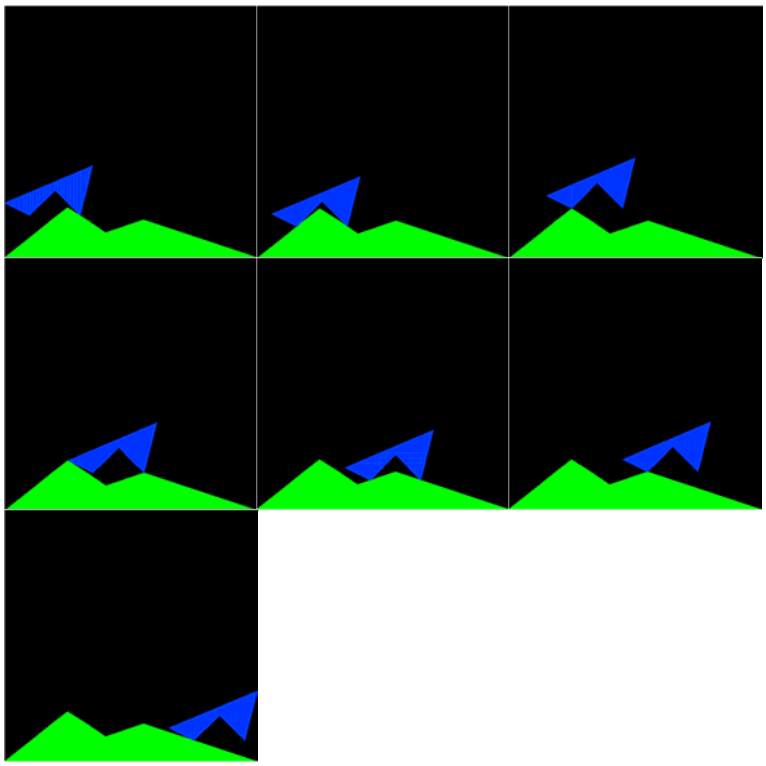

Figure I.4.4: Succession of moves as a part travels thru the profile across the associated breakpoints.

The proposed placement heuristic builds on top of this proof by initially aligning each of the edges of the part with each of the edges of the profile and running the non-oriented placement heuristic. Pseudo-code 3.2.1 which shows the online heuristic is given below:

```
Begin
{
   Do for all edges in profile
   {
         Do for all edges in part
         {
               alignPart( part edge, profile edge)
               place2Dnon-oriented(part)
         }
   }
}
```

Pseudo-Code I.4.1: Proposed Online Placement Heuristic

I.4.15 Offline Ordering Algorithm

A simulated annealing algorithm is used to generate the next ordering based on the void area of the previous ordering. In simulated annealing an initial ordering or state is generated. The void area of this ordering is generated by passing the ordering to the placement heuristic. The annealing temperature is initialized and the algorithm goes into a loop. Inside the loop a new ordering is generated by using the move function (which will be explained later on). The area associated with this new ordering is obtained by passing the ordering to the placement heuristic. If the new area is

less than the current area the new ordering is accepted. However if the new area is less than the current one the area is accepted based on the following probability function:

$$\Pr = e^{-\frac{NewArea - CurrentArea}{T}}$$

where T is the annealing temperature. This probability of accepting an inferior move or ordering gives the algorithm a hill climbing property, i.e. allows the algorithm to search some other areas of the solution space in hopes of finding the global optimum and a recourse to get out of local minima. High annealing temperatures will yield higher probabilities of accepting an inferior move whereas lower temperatures will in turn lower this probability. Initially the annealing temperature is set high and as the algorithm progresses this temperature is lowered by an annealing schedule function. This allows the algorithm to perform a global search initially and as the temperature is lowered the search will be local around the best solution obtained so far. The simulated annealing general structure is given in pseudo-code I.4.4-2 below.

```
Begin
{
   current ordering = random initial ordering
   current area  = placementHeuristic( current ordering )
   T = initialize_temperature
   begin outer loop
   {
      begin inner loop
      {
         new ordering = move( current ordering )
         new area  = placementHeuristic( new ordering )
           if(new area < current area)
              current ordering = new ordering
           else if( rand()<exp(-(current area – new area)/T))
              current ordering = new ordering
           check_inner_loop_termination()
      }
     reduce_temperature(T)
     check_outer_loop_termination()
   }
}
```

Pseudo-Code I.4.2: Simulated Annealing General Structure

I.4.16 Annealing Schedule

The annealing schedule dictates how the initial temperature is chosen and how the temperature is lowered as the algorithm progresses. The most general one is known as fixed annealing schedule and as the name implies the temperature is lowered by a constant factor M which has typical values that range from 0.9 to 0.99:

$T_{i+1} = T_i * M$

The major problem for this type of schedule is that is does not take into account the nature of the problem at hand. For this purpose an adaptive annealing schedule was developed. On this schedule the initial temperature is given as a function of the problem standard deviation as follows:

$$T_i = \frac{-3 * \sigma}{\ln(P)}$$

Where σ is the standard deviation of the problem which is obtained by performing a random walk through the solution space accepting every move or ordering and P is a user defined parameter with recommended values around 0.85 to 0.9. Subsequent temperatures are generated from the following formula:

$$T_{i+1} = T_i + e^{\frac{-\lambda * T_i}{\sigma}}$$

The value of λ is another user defined parameter with recommended values around 0.7. The benefit of this annealing schedule is that it provides a better probability which depends in part on the standard deviation of the problem.

I.4.17 Move Function

The move function generates a new ordering based on the previous one. A typical move function for the geometric bin packing where the problem is not decoupled (i.e. there is not subdivision of online and offline problems) involves translation, rotation and swap in place of the three dimensional parts. For the decoupled case there is no actual geometry to consider only orderings. For this case the move function has only to generate a new combination of parts based on the previous one. To this end a concept from genetic algorithms was used to generate the new ordering.

Genetic algorithms are based on survival of the fittest. A normal GA has an initial population and from it pair of individuals is selected to act as parents. The parents reproduce and a new offspring is formed and added to the population. In the context of orderings of parts, the population is a subset of all the possible orderings that the problem posses (n!). A specific ordering will then be an individual. Two individuals (orderings) are selected and reproduced. The reproduction involves crossover, mutation and other operators to which the offspring can be subject to. Typically as the algorithm progresses the offspring will posses the good qualities of the parents and discard the bad ones.

Among the different operators an offspring can be subject to there is one in particular that has proven very useful in large combinatorial problems such as bin packing and the traveling salesman: The Inver-Over Operator. The best way of explaining how this operator works is through an example: The operator has an active part called p a current ordering S and an inver-to part called p'. The operator also has a parameter ρ which determines if the new ordering will be generated by using solely the current ordering S or by using another randomly generated ordering S'. If the individual creates a new ordering based solely on itself the reproduction is said to be asexual, whereas if it needs another individual is said to be sexual.

Suppose the current ordering is given by S = (2,3,9,4,1,5,8,6,7) and that the active part p is 3. A random number between 0 and 1 is generated and if that random number is less than ρ the reproduction is asexual. Let's assume that the reproduction is asexual for this case. A inver-to part p' is then randomly selected from the remaining parts from S=(2,9,4,1,5,8,6,7). Assume p' is 8, then the new ordering is the current ordering with the numbers from 9 until 8 inverted. The new ordering is S = (2,3,8,5,1,4,9,6,7) and the new active part is p=p'=8. Since the algorithm will continue until there are no more inversions a new random number has to be generated and compared to the ρ parameter.

Let's assume that this time the random number is greater than ρ, this means that the current reproduction will be sexual. A new individual S' is selected from the population: S'=(5,6,4,3,1,7,9,2,8). The inver-to part p' is then selected as the part from S' next to the active part

p=8. The part next to 8 in S' is 5. Going back to S the parts in S are inverted from the number next to p up to p'. In this case the part next to p in S is 5 and since p' is 5 as well the operator ends and the new ordering is S = (2,3,8,5,1,4,9,6,7).

The pseudo code for the operator is given below:

```
current state S
begin
{
        randomly select a part p from S
        begin loop
        {
                if(rand()<ρ)
                        select p' from S
                else
                {
                        select a new state S' from P
                        assign p' to the next part to the part p in S'
                }
                if(p'==p+1 || p'==p-1)
                        exit loop
                inverse the section from p+1 to p' in S
                p=p'
        }
}
```

Pseudo-Code I.4.3: The Inver-Over move function.

I.4.18 Implementation

The proposed approach is currently being developed in Linux. The program is written in C++ which should improve the performance over the previous implementation's Java code. The graphical user interface uses Lesstif and Open Inventor for the on-screen 2D graphics. The simulated annealing, inver-over operator and randomized ordering part of the code are already developed, and work is underway in the online placement heuristic. The following figures depict a single part being placed on the profile. Figure I.4.5 presents a general view of the program with a drawn part.

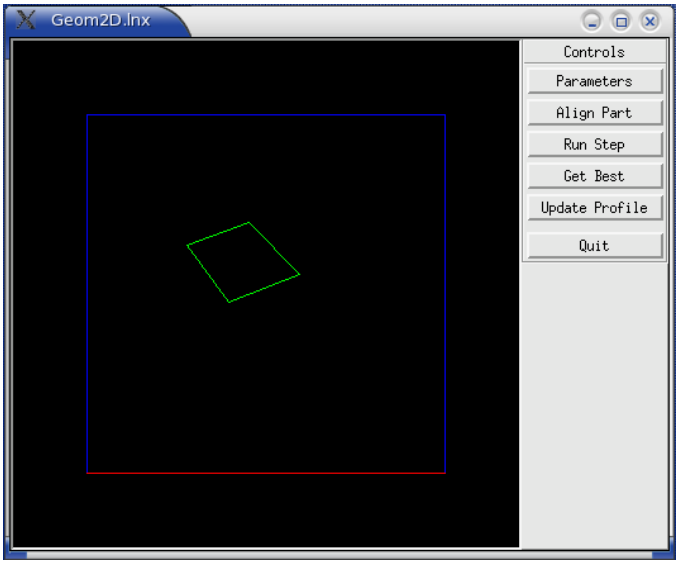

Figure I.4.5: General View

The align part button shows the functionality of the written code to align each of the edges of the part with each of the edges of the profile. Figure I.4.6 shows the drawn part of the previous figure after one of its edges was aligned with the profile. The part was placed on the profile and the best placement is shown in Figure I.4.6. Figure I.4.7 shows the updated profile with the placed part added to it.

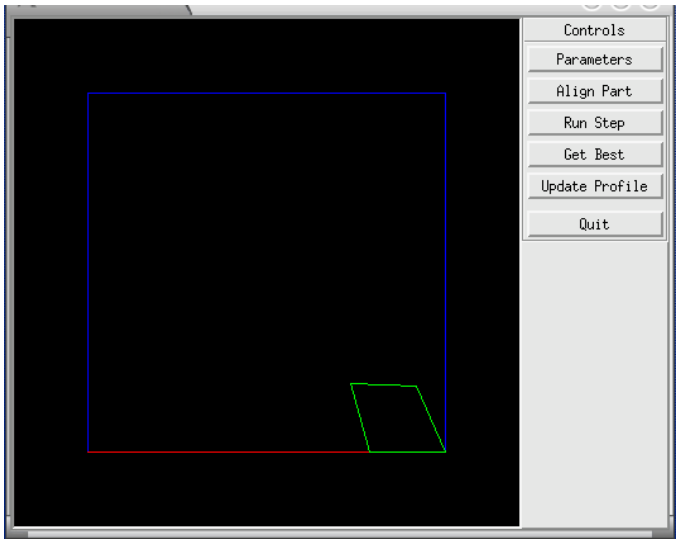

Figure I.4.5: After one edge was aligned with the profile

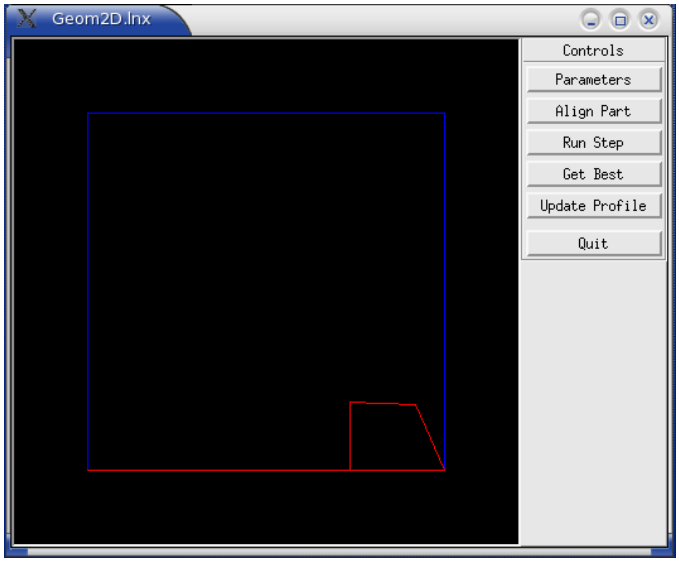

Figure I.4.6: The best placement

The align part button shows the functionality of the written code to align each of the edges of the part with each of the edges of the profile. Figure I.4.7 shows the drawn part of the previous figure after one of its edges was aligned with the profile. The part was placed on the profile and the best placement is shown in Figure I.4.7. Figure I.4.8 shows the updated profile with the placed part added to it.

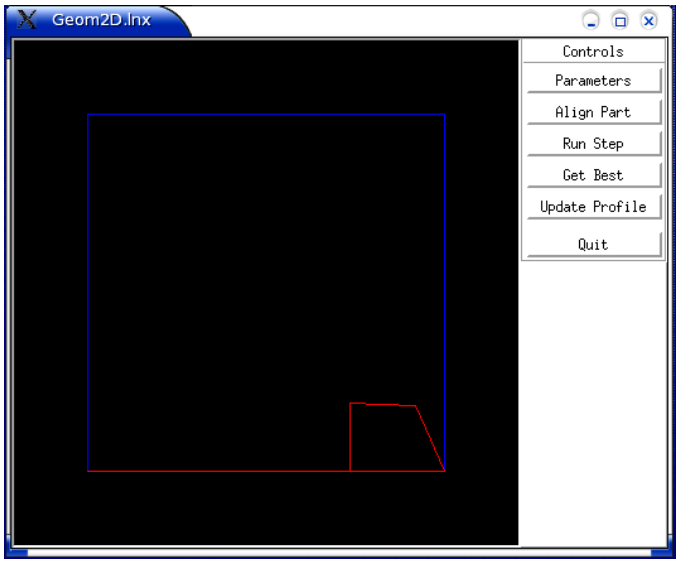

Figure I.4.8: The updated profile with the placed part added

I.4.18 Conclusions and Discussion

A packing algorithm was developed and implemented using a hybrid approach in the form of SA-GA. The results do show a performance improvement over the previous implementation, partly due to the language used which was c++ that does have a computing advantage over Java code. Since the program ran on a Linux emulation on top of Windows one can expect a faster code if it's allowed to run natively on the system instead of an emulated one. However the performance increase is too big to credit just to the advantageous C++ code and more testing will need to be conducted to allow for a fair comparison. Additional work must be done to give some meaning to the annealing temperature in relation to any specific scenario. This will be done using the adaptive annealing schedule that was described in this work instead of the fixed one that was used.

II.1 Force Reflecting Controller Development

II.1.1 Objective

This research concentrates on the geometric stability of parallel platform based manipulators. The aim is to develop a reconfigurable device that can attain any desired compliance matrix relationship (the compliance matrix relates the displacement of the top of the platform to the force/torque applied to the top of the platform). A variable-damping device will be designed and built to adjust the damping of the connectors in real-time. The best candidate device used to achieve variable-damping is the magnetorheological (MR) damper.

II.1.2 Background

Semi-active control has recently been an area of much interest because of its potential to provide the adaptability of active devices without requiring a significant external power supply for actuators. A semi-active control system cannot provide energy to a system comprising the structure and actuator, but by altering the properties of the system, such as stiffness and damping, it can achieve favorable results[1]. Unlike an active system, the control forces developed are related to the motion of the structure. Furthermore, the stability of the semi-active system is guaranteed as the control forces typically oppose the motion of the structure[2].

The robustness and the simple mechanical design of magnetorheological (MR) dampers make them a natural candidate for a semi-active control device. They require minimal power while delivering high forces suitable for full-scale applications. They are fail-safe since they behave as passive devices in case of a power loss[3]. The focus of this report is to review models that effectively predict the behavior of magnetorheological devices while giving preliminary test results from an MR damper designed and built.

MR fluids are suspensions of small iron particles in a base fluid. They are able to reversibly change from free-flowing, linear viscous liquids to semi-solids having controllable yield strength under a magnetic field. When the fluid is exposed to a magnetic field, the particles form linear chains parallel to the applied field as shown in Figure II.1.1. These chains impede the flow and solidify the fluid in a matter of milliseconds. This phenomenon develops a yield stress which increases as the magnitude of the applied magnetic field increases[4].

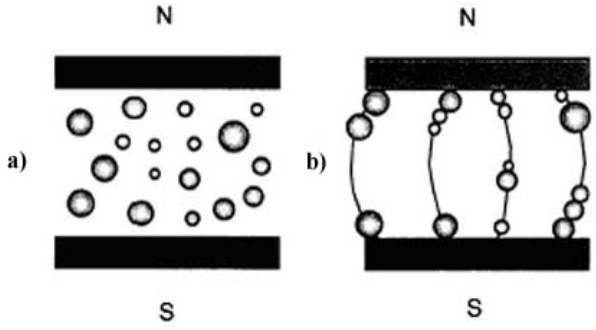

Figure II.1.1 Magnetorheological fluid: a) no magnetic field, b) with magnetic field[4]

MR devices can be divided into three groups of operational modes or a combination of the three based on the design of the device components. These modes are shown in Figure II.1.2. In the valve mode, of the two surfaces that are in contact with the MR fluid, one of them moves relative to the fluid. This relative motion creates a shear stress in the fluid. The shear strength of the fluid may be varied by applying different levels of magnetic field. In the direct shear mode, the fluid is pressurized to flow between two surfaces which are stationary. The flow rate and the

pressure of the fluid may be adjusted by varying the magnetic field. In the squeeze film mode, two parallel surfaces squeeze the fluid in between and the motion of the fluid is perpendicular to that of the surfaces. The applied magnetic field determines the force needed to squeeze the fluid and also the speed of the parallel surfaces[5].

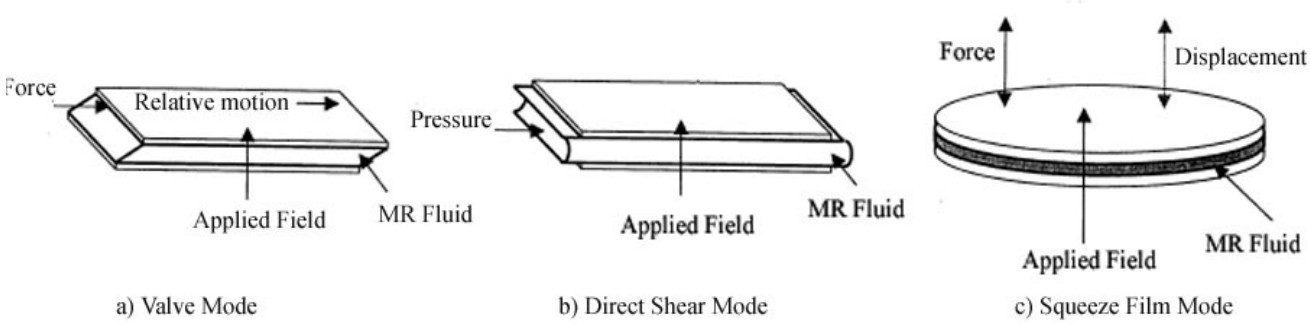

Figure II.1.2 Flow modes of MR devices: a) Valve Mode b) Direct Shear Mode c) Squeeze Film Mode[5]

A magnetic circuit is necessary to induce the changes in the viscosity of the MR fluid. A simple and typical electromagnet is shown in Figure II.1.3. The magnetic circuit typically uses low carbon steel, which has a high magnetic permeability and saturation. This steel effectively directs magnetic flux into the fluid gap. In an optimal design, magnetic field energy in the fluid gap is kept at a maximum while the energy lost in steel flux conduit and regions of non-working areas is minimized. This requires the total amount of steel in the magnetic circuit to be minimized. However, sufficient cross-section of steel must be maintained such that the magnetic field intensity in the steel is very low.

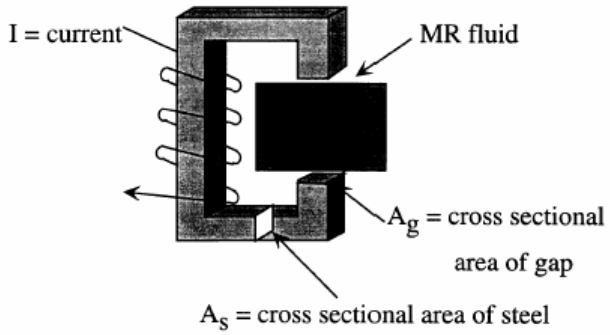

Figure II.1.3 Magnetic Circuit

Several different designs of MR dampers have been built and tested in the past. The first of these designs is the bypass damper where the bypass flow occurs outside the cylinder and an electromagnet applies a magnetic field to the bypass duct[6,7]. While this design has a clear advantage that the MR fluid is not directly affected by the heat build-up in the electromagnet, the presence of the bypass duct makes it a less compact design. In another design by the Lord Corporation, the electromagnet is inside the cylinder and the MR fluid passes through an annular gap around the electromagnet. This design uses an accumulator to make up for the volume of fluid displaced by the piston rod which is going into the damper[8,9]. A way to get rid of this accumulator and simplify the design is to build a double-shafted damper[10]. However, all of these dampers were intended for large-scale applications, mostly for the vibration isolation of structures. A linear,

double-shafted MR damper with a simple design which can be used for small-scale applications is the focus of this research.

II.1.3 Approach

The MR damper utilizes the unique properties of the MR fluid. In this design, the MR fluid flows through the annular gap between the housing and the magnetic body as seen in Fig. 8. The damper operates in a combination of valve and direct shear modes. A magnetic field is created along this gap through the use of a coil which is wrapped around the magnetic body. When the magnetic field is applied, the viscosity of the magnetorheological fluid increases in a matter of milliseconds. The field causes a resistance to the flow of fluid between the two reservoirs. This way, the damping coefficient of the damper is adjusted. Therefore, the damping coefficient of the damper can be adjusted by feeding back a conditioned sensor signal to the coil.

All the parts of this damper were manufactured from low-carbon steel which has a high magnetic permeability. The magnetic body was designed to divide the coil into two parts which creates three effective magnetic surfaces. The two coils were wound in directions opposite to each other so that the flux lines would add up in the middle, as shown in Fig. 8. The flux lines are perpendicular to the flow of the MR fluid. To increase the total magnetic field intensity, the length of the steel path and the fluid path were kept at a minimum. The thickness of the housing is 4.75 mm. The annular gap between the magnetic body and the housing is 0.030 mm.

The total length of the damper, shown in Fig. 9 is 220 mm, while its stroke is 62 mm.

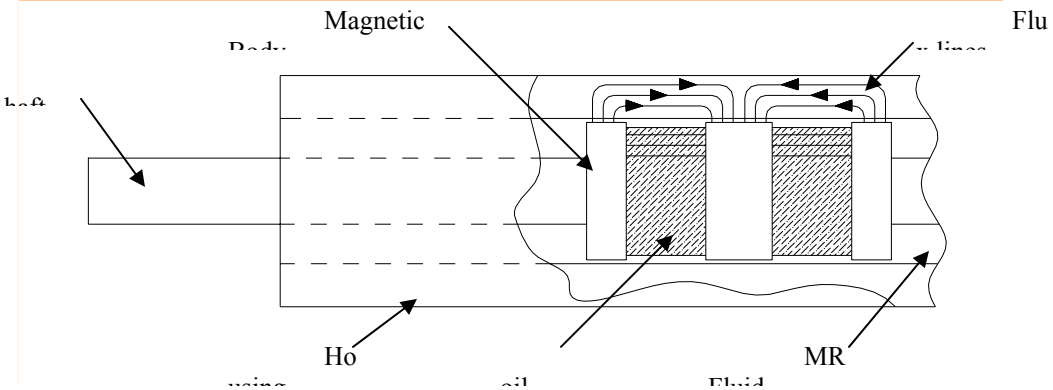

Fig. II.1.4 Schematic of the double-shaft MR damper

Fig. II.1.5 Double-shaft MR damper made from low-carbon steel

Preliminary tests were conducted on an Instron universal tester to determine the force characteristics of the damper built. The plots given below are the results of tension tests carried out. For velocities 1, 2, 3, 4, and 5 in/min, the damping force generated by the damper was measured for varying magnitudes of the magnetic field. The force vs. displacement plot was obtained from data at velocity 5 in/min for a 1.5 in. displacement of the stroke. The mean values of the force for varying velocities were calculated for the force vs. velocity plot. It was noted that a significant increase in the damping force did not occur for currents above 0.4A due to saturation of the coil. Therefore, the maximum damping force that can be generated by the damper is approximately 40 lbs.

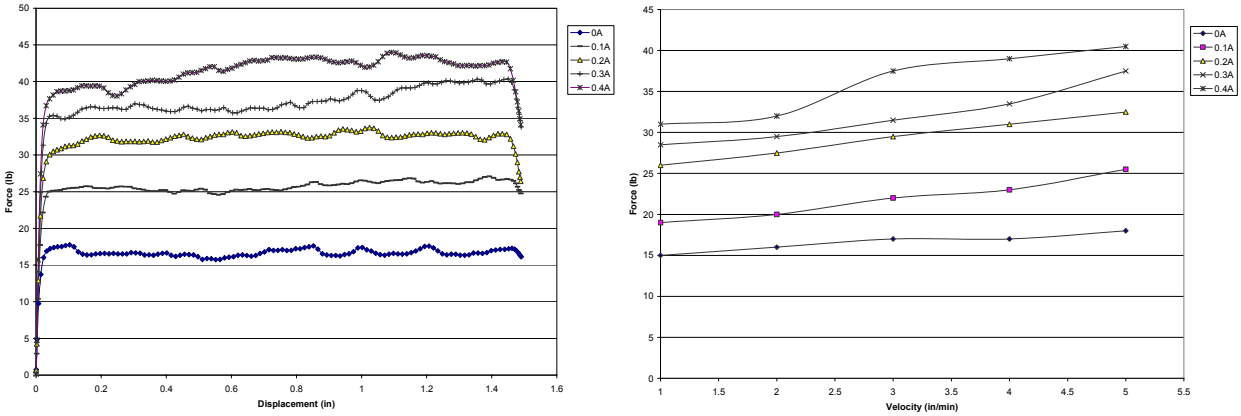

Figure II.1.6 Force vs. displacement and force vs. velocity curves for varying magnetic field

The next step in the MR damper is to compare the frequency response of the damper different analytical models to determine which of the models best predict the behavior of the damper. The future work will focus on developing a control scheme based on the model adopted and implementing MR dampers in the connector legs of a parallel platform mechanism to vary the damping of each leg individually. To have an effective range of damping, the inherent friction in the system needs to be kept low and the electromagnet should be capable of delivering a high enough magnetic field.

II.1.4 References:

- Dyke, S. J., Spencer, B. F., Sain, M. K., and Carlson, J. D., "Experimental Verification of Semi-Active Structural Control Strategies Using Acceleration Feedback", *Proceedings of the 3rd International Conference on Motion and Vibration Control*, September 1-6, Chiba, Japan, Vol. III, pp. 291-296, 1996.
- Scruggs, J. and Lindner, D., "Active Energy Control in Civil Structures*," Proceedings of the SPIE - The International Society for Optical Engineering*, Newport Beach, CA, Vol. 3671, pp. 194-205, 1999.
- Symans, M.D. and M.C. Constantinou, "Experimental Testing and Analytical Modeling of Semi-Active Fluid Dampers for Seismic Protection," *Journal of Intelligent Material Systems and Structures*, Vol. 8, No. 8, pp. 644-657, August 1997.
- Jolly, Mark R., Bender, Jonathan W., and Carlson, J. David, "Properties and Applications of Commercial Magnetorheological Fluids," *Proceedings of SPIE - The International Society for Optical Engineering*, Vol. 3327, pp. 262-275, 1998.
- Yalcintas, M., "Magnetorheological Fluid Based Torque Transmission Clutches," *Proceedings of the 1999 9th International Offshore and Polar Engineering Conference*, 1999.

- Sunakoda, K., Sodeyama, H., Iwata, N., Fujitani, H., and Soda, S., "Dynamic Characteristics of Magneto-Rheological Fluid Damper," *Proceedings of SPIE - The International Society for Optical Engineering* Vol. 3989 Society of Photo-Optical Instrumentation Engineers, USA, pp. 194-203, 2000.
- Sodeyama, H., Sunakoda, K., Fujitani, H., Soda, S., Iwata, N., and Hata, K., "Dynamic Tests and Simulation of Magneto-Rheological Dampers*," Computer-Aided Civil and Infrastructure Engineering* Vol. 18 n 1, pp. 45-57, January 2003.
- Snyder, R.A., and Wereley, N. M., "Characterization of a Magnetorheological Fluid Damper Using a Quasi-Steady Model," Proceedings *of the 1999 Smart Structures and Materials - Smart Structures and Integrated Systems* Newport Beach, CA, USA, 1999.
- Snyder, R. A., Kamath, G. M., and Wereley, N. M., "Characterization and Analysis of Magnetorheological Damper Behavior Under Sinusoidal Loading," *AIAA Journal* Vol. 39 n 7, pp. 1240-1253, July 2001.
- Yang, G., Spencer, Jr., Carlson, J. D., and Sain, M. K., "Large-Scale MR Fluid Dampers: Modeling and Dynamic Performance Considerations," *Engineering Structures* Vol. 24 n 3, pp. 309-323, March 2002.

II.2 Development of Three-Dimensional Visualization Device

For the program, the control program was developed, the control box was assembled and wired, and the assembly of the physical display was begun. Figure II.2.1 shows the assembled physical display drawn in Mechanical Desktop. The drawing includes all parts of the display except for the nine hundred moving pins with their miniature clamp systems, which pass through the plates. All that remains to be done is assembling, testing, and renovating.

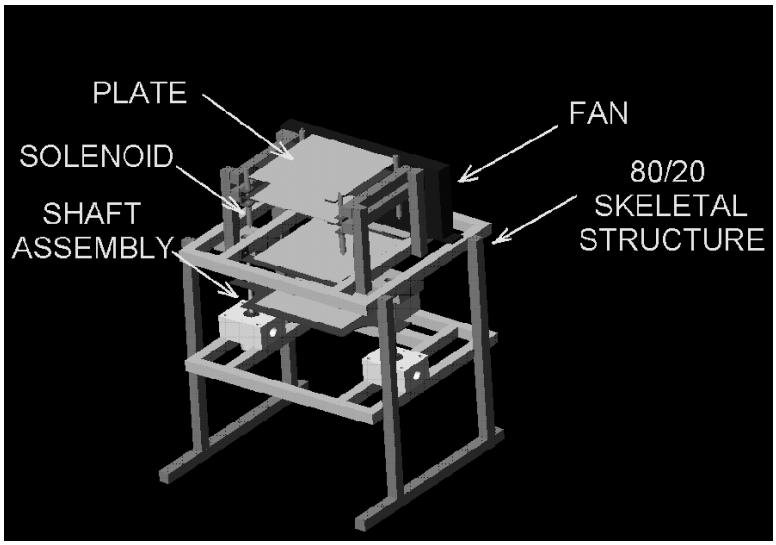

Figure II.2.1: 3-D View of Fully Assembled Physical Display Device

The frame for the physical display was fabricated and assembled. Figure II.2.2 shows the original CAD design of the frame. The frame was designed with the purpose of being capable of holding together all display's working parts, bearing the weight and forces from display's actions, and still being open for easy viewing and maintenance. It was made from extruded aluminum and connected using groove-fitted screws and nuts. Figure II.2..3 shows the assembled frame with the cooling fan attached.

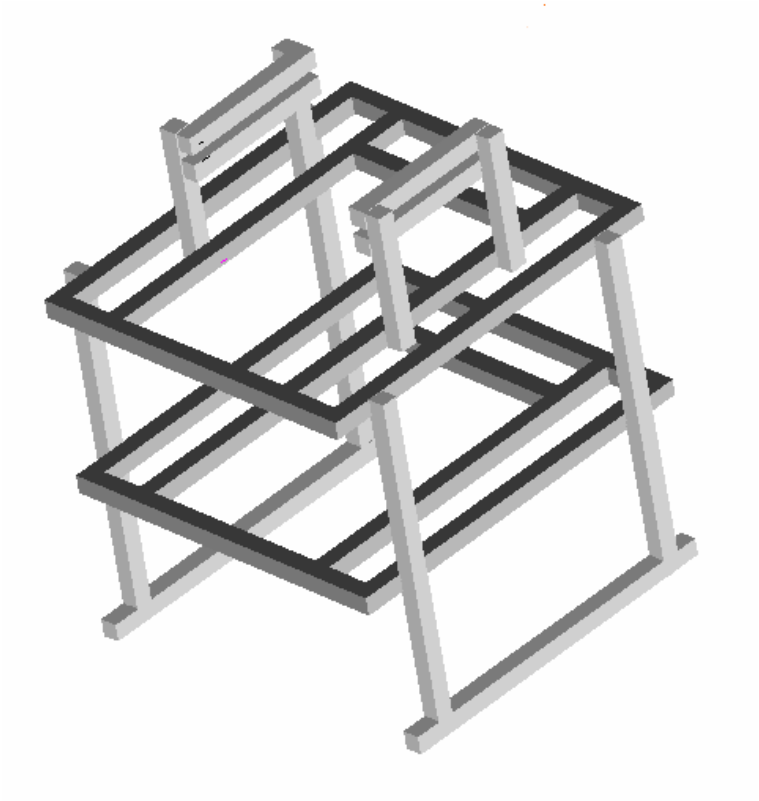

Figure II.2.2: Virtual 3-D Display Frame

Figure II.2.3: Assembled 3-D Display Frame with Fan

Bracket Fabrication

Brackets were designed to attach the various plates to the to the machine frame. Each design took into consideration the fit of the parts around it, the actions it would be making, and the forces that it would have to withstand. It was decided that making the brackets from steel would be structurally sound while still being economically efficient. Figure II.2.4 shows the detailed

dimensioned drawing of the brackets for the top plate. The two L-shaped brackets will be attached to opposing ends of the top plate. The top plate will be screwed to one section of the "L" and the top plank of 80/20 extruded aluminum will be screwed to the other section. These brackets will hold the top board rigid while allowing for free movement of the solenoids (which move the ground plate) around the brackets.

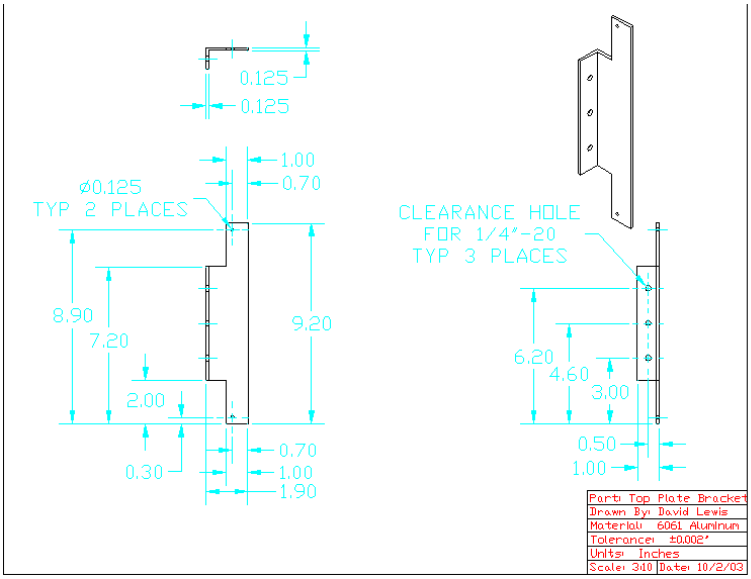

Figure II.2.4: Top Plate Bracket

Figure II.2.5 shows the detailed dimensioned drawing of the brackets for the ground plate. These brackets will be screwed to the opposing ends of the ground board for a rigid attachment. The other ends of the brackets will be attached to four push solenoids each. Two solenoids will be inserted into opposing ends of each hole in the brackets. Pushing from the solenoids on the brackets will lead to a corresponding movement of the ground plate.

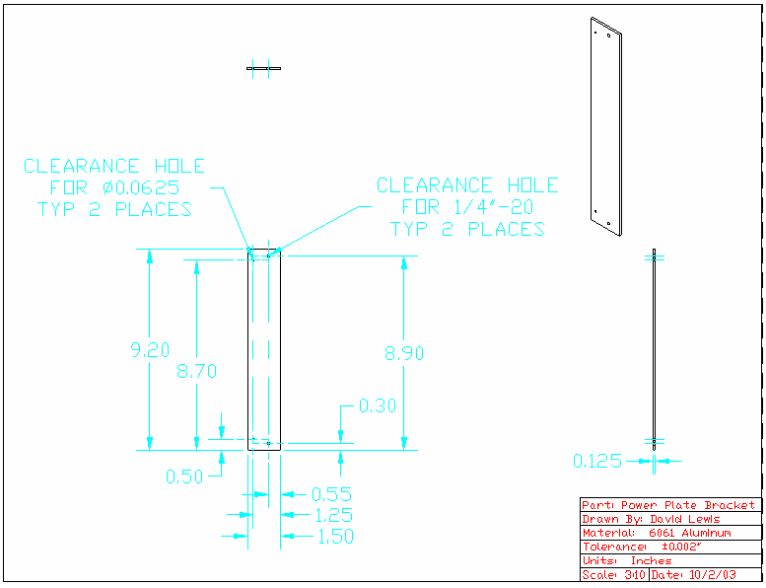

Figure II.2.5: Ground Plate Bracket

Figure II.2.6 shows the detailed dimensioned drawing of the brackets for the power plate. Opposing ends of the power plate will be screwed to the inside on the longest section of these two C-shaped brackets. The two smaller symmetric sections of the brackets will be to planks of 80/20 on the level of the frame that is third from the top. These brackets will hold the power plate rigid even when the attached SMA wires are pulling on it.

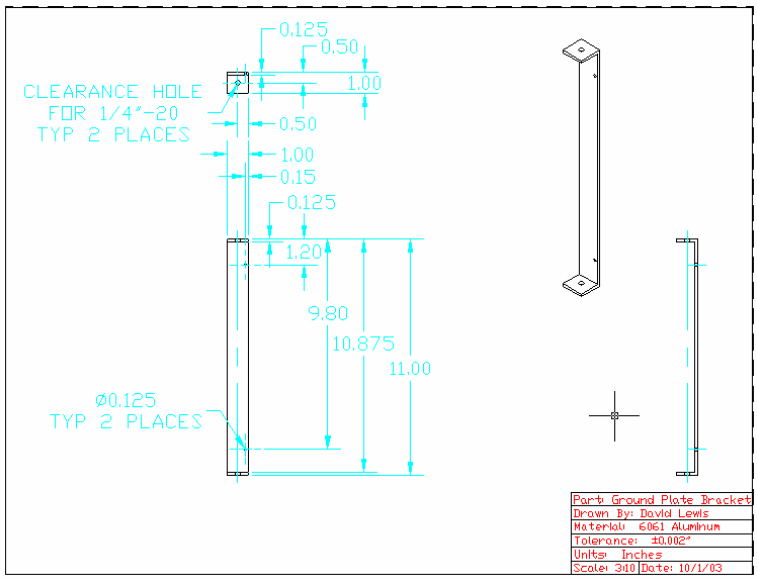

Figure II.2.6: Power Plate Bracket

Figure II.2.7 shows the detailed dimensioned drawing of the bracket for the sensor plate. The sensor plate will be screwed to this singular piece for a rigid attachment. The three arms of the bracket will be screwed to the nuts on the three motor / shaft assemblies. Turning the shafts in unison will result in a symmetric movement of the nuts. This will, in turn, move the bracket and sensor plate up and down (lowering the sensor plate allows for movement of the pins).

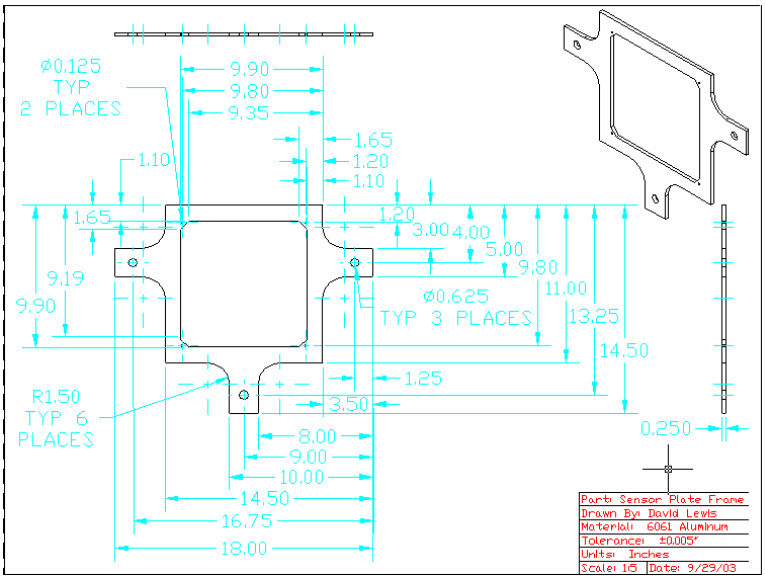

Figure II.2.7: Sensor Plate Bracket

All the parts that were designed specifically for the display device were manufactured. The following list of parts was created in the UF machine shop:

1. Two Top Plate Brackets
2. Two Ground Plate Brackets
3. Two Power Plate Brackets
4. Three Upper Bearing Mounts
5. Three Motor Mounts
6. Four Solenoid Mounts
7. Six Bushings
8. Six Screw Shafts

To make the top plate bracket, a precise milling machine was required; because this was not available in the UF shop, the piece was created by an out-of-house manufacturer. The pieces were press-fit together as with their associated parts.

Clamp System Design and Tests

The clamp system was again adjusted and redesigned. Figure II.2.8 shows the clamp design at the beginning of the quarter. The system was assembled using the following steps:

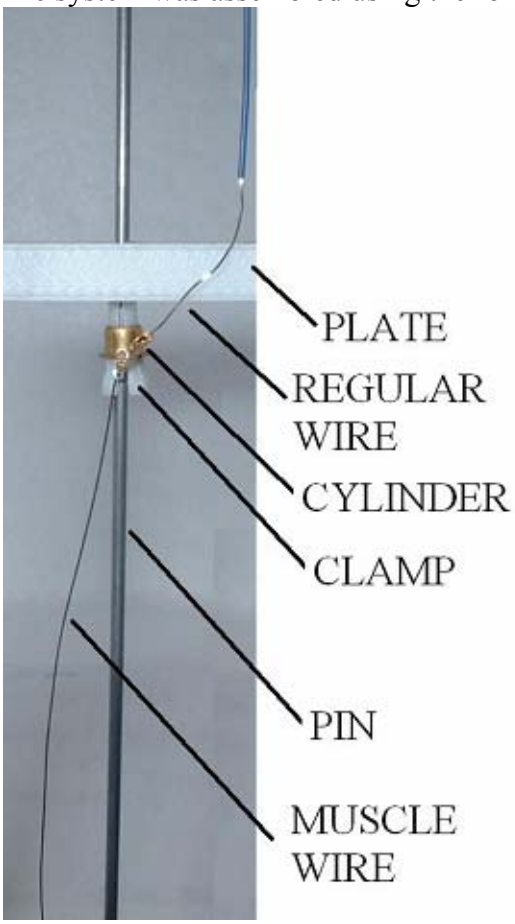

Figure II.2.8: Previous Pin-Clamp System

Step 1: A 3.5" SMA wire is attached to the outgoing end of a diode with a crimp

Step 2: The ingoing end of the diode is soldered to its respective trace hole on the power plate

Step 3: Two small holes are drilled into the rim of the bronze freedom ring

Step 4: A two-inch wire-wrap wire is threaded up through the first rim hole, wrapped halfway around the freedom ring and back down the other hole

Step 5: A three-inch metal tube it threaded through the respective holes of the top plate and ground plate and glued to the top plate

Step 6: One end of the wire-wrap wire is soldered to the ground plate

Step 7: The freedom ring is placed around the clamp and the non-functioning end of the clamp is inserted into the bottom of the metal tube

Step 8: The unused end of the wire-wrap is attached to the SMA wire with a crimp

Step 9: Lower the pin through the metal tube, down to the sensor plate

Giving power to the power plate and a ground to the ground plate will cause the SMA wire to be heated and contract; thus, the freedom ring will be pulled down on the clamp, close it, and the pin will not be able to move. Moving the ground plate upward will cause the freedom rings to be pulled upward; thus, opening all the clamps and allowing for free movement of the pins.

While the system proved to be reliably functional for a single pin, prototyping a system with multiple pins and clamps within an accurate environment lead to several new problems. There were numerous locations where short circuits occurred, hand assembly was difficult, and several connections were structurally unreliable.

Switching to the design shown in Figure II.2.9 reduced the severity of these problems. This updated design allows for the system to be assembled in a more convenient step-by-step process and minimizes the chance of short circuits.

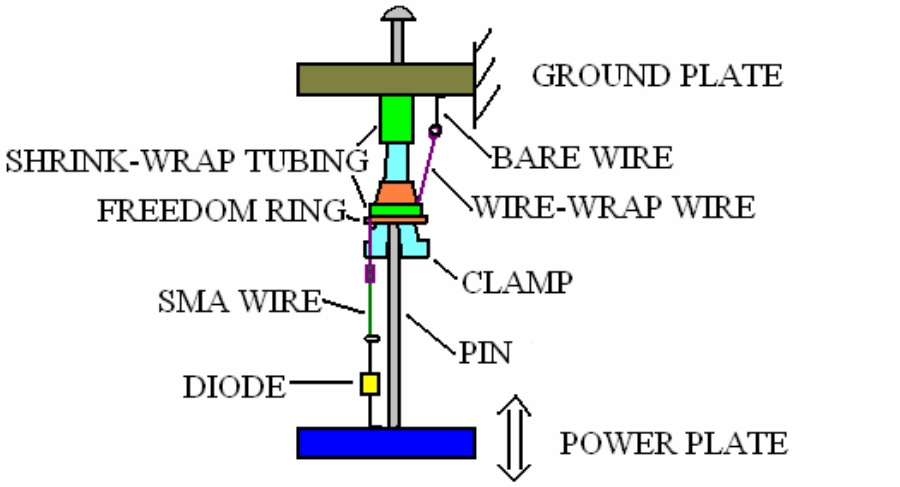

Figure II.2.9: New Pin-Clamp System

The updated design uses the following assembly procedure:

Step 1: Curl the outgoing end of the diode into a spiral

Step 2: Curl the ingoing end of the diode into an L-shape

Step 3: Solder the ingoing end of the diode to its respective trace hole on the power plate

Step 4: Place center of wire-wrap wire against side of bronze freedom ring and place shrink-wrap tubing with 3/16" diameter around both

Step 5: Tighten the shrink-wrap tubing by heating it was a hot fan

Step 6: Loop both ends of wire-wrap wire

Step 7: Loop one end of 4" long SMA wire

Step 8: Place straight end of the SMA wire through the wire-wrap loop and twist the loop around the SMA wire so that the wires are tightly gripped

Step 9: Curl one end of a 1" long bare wire so that it spirals and curl the other end so that it makes an L-shape

Step 10: Solder the L-shaped end of the wire to the respective trace hole on the ground plate

Step 11: Place the looped end of the wire-wrap wire around the spiral curl on the bare wire and tighten with pliers

Step 12: Place a 1/16" long strand of semi-rigid tubing within a two-inch long strand of shrink-wrap tubing, a quarter-inch from the end of the tubing

Step 13: Shrink the tubing with a heating fan

Step 14: Thread the tubing through the top plate and then the ground plate until the semi-rigid plastic tubing prevents further movement

Step 15: Place the clamp through the freedom ring and press the small end into the shrunken tubing

Step 16: Place the looped end of the SMA wire around the looped end of the diode and tighten with pliers

Step 17: Lower the pin through the shrunken tubing, down to the sensor plate

The use of the shrink-wrap tubing eliminated most current shorting difficulties and actually allowed for a smoother flow of the pin. Using looped and curled wire end eliminated the need for crimps and allowed for a simpler assembly and a better situation for maintenance.

Each of the 900 moving pins on the physical display device will require a working clamp with a freedom ring to lock its position. Each clamp and freedom ring needed to be removed from a single Pentel Crayz 1.3 mm Mechanical Pencil. Therefore 996 pencils were ordered and stripped down to the clamp and freedom ring. Because of the large number pencils, the stripping process was broken down into five specific steps.

Step 1: Disassembly

All parts of the mechanical pencil that were capable of being removed by hand were detached and collected. The detached parts included the eraser cap, eraser, two sticks of lead, the pencil cap, and the cone cover.

Step 2: Shell Removal

The clamp is attatched to a long cylindrical, semi-rigid plastic sleeve. A much harder plastic shell surrounds all this, which is what the user grips when writing with the pencil. The hard shell could only be removed by being broken off. The pencil was placed in a vice and when the vice increased the pressure, the shell would fracture linearly and could be peeled off.

Step 3: Sleeve Slicing

The semi-rigid plastic sleeve holds the clamp in place and an increase in the sleeve's diameter holds the freedom ring and spring over the clamp. A dremel with circular blade was use to slice the sleeve through its smaller diameter where it starts to cover the clamp. This removed all of sleeve except for a thin ring, and, it allowed for the following step.

Step 4: Spring Removal

Without the sleeve to hold it in place, the springs could be removed from around the clamp and placed and bin where they would be used later.

Step 5: Sleeve Dissection

In order to remove the remaining ring from the plastic sleeve around the clamp, the dremel with the circular blade was used to carefully slice through the ring on two sides. The ring was, in turn, dissected into two pieces that would just fall off. Because the clamp was made of a harder plastic than the sleeve, the dremel could be set at a low enough spinning rate that it would cut easily through the sleeve and cause a negligible amount of damage to the clamp. Once the sleeve was removed the freedom ring could be pulled off and the clamp and ring could be stored in their associated bins, as seen in Figure II.2.10.

Figure II.2.10: Bins of Separated Materials

The control box was assembled and carefully wired. The box will hold all the terminal boxes that will break the ribbon cables to individual wires, the opto-isolators that will switch computer signal for power signals and vice versa, and the terminal boxes that will unite the

individual wires into singular ribbon cables. The control box has three racks that with all the terminals attached to them. The terminals were wired to one another with color-coded wires. Figure II.2.11 shows the wired box with the racks hanging out.

Figure II.2.11: Control Box

II.3 Force Control via Parallel Architecture Mechanisms, Passive

In order to get accurate force/displacement relation for each leg, a calibration experiment is designed and finished to test the linearity for the out put of the load cell. 3 sets of experiments with standard weight sets are done by researchers, and the experimental data are analyzed by a Matlab program.

The input/output relationship is show in figure II.3.1 The red/orange/purple curve show the main relationship, which has the input load force (unit: gram) as the X variable and the output load cell voltage (unit: Volt) as the Y variable. The green/yellow curve show the error/input relationship, where the error comes as the difference between the real output data and the least squares solutions for the input/output equation. From the result, it is quite clear the error is small enough to provide accurate experimental data.

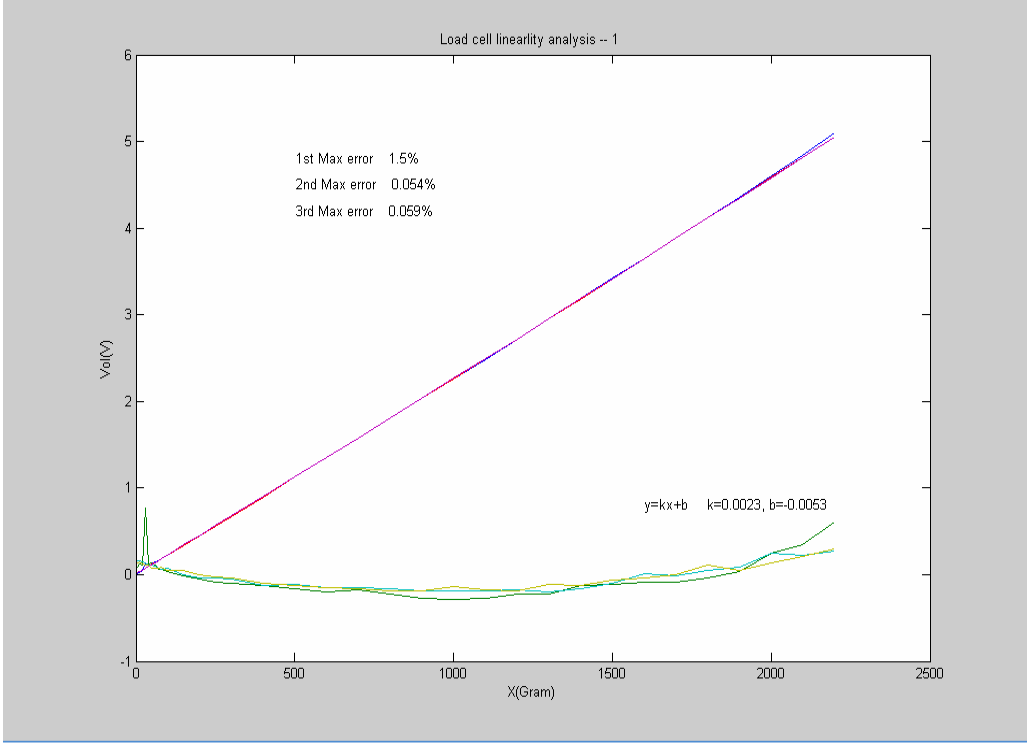

Figure II.3.1 load cell calibration test data.

All designed parts are manufactured and ready to be assembled. The ground-end spring, optical encoder and strips are successfully assembled with the 3 segment leg. A new optical encoder/ strip with higher resolution and index capacity will be released by the vendor and since it has exactly the same dimension values, it should be quite simply to replace the old ones.

The 6-DOF passive parallel structure prototype is being assembled, before the whole platform is finalized, the shafts of the legs should be cut in order to get the desired leg length to perform the right tasks. Two different methods developed in order to measure the free length of the compliance part.

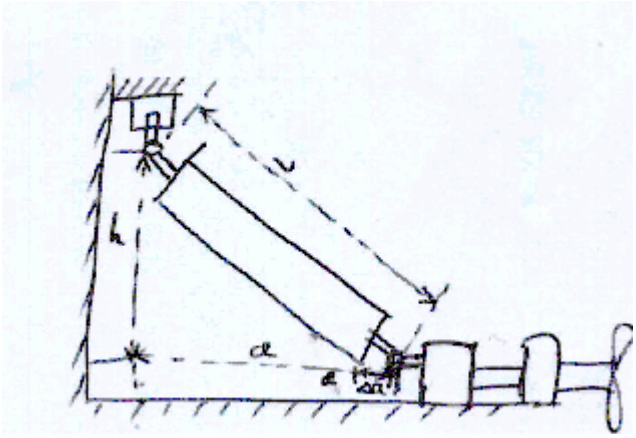

Figure II.3.2 Free Leg Length Measurement

In order to assembly the whole parallel platform, the free length of the legs should be carefully measured and machined to the desired theoretical values. Here the free length means the distance between the center of the hook joint connecting to the base platform and the center of the hook joint connecting the top platform for each leg with no external load applied on it.

Two different methods are inspired and investigated thoroughly. The first method comes from a different, a more theoretical direction: Measure the length variations alone the leg and one other direction and based on the experimental data to get real free length. The experiment diagrammatic sketch is shown in figure II.3.2

The leg is placed so that it is the sloped edge of a right triangle, and the hook joint are fixed so that they are in the direction of the right-angle side. The free length of the leg is L, and the other two right-angle side are H and A.

$$L^2 = A^2 + H^2$$
$$H^2 = L^2 - A^2$$

$$H^2 = (L + \Delta l_1)^2 - (A + \Delta a_1)^2$$
$$H^2 = (L + \Delta l_2)^2 - (A + \Delta a_2)^2$$
$$H^2 = (L + \Delta l_3)^2 - (A + \Delta a_3)^2$$

Where L, A , H are unknown and $\Delta l_1, \Delta l_2, \Delta l_3$ are know, so with 3 unknowns and 3 equations, L could be calculated.

This method required very accurate perpendicular right-angel, and precision fixture in order to get the ideal configuration. And most important is to measure the Δa, Δl very accurately. This method is very creative and theoretical correct, but it need a lot of additional work to design a measuring bench with high precision fixtures, and additional precision instrument for displacement measurement. And the final result is quite sensitive about the accuracy of the experimental data.

The other method which we are currently using is pure photographing method, one group of pictures of the experiment for this method is provided in figure II.3.3. With the state of the art of the digital photographing technology and carefully designed experimental procedure, the center for both the hook joints could be clearly located in a very detailed and well focused digital picture. And the measurement resolution is high enough for the application. For each single leg , a group of 3 photos which are related to each other will provide enough information for the cutting-counting measurement.

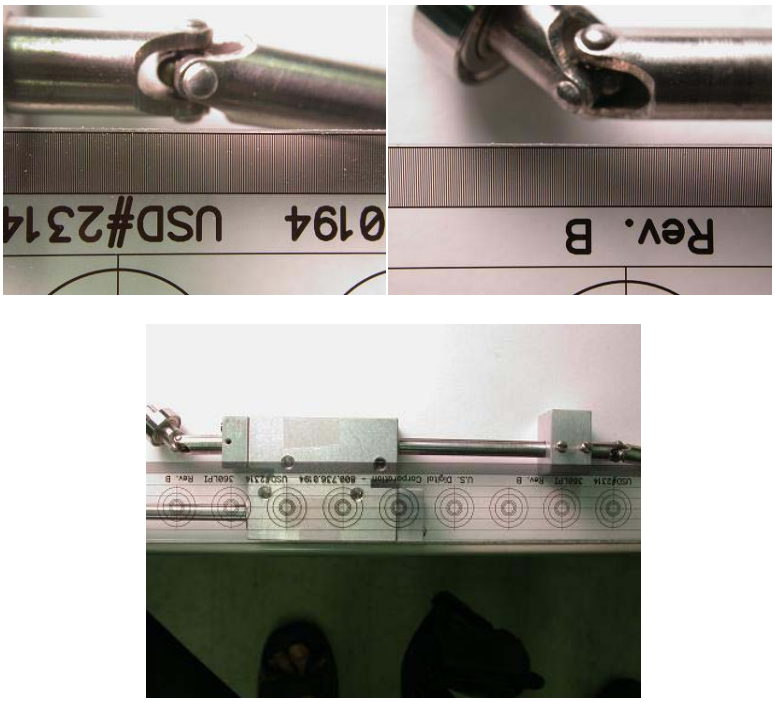

Figure II.3.3 Free Leg Length Measurement option 2

By investigating the whole group of photos, the free length of the legs could be measured by accounting the number of the cuts of the encoder strips. The first two figures could provide detailed counting information for both the left and right hook joint (or top and base connecting hook joints), while the last one could provide the overall picture of the whole leg, which provides a very convenient way for the researcher to locate the centers of the circle on the optical strip, which is quite essential to connect to the left and right detailed picture, helps to measure the over all length of the leg which is not shown in the first two pictures.

This method is pretty straight forward and easy to carry, and as long as the picture is clear enough to zoom in to the desired extent; it could provide quite accurate non-contact measurement. With several experiments and analysis, the researchers have already found a way to take pictures quickly, accurately and solved the problem that the cutting of the strip and the center of the hook joint could not been focused at the same time. The new pictures, which are too big to be shown here, could provide satisfied results for the measurement.

To fully understand the compliance property of the legs, a displace/load relationship experiment should be designed and tested in order to get the check point table. There are two reasons that this step is postponed:

Reason 1. The encoder manufacture company promised to release the higher resolution encoder with index this fall, but it is still not available now; while it index encoder is essential for the measurement of the displacement.

Reason 2. It is still not very clear where should the index of the strip be located when finishing assembly the platform, since the distance between both center of the hook joint to the encoder detecting point are all different and it should also consider the feasible and easiness of installing.

Assembly of Platform

All the legs are cut according to the theoretical value of the analysis, and all the parts are assembled together and the 6-6 in-parallel platform are shown in figure II.3.4. The optical encoder head are disconnected with the cables, and the index strip are not attached in on the leg, the reason is explained above.

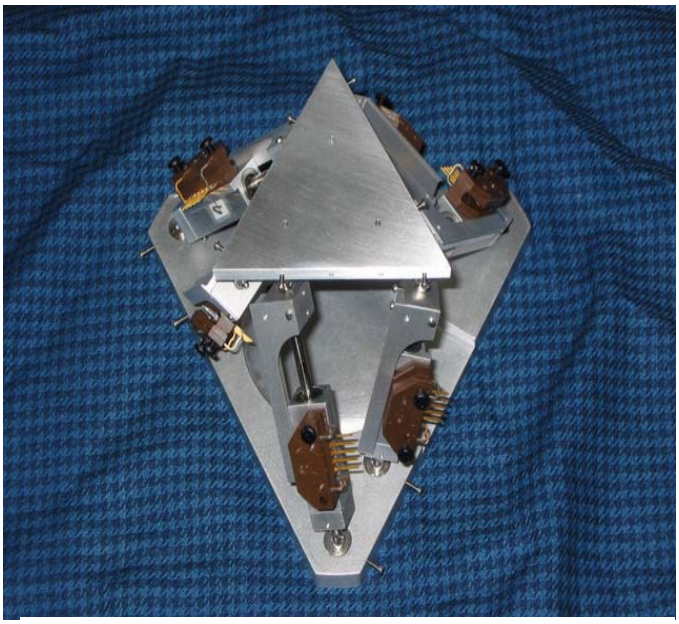

II.3.4 Assembled 6-6 in-parallel

II.4 Force Control via Parallel Architecture Mechanisms, Active

The system architecture is separated into two parallel geometry mechanism based machines. One acts as the prime mover, orienting the output or moving platform with respect to the base. The second serves to measure the location of the moving platform relative to the base.

The actuation frame is servo-hydraulic actuated. The valves, cylinders, and joints are in-house. Strain gauge based load cells are incorporated in the connectors and are also in-house. The attachment configuration of the connectors is established using an optimizing design methodology. The goal is to arrive at a mechanism with uniform loading in the connectors for a uniform gravity load on the moving platform. The load cell and joint configuration has been the subject of much design work. Integrating these components for maximum joint range has been a challenge. The current design is considered suitable.

The universal joints utilized require modification from their off the shelf geometry. This involves disassemble, machining, and reassembly. The load cells are limited to a maximum load of 10,000 N, but an upset condition in the actuator could generate in excess of 40,000 N. A load carrying structure is incorporated to take excessive deflections in the load cell.

As previously presented, a design methodology for parallel kinematic mechanisms has been developed. This methodology has been applied to the actuation frame and the results are acceptable. The methodology is currently being applied to the metrology frame. The objective function development is difficult as both positional and rotational errors are of concern. The methodology is illustrated in Figure II.4.1 for completeness, and the process is discussed.

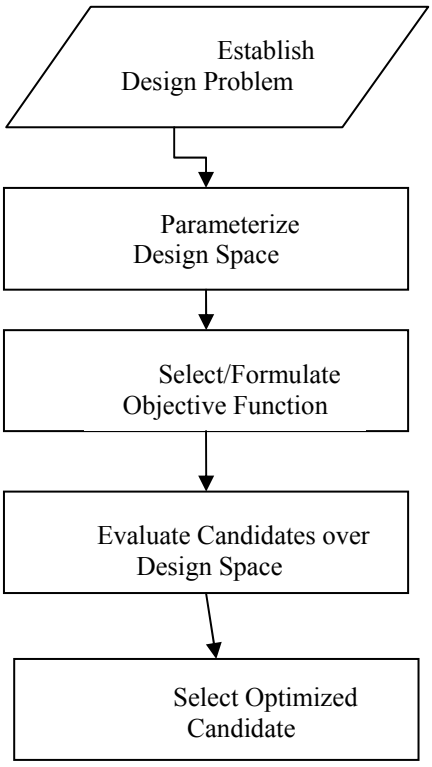

Figure II.4.1 Design Methodology Overview.

The design problem needs to be defined as accurately as possible. Primary functional characteristics are needed. Expected loading, positions, velocities, and accelerations should be bounded. Volume available for the mechanism to occupy is also important.

A parameterization for a general 6 degree of freedom parallel kinematic mechanism, with planar connector joints for each platform has been developed. This parameterization allows the design space of candidate mechanism to be easily defined based on these six kinematic parameters. The parameterization is symmetric for the fixed platform and moving platform, simplifying the design space significantly. If an application would benefit form a non-symmetric mechanism, then further parameterization is necessary. Figure II.4.2 illustrates the symmetric parameterization of a PKM.

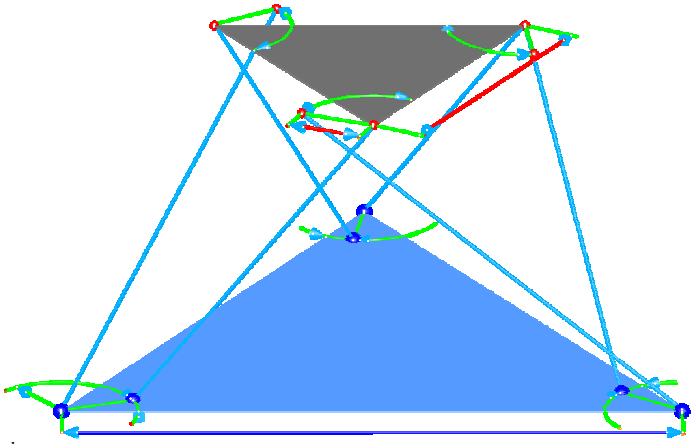

Figure II.4.2 Parameterization of the 6-6 design space

Selection of an objective function is driven by the requirements for the PKM. The application at hand has two PKM's with differing requirements. The actuation PKM is intended to be the prime mover of the machine. An objective function that examines the force generating capabilities of candidate mechanisms is desired. The metrology PKM determines the machine's position and orientation. An objective function that examines the accuracy of this determination is desired.

The search over the design space to identify the optimized candidate mechanism is done in a discrete manner. The workspace evaluation of each candidate is also performed in a discrete manner. Figure II.4.3 illustrates the methodology applied to evaluate the design space and the candidates represented.

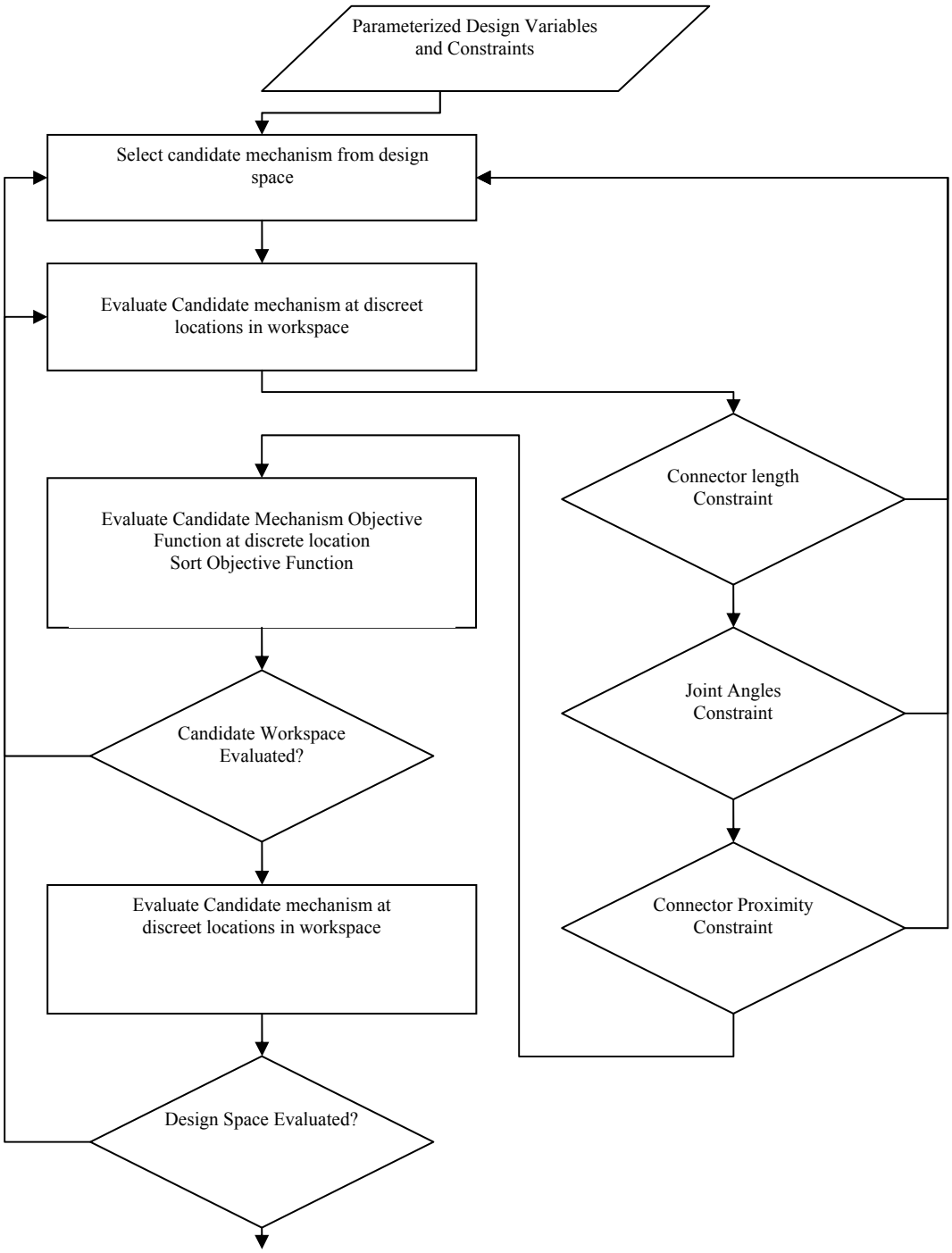

Figure II.4.3 Design space search methodology

The methodology has been applied with results to the actuation frame, as reported. The metrology PKM requires a geometry for which a forward kinematic analysis exists in closed form. A "special" 6-6 type PKM has a known forward analysis. Figure II.4. 4 illustrates the parameterization of this geometry.

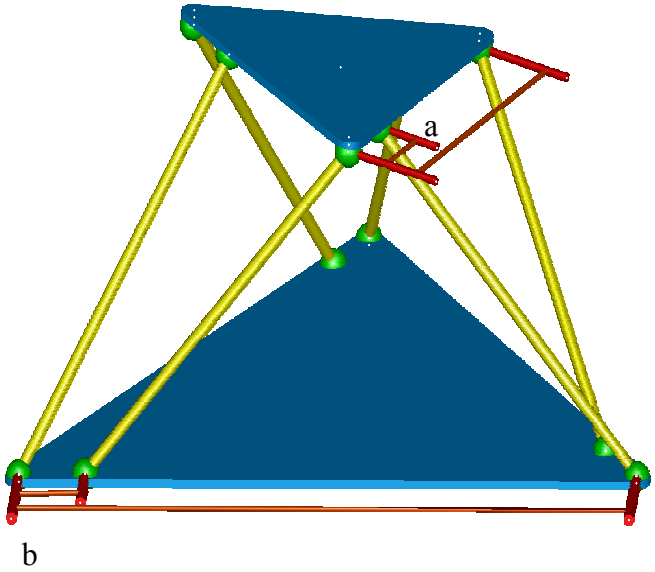

Figure II.4.4 Parameterization of design space, special 6-6.

A procedure based on error propagation via the position analysis is being developed. The result of the analysis is a maximum expected error for the position and rotation of the moving platform with respect to the precision of the measurement scheme implemented in the connectors. Quantification of this error can consist of evaluation of rotational and position errors. A methodology is introduced in which the absolute value of the error in the location of a set of points is calculated. This procedure eliminates the mixed unit's problem in the objective function, and allows comparison of candidate mechanisms. This sum is utilized to evaluate a candidate mechanism for suitability in the metrology frame design.

The procedure for evaluating measurement precision is to calculate the error in location of a set of known points located in the moving platform. Then the sum of the magnitude of these errors will represent a measure of the precision of the candidate PKM. This objective function is utilized in the search procedure detailed in Figure II.4.3. Figure II.4.5 provides motivation for this approach. The four points that make up the tetrahedron on the moving platform have known location relative to the moving platform. Their location can be calculated for a given pose. The inclusion of measurement error will induce an error in the calculated position of the four points.

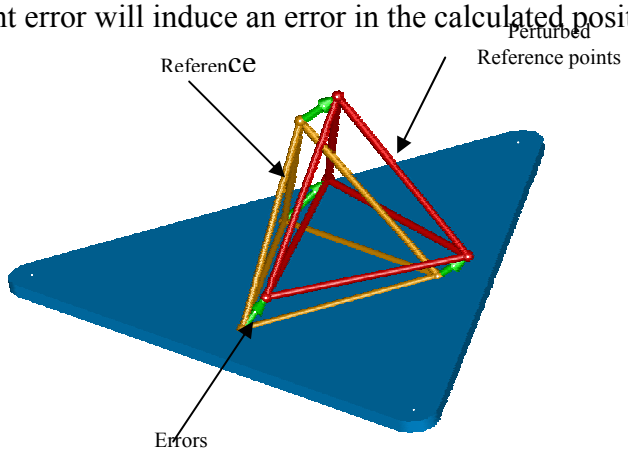

Figure II.4.5 Parameterization of design space, special 6-6.

The optimization procedure follows the methodology previously introduced. Parameterization of the design space is undertaken. A candidate mechanism is chosen for the

design space defined by a, b, ra, and rb. An error analysis is performed based on an assumed level of precision from the metrology connectors. A worst case error sum as discussed is found by searching over the desired workspace. This value is used to compare the candidate mechanism with other candidate mechanisms. The constraints on joint angle and connector ranges are applied as with the actuation PKM. The connector proximity constraint considers the metrology connectors and the actuation connectors. Table II.4.2 details the constraints on the metrology frame arising from the actuation PKM's design and from component limits.

Table II.4.2. Constraint specifications for the metrology PKM

Workspace: Volume	0.25 m radius X 0.5 m tall cylinder
Workspace: Orientation	± 25° about a line parallel to the volume cylinder ends
Position Resolution	± 0.1 mm
Parameter range: a	0.3m < a < 0.5m
Parameter range: ra	0.1m < ra < 0.5*a
Parameter range: b	0.4m < b < 0.7m
Parameter range: rb	0.1m < rb < 0.5*a

The implementation of the methodology is functional, but results are not finalized. The discretization of the design space is straight forward, but the evaluation of the objective function for each candidate mechanism is computationally costly. The workspace of the candidate mechanism is defined as a cylinder of fixed dimension over which an angular range of freedoms exist. For this case, the angular range is taken as ±25° of rotation about any line lying in a plane parallel to the ends of the cylinder.

For each discritized point in the workspace, the worst case for error propagation must be examined. The measurement scheme anticipated is linear encoder based. The precision of the encoders is +- 20 microns. Pose error is evaluated for any up to all legs being affected by variations up to the precision of the encoders. The degree to which the error propagation is evaluated greatly affects the computational cost.

The initial results show a typical error magnitude of 5 to 6 times the precision of one connector. The variability of the magnitude of the error does not show consistency. This characteristic leads to exhaustive type search methodologies. The exhaustive nature has lead to considerable computation time.

The current system design, including the previous metrology frame design, is illustrated in Figure II.4.5. At present, the metrology frame design is the only section unspecified. All components are in-house except for the fixed and moving platforms.

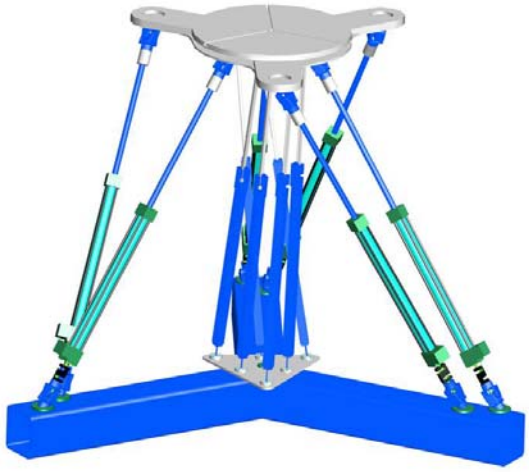

Figure II.4.6 WCPMMI design

The hydraulic circuit for the apparatus is laid out and all fittings and hoses are in-house. The hydraulic power supply that will be utilized supplies another research device, and the hydraulic circuit has to take this into account. The cylinders are being plumbed for flushing. The design allows flushing while the assembly of the actuation frame is underway.

APPENDIX A: High Level Code to format, encode and decode chip data.

```
/*****************************************
This program was produced by the
CodeWizardAVR V1.23.7a Standard
Automatic Program Generator
© Copyright 1998-2002 HP InfoTech s.r.l.
http://www.hpinfotech.ro
e-mail:office@hpinfotech.ro

Project : DOE 780
Version : D01.32.00
Date    : 04/17/2003
Author  : Cyril Kurien
Company : Electronics Communications Lab
Comments:

Chip type           : ATmega128
Program type        : Application
Clock frequency     : 18.432000 MHz
Memory model        : Small
Internal SRAM size  : 4096
External SRAM size  : 0
Data Stack size     : 1024
*****************************************/

#include <mega128.h>
#include <delay.h>

bit dataReceived=0x00;    // boolean variable that indicates whether address received or not
bit zeroMode = 1;
bit manchesterDecodeError = 0;
bit hammingDecodeError = 0;
unsigned char bitNumber = 0x00;
unsigned char rxData[16] = {3,3,3,3,3,3,3,3,3,3,3,3,3,3,3,3};
unsigned char hammingData[8] = {0,0,0,0,0,0,0,0};
unsigned char packetData[4] = {0,0,0,0};

// Timer 1 output compare A interrupt service routine
interrupt [TIM1_COMPA] void timer1_compa_isr(void){
// Sample the RSSI
        ADCSRA |= 0x40;
}

interrupt [TIM1_COMPB] void timer1_compb_isr(void){
        PORTA=0xF;
        PORTA.0 = PIND.4;
```

```
        PORTA=0x0;
        if(zeroMode == 1){
                if(bitNumber == 0 && PIND.4 == 1){
                        bitNumber = 1;
                }
                else if(bitNumber == 1 && PIND.4 == 0){
                        bitNumber = 0;
                }
                else{
                        rxData[0] = 0x01;
                        bitNumber = 1;
                        zeroMode = 0;
                        PORTA.1=1;
                }
        }
        else{                                   // no longer zero mode
                if(bitNumber < 128){            // read in encoded address bits
                        rxData[bitNumber/8] <<= 1;
                        rxData[bitNumber/8] = rxData[bitNumber/8] | PIND.4;
                }
                if (bitNumber<=128) {
                        dataReceived = 1;
                        bitNumber = 0;
                        ADCSRA=0x88;
                        TIMSK=0x10;// Turn off timer 1 output compare ISR
                        PORTA.1=0;
                 }
                bitNumber++;
        }
} //end of timer 1 output compare b interrupt

interrupt [TIM1_COMPC] void timer1_compc_isr(void){
        TIFR|=0x08;
        TIMSK=0x08;
        ETIMSK=0x00;
        }

// Timer 1 input capture interrupt service routine
bit edgeNumber = 1;
unsigned int counter1, counter2, edgeTime;

interrupt [TIM1_CAPT] void timer1_capt_isr(void){
        if(edgeNumber == 1){
                counter1=ICR1H;
                counter1=counter1<<8 | ICR1L;
                edgeNumber = 2;
        }
        else{
                counter2=ICR1H;
```

```
                counter2=counter2<<8 | ICR1L;

            if(counter1 > counter2)
                    edgeTime = 0xFFFF - counter1 + counter2;
            else
                edgeTime = counter2 - counter1;

            if(edgeTime < 0x3C1 && edgeTime >= 0x3BB){
                edgeNumber = 1;
            // Set up Timer1C OC Interrupt

                        TCCR1B&=0xF8;
                        TIFR|=0x01;
                        ETIMSK=0x01;
                        TCCR1B=0x49;
                        TCNT1H=0x00;
                        TCNT1L=0xF0;
            }
            else
                edgeNumber = 1;
        }
}

//unsigned char lastADCData;
unsigned char adcData;
unsigned char adcSamples;

#define ADC_VREF_TYPE 0x20
#define RSSI_THRESHOLD 0x40
// ADC interrupt service routine
interrupt [ADC_INT] void adc_isr(void){
// Store previous state and get current state
        adcData = ADCH;

// Check if threshold broken
        if(ADCH > RSSI_THRESHOLD)
                if(adcSamples >= 192){
                // Turn off ADC
                        ADCSRA = 0x00;
                // Reset ADC samples
                        adcSamples = 0;
        // Set up IC1 for rising edge detect and turn on interrupt
                TIFR|=0x20;
                        TIMSK=0x20;
                }
                else
                        adcSamples++;
        else
                adcSamples = 0;
```

```
}

void main(void)
{
unsigned char iso1, iso2, iso3, s1, s2, s3, s;
unsigned char result = 0x00;
int i;

// Input/Output Ports initialization
// Port A initialization
// Func0=Out Func1=Out Func2=Out Func3=Out Func4=Out Func5=Out Func6=Out
Func7=Out
// State0=T State1=T State2=T State3=T State4=T State5=T State6=T State7=T
PORTA=0x00;
DDRA=0xFF;

// Port B initialization
// Func0=In Func1=In Func2=In Func3=In Func4=In Func5=Out Func6=Out Func7=Out
// State0=T State1=T State2=T State3=T State4=T State5=0 State6=T State7=T
PORTB=0x00;
DDRB=0xE0;

// Port C initialization
// Func0=Out Func1=Out Func2=Out Func3=Out Func4=Out Func5=Out Func6=Out
Func7=Out
// State0=T State1=T State2=T State3=T State4=T State5=T State6=T State7=T
PORTC=0xAA;
DDRC=0xFF;

// Port D initialization
// Func0=In Func1=In Func2=In Func3=In Func4=In Func5=In Func6=In Func7=In
// State0=T State1=T State2=T State3=T State4=T State5=T State6=T State7=T
PORTD=0x00;
DDRD=0x00;

// Port E initialization
// Func0=In Func1=In Func2=In Func3=In Func4=In Func5=In Func6=In Func7=In
// State0=T State1=T State2=T State3=T State4=T State5=T State6=T State7=T
PORTE=0x00;
DDRE=0xFF;

// Port F initialization
// Func0=In Func1=In Func2=In Func3=In Func4=In Func5=In Func6=In Func7=In
// State0=T State1=T State2=T State3=T State4=T State5=T State6=T State7=T
PORTF=0x00;
DDRF=0x00;

// Port G initialization
// Func0=In Func1=In Func2=In Func3=In Func4=In
```

```
// State0=T State1=T State2=T State3=T State4=T
PORTG=0x00;
DDRG=0x00;

// Timer/Counter 0 initialization
// Clock source: System Clock
// Clock value: Timer 0 Stopped
// Mode: Normal top=FFh
// OC0 output: Disconnected
ASSR=0x00;
TCCR0=0x00;
TCNT0=0x00;
OCR0=0x00;

// Timer/Counter 1 initialization
// Clock source: System Clock
// Clock value: 18432.000 kHz
// Mode: CTC top=OCR1A
// OC1A output: Toggle
// OC1B output: Discon.
// OC1C output: Discon.
// Noise Canceler: Off
// Input Capture on Falling Edge
TCCR1A=0x54;
TCCR1B=0x49;     //0x49
TCNT1H=0x00;
TCNT1L=0x00;
OCR1AH=0x03;
OCR1AL=0xC0; //C0
OCR1BH=0x01;  //01
OCR1BL=0xE0; //changed from 0xe0
OCR1CH=0x01;//03
OCR1CL=0xE0;//c0

// Timer/Counter 2 initialization
// Clock source: System Clock
// Clock value: Timer 2 Stopped
// Mode: Normal top=FFh
// OC2 output: Disconnected
TCCR2=0x00;
TCNT2=0x00;
OCR2=0x00;

// Timer/Counter 3 initialization
// Clock source: System Clock
// Clock value: Timer 3 Stopped
// Mode: Normal top=FFFFh
// OC3A output: Discon.
// OC3B output: Discon.
```

```
// OC3C output: Discon.
TCCR3A=0x00;
TCCR3B=0x00;
TCNT3H=0x00;
TCNT3L=0x00;
OCR3AH=0x00;
OCR3AL=0x00;
OCR3BH=0x00;
OCR3BL=0x00;
OCR3CH=0x00;
OCR3CL=0x00;

// External Interrupt(s) initialization
// INT0: Off
// INT1: Off
// INT2: Off
// INT3: Off
// INT4: Off
// INT5: Off
// INT6: Off
// INT7: Off
EICRA=0x00;
EICRB=0x00;
EIMSK=0x00;

// Timer(s)/Counter(s) Interrupt(s) initialization
TIMSK=0x10;
ETIMSK=0x00;

// Analog Comparator initialization
// Analog Comparator: Off
// Analog Comparator Input Capture by Timer/Counter 1: Off
// Analog Comparator Output: Off
ACSR=0x80;
SFIOR=0x00;

// ADC initialization
// ADC Clock frequency: 144.000 kHz
// ADC Voltage Reference: AREF pin
// ADC High Speed Mode: Off
// Only the 8 most significant bits of
// the AD conversion result are used
ADMUX=ADC_VREF_TYPE;
ADCSRA=0x88;
SFIOR&=0xEF;

// Global enable interrupts
#asm("sei")
```

```
while (1){
        if (dataReceived==0x01){
            // Manchester decode address stored in rxData
            // the following assumes that the data has been read in
perfectly

            for(i = 1; i < 16; i+=2){
                switch(rxData[i]){
                    case 0xAA: hammingData[i/2]=0x00; break;
                    case 0xA9: hammingData[i/2]=0x10; break;
                    case 0xA6: hammingData[i/2]=0x20; break;
                    case 0xA5: hammingData[i/2]=0x30; break;
                    case 0x9A: hammingData[i/2]=0x40; break;
                    case 0x99: hammingData[i/2]=0x50; break;
                    case 0x96: hammingData[i/2]=0x60; break;
                    case 0x95: hammingData[i/2]=0x70; break;
                    case 0x6A: hammingData[i/2]=0x80; break;
                    case 0x69: hammingData[i/2]=0x90; break;
                    case 0x66: hammingData[i/2]=0xA0; break;
                    case 0x65: hammingData[i/2]=0xB0; break;
                    case 0x5A: hammingData[i/2]=0xC0; break;
                    case 0x59: hammingData[i/2]=0xD0; break;
                    case 0x56: hammingData[i/2]=0xE0; break;
                    case 0x55: hammingData[i/2]=0xF0; break;
    default  : hammingData[i/2]=0x00;
                  manchesterDecodeError = 1;
                  break;
                }
            }

            for(i = 0; i < 16; i+=2){
                switch(rxData[i]){
                    case 0xAA: hammingData[i/2]|=0x0; break;
                    case 0xA9: hammingData[i/2]|=0x1; break;
                    case 0xA6: hammingData[i/2]|=0x2; break;
                    case 0xA5: hammingData[i/2]|=0x3; break;
                    case 0x9A: hammingData[i/2]|=0x4; break;
                    case 0x99: hammingData[i/2]|=0x5; break;
                    case 0x96: hammingData[i/2]|=0x6; break;
                    case 0x95: hammingData[i/2]|=0x7; break;
                    case 0x6A: hammingData[i/2]|=0x8; break;
                    case 0x69: hammingData[i/2]|=0x9; break;
                    case 0x66: hammingData[i/2]|=0xA; break;
                    case 0x65: hammingData[i/2]|=0xB; break;
                    case 0x5A: hammingData[i/2]|=0xC; break;
                    case 0x59: hammingData[i/2]|=0xD; break;
                    case 0x56: hammingData[i/2]|=0xE; break;
                    case 0x55: hammingData[i/2]|=0xF; break;
    default  : hammingData[i/2]|=0x0;
```

```
                manchesterDecodeError = 1;
                break;
                }
            }

            for(i = 1; i < 8; i+=2){
                packetData[i/2] = (((hammingData[i] >> 3) & 0x0E) |
((hammingData[i] >> 2) & 0x01))<<4;
                iso1 = (hammingData[i] & 0x74); // Isolate s1
                iso2 = (hammingData[i] & 0x6C); // Isolate s2
                iso3 = (hammingData[i] & 0x59); // Isolate s3

                s1 =
(iso1>>7)^(iso1>>6)^(iso1>>5)^(iso1>>4)^(iso1>>3)^(iso1>>2)^(iso1>>1)^(iso1);
                s2 =
(iso2>>7)^(iso2>>6)^(iso2>>5)^(iso2>>4)^(iso2>>3)^(iso2>>2)^(iso2>>1)^(iso2);
                s3 =
(iso3>>7)^(iso3>>6)^(iso3>>5)^(iso3>>4)^(iso3>>3)^(iso3>>2)^(iso3>>1)^(iso3);

                s = (s1<<2)|(s1<<1)|(s1<<0);

                switch(s){
                    case 3 :
packetData[i/2]=(packetData[i/2]^0x04)<<4; break;
                    case 5 :
packetData[i/2]=(packetData[i/2]^0x10)<<4; break;
                    case 6 :
packetData[i/2]=(packetData[i/2]^0x20)<<4; break;
                    case 7 :
packetData[i/2]=(packetData[i/2]^0x40)<<4; break;
                    default: break;
                }
            }

            for(i = 0; i < 8; i+=2){
                packetData[i/2]|= (((hammingData[i] >> 3) & 0x0E) |
((hammingData[i] >> 2) & 0x01));
                iso1 = (hammingData[i] & 0x74); // Isolate s1
                iso2 = (hammingData[i] & 0x6C); // Isolate s2
                iso3 = (hammingData[i] & 0x59); // Isolate s3

                s1 =
(iso1>>7)^(iso1>>6)^(iso1>>5)^(iso1>>4)^(iso1>>3)^(iso1>>2)^(iso1>>1)^(iso1);
                s2 =
(iso2>>7)^(iso2>>6)^(iso2>>5)^(iso2>>4)^(iso2>>3)^(iso2>>2)^(iso2>>1)^(iso2);
                s3 =
(iso3>>7)^(iso3>>6)^(iso3>>5)^(iso3>>4)^(iso3>>3)^(iso3>>2)^(iso3>>1)^(iso3);

                s = (s1<<2)|(s1<<1)|(s1<<0);
```

```
                                        switch(s){
                                                case 3 : packetData[i/2]|=packetData[i/2]^0x04;
break;
                                                case 5 : packetData[i/2]|=packetData[i/2]^0x10;
break;
                                                case 6 : packetData[i/2]|=packetData[i/2]^0x20;
break;
                                                case 7 : packetData[i/2]|=packetData[i/2]^0x40;
break;
                                                default: break;
                                        }
                                }

                                PORTA.1=0;
                                PORTA.2=1;
                                dataReceived=0x00; // done decoding address set flag back to
0
                                zeroMode = 1;
                        }
                };
        }
```

APPENDIX B: Low Level Code

```
// CodeVisionAVR C Compiler
// (C) 1998-2001 Pavel Haiduc, HP InfoTech S.R.L.

// I/O registers definitions for the ATmega128

#ifndef _MEGA128_INCLUDED_
#define _MEGA128_INCLUDED_

#pragma used+
sfrb PINF=0;
sfrb PINE=1;
sfrb DDRE=2;
sfrb PORTE=3;
sfrb ADCL=4;
sfrb ADCH=5;
sfrw ADCW=4;      // 16 bit access
sfrb ADCSRA=6;
sfrb ADMUX=7;
sfrb ACSR=8;
sfrb UBRR0L=9;
sfrb UCSR0B=0xa;
sfrb UCSR0A=0xb;
sfrb UDR0=0xc;
sfrb SPCR=0xd;
sfrb SPSR=0xe;
sfrb SPDR=0xf;
sfrb PIND=0x10;
sfrb DDRD=0x11;
sfrb PORTD=0x12;
sfrb PINC=0x13;
sfrb DDRC=0x14;
sfrb PORTC=0x15;
sfrb PINB=0x16;
sfrb DDRB=0x17;
sfrb PORTB=0x18;
sfrb PINA=0x19;
sfrb DDRA=0x1a;
sfrb PORTA=0x1b;
sfrb EECR=0x1c;
sfrb EEDR=0x1d;
sfrb EEARL=0x1e;
sfrb EEARH=0x1f;
sfrw EEAR=0x1e;   // 16 bit access
sfrb SFIOR=0x20;
sfrb WDTCR=0x21;
```

```
sfrb OCDR=0x22;
sfrb OCR2=0x23;
sfrb TCNT2=0x24;
sfrb TCCR2=0x25;
sfrb ICR1L=0x26;
sfrb ICR1H=0x27;
sfrw ICR1=0x26;   // 16 bit access
sfrb OCR1BL=0x28;
sfrb OCR1BH=0x29;
sfrw OCR1B=0x28;  // 16 bit access
sfrb OCR1AL=0x2a;
sfrb OCR1AH=0x2b;
sfrw OCR1A=0x2a;  // 16 bit access
sfrb TCNT1L=0x2c;
sfrb TCNT1H=0x2d;
sfrw TCNT1=0x2c;  // 16 bit access
sfrb TCCR1B=0x2e;
sfrb TCCR1A=0x2f;
sfrb ASSR=0x30;
sfrb OCR0=0x31;
sfrb TCNT0=0x32;
sfrb TCCR0=0x33;
sfrb MCUCSR=0x34;
sfrb MCUCR=0x35;
sfrb TIFR=0x36;
sfrb TIMSK=0x37;
sfrb EIFR=0x38;
sfrb EIMSK=0x39;
sfrb EICRB=0x3a;
sfrb RAMPZ=0x3b;
sfrb XDIV=0x3c;
sfrb SPL=0x3d;
sfrb SPH=0x3e;
sfrb SREG=0x3f;
#pragma used-

#define DDRF *(unsigned char *) 0x61
#define PORTF *(unsigned char *) 0x62
#define PING *(unsigned char *) 0x63
#define DDRG *(unsigned char *) 0x64
#define PORTG *(unsigned char *) 0x65
#define SPMCSR *(unsigned char *) 0x68
#define EICRA *(unsigned char *) 0x6a
#define XMCRB *(unsigned char *) 0x6c
#define XMCRA *(unsigned char *) 0x6d
#define OSCCAL *(unsigned char *) 0x6f
#define TWBR *(unsigned char *) 0x70
#define TWSR *(unsigned char *) 0x71
#define TWAR *(unsigned char *) 0x72
```

```
#define TWDR *(unsigned char *) 0x73
#define TWCR *(unsigned char *) 0x74
#define OCR1CL *(unsigned char *) 0x78
#define OCR1CH *(unsigned char *) 0x79
#define TCCR1C *(unsigned char *) 0x7a
#define ETIFR *(unsigned char *) 0x7c
#define ETIMSK *(unsigned char *) 0x7d
#define ICR3L *(unsigned char *) 0x80
#define ICR3H *(unsigned char *) 0x81
#define OCR3CL *(unsigned char *) 0x82
#define OCR3CH *(unsigned char *) 0x83
#define OCR3BL *(unsigned char *) 0x84
#define OCR3BH *(unsigned char *) 0x85
#define OCR3AL *(unsigned char *) 0x86
#define OCR3AH *(unsigned char *) 0x87
#define TCNT3L *(unsigned char *) 0x88
#define TCNT3H *(unsigned char *) 0x89
#define TCCR3B *(unsigned char *) 0x8a
#define TCCR3A *(unsigned char *) 0x8b
#define TCCR3C *(unsigned char *) 0x8c
#define UBRR0H *(unsigned char *) 0x90
#define UCSR0C *(unsigned char *) 0x95
#define UBRR1H *(unsigned char *) 0x98
#define UBRR1L *(unsigned char *) 0x99
#define UCSR1B *(unsigned char *) 0x9a
#define UCSR1A *(unsigned char *) 0x9b
#define UDR1 *(unsigned char *) 0x9c
#define UCSR1C *(unsigned char *) 0x9d

// Interrupt vectors definitions

#define EXT_INT0 2
#define EXT_INT1 3
#define EXT_INT2 4
#define EXT_INT3 5
#define EXT_INT4 6
#define EXT_INT5 7
#define EXT_INT6 8
#define EXT_INT7 9
#define TIM2_COMP 10
#define TIM2_OVF 11
#define TIM1_CAPT 12
#define TIM1_COMPA 13
#define TIM1_COMPB 14
#define TIM1_OVF 15
#define TIM0_COMP 16
#define TIM0_OVF 17
#define SPI_STC 18
#define USART0_RXC 19
```

```
#define USART0_DRE 20
#define USART0_TXC 21
#define ADC_INT 22
#define EE_RDY 23
#define ANA_COMP 24
#define TIM1_COMPC 25
#define TIM3_CAPT 26
#define TIM3_COMPA 27
#define TIM3_COMPB 28
#define TIM3_COMPC 29
#define TIM3_OVF 30
#define USART1_RXC 31
#define USART1_DRE 32
#define USART1_TXC 33
#define TWI 34
#define SPM_RDY 35

#endif
```

```
// CodeVisionAVR C Compiler
// (C) 1998-2000 Pavel Haiduc, HP InfoTech S.R.L.

#ifndef _DELAY_INCLUDED_
#define _DELAY_INCLUDED_

#pragma used+

void delay_us(unsigned int n);
void delay_ms(unsigned int n);

#pragma used-

#endif
```

REFERENCES

[1] Latchman, H.A. *Computer Communication Networks and the Internet*, McGraw Hill, 1997.

[2] Tannenbaum, Andrew S. *Computer Networks*, Prentice Hall, Upper Saddle River, New Jersey, 1996.

[3] Kurien, Cyril. "Comparison of FPGA and Microcontroller Technology," Report to James Kurtz, October 3, 2002.

[4] Electronic Communications Laboratory, "Design and Development of Wireless Components for Radiation Environments," University of Florida Electronic Communications Laboratory report to Argonne National Laboratories – West, April 2002.

[5] King, K.N. *C Programming: A Modern Approach*, W.W. Norton, New York, 1996.

[6] "ATmega128(L) Preliminary Complete Data Sheet," February 2003. http://www.atmel.com/dyn/resources/prod_documents/doc2467.pdf.

[7] "Atmel AVR STK 500 Data Sheet," March 2003. http://www.atmel.com/dyn/products/tools_card.asp?tool_id=2735.

[8] "RF Micro Devices RF2905 Transceiver Data Sheet," April 2003. http://www.rfmd.com/DataBooks/db97/2905.pdf.